UP

THE EFFECT OF ALUMINA PICK-UP ON MOULD FLUX BEHAVIOUR IN CONTINUOUS CASTING

by

Gert Adrian Bezuidenhout, B ENG.

Dissertation submitted in partial fulfilment of the degree

Master of Engineering

in the

Department of Materials Science and Metallurgical Engineering,

Faculty of Engineering

at the

University of Pretoria

Leader: Prof. P.C. Pistorius

PRETORIA

1999

Abstract

Title	:	The effect of alumina pick-up on mould flux behaviour in continuous casting
Author	:	Gert Adrian Bezuidenhout
Leader	:	Prof. P.C. Pistorius
Department	:	Materials Science and Metallurgical Engineering
Degree	:	Master of Engineering

The aim of this study was to determine the influence of alumina increase on the functioning of casting powder during continuous casting. Two aspects of the powder's performance were experimentally measured, namely the influence of alumina on the viscosity and the crystallisation behaviour. These two aspects were then related to the in-mould functioning of the casting powder with the aid of literature references.

Casting slag must provide lubrication between the mould surface and the thin steel shell. Alumina increase will cause viscosity increase in casting slags and will hinder lubrication when the inflow of casting slag into the mould/strand gap deteriorates. Heat transfer across the gap is determined by the amount of solid casting slag and the form (glass or crystalline) thereof. Heat transfer across a crystalline material may be up to seven times lower than that across a glass phase. The increased alumina will serve to increase the ratio of glassy phase to crystalline phase in the gap, so increasing the heat transfer.

To determine the true extent of alumina increase with modern clean steel practice, samples were taken from the moulds of both the V1 and V2 continuous casters at ISCOR Vanderbijlpark. The influence of this alumina increase on the viscosity and the crystallisation behaviour of the casting slag were experimentally measured. Viscosity measurements were done with a rotating bob viscometer (in a vertical tube furnace) on two commercial casting powders (with increasing Al_2O_3 content). Viscosity prediction models were evaluated with the data from the measured viscosity values. Crystallisation measurements were done by quench experiments with the aid of the hot thermocouple technique. Crystallisation behaviour after a specified heat cycle was presented as the percentage opaque material (crystalline) to vitreous material (glassy) measured with an optical microscope.

For the seven sequence casts during which samples were collected from the mould, it was found that the alumina content of the casting slag reached a steady-state value within the first ladle (first 40 minutes) with an increase of 3 to 4 mass %. The influence of a 4 mass % alumina increase on the measured viscosity is small enough that proper lubrication function of the slag will not be negatively affected. Viscosity prediction models vary in their accuracy and are limited with respect to the composition range of the casting powder and the temperature range for which they are valid.

The increased alumina content was found to have a strong influence on the percentage crystalline material present. After the sample was heated to 1300°C, kept there for 10s, and then quenched, the crystalline material will decrease from 60 % to 30 % for 5 mass % alumina added. This decreased crystalline material present may notably increase heat transfer. Full crystallisation does not occur at a single temperature, and crystallisation occurs over a temperature interval (of up to 200°C). This means that crystallisation temperature values quoted by casting powder manufacturers depend on the heat cycle and the technique used during crystallisation measurements. Several crystalline phases are usually present in solidified casting slag and these crystalline phases are strongly influenced by the alumina content: the stable crystalline phases may change as alumina content increases.

For the current alumina increase in casting powders the effect on viscosity is small, while crystallisation behaviour may be influenced to a greater extent.

Key terms: continuous casting, mould, casting powder, alumina, viscosity, viscosity prediction model, crystallisation, hot thermocouple technique, lubrication, heat transfer

Samevatting

Titel : Die effek van aluminatoename op gietpoeiergedrag tydens stringgieting
Outeur : Gert Adrian Bezuidenhout
Studieleier : Prof. P.C. Pistorius
Departement : Materiaalkunde en Metallurgiese Ingenieurswese
Graad : Meester in Ingenieurswese

Die doel van hierdie studie was om die invloed van die toename in alumina op die funksionering van gietpoeier tydens stringgieting te bepaal. Twee aspekte van die poeiergedrag is eksperimenteel gemeet, naamlik die invloed van alumina op viskositeit en kristallisasiegedrag. Hierdie twee aspekte is daarna met die hulp van literatuurverwysings na die funksionering van die gietpoeier in die gietvorm herlei.

Die gietslak moet smering bied tussen die wand van die gietvorm en die dun staalskil. Alumina toename sal die viskositeit van 'n gietpoeier verhoog wat die smering sal benadeel sodra dit die invloei van gietslak in die gietvorm/staalskil gaping beïnvloed. Hitte-oordrag oor die gaping word bepaal deur die hoeveelheid gestolde gietslak, asook die aard (glas of kristallyn) daarvan. Hitte-oordrag oor 'n kristallyne materiaal kan soveel as sewe keer laer wees as oor 'n glasfase. Die verhoogde aluminatoename sal tot gevolg hê dat die verhouding van glas tot kristalfase in die gaping vergroot, wat die hitte-oordrag ooreenkomstig sal verhoog.

Om die ware omvang van alumina toename in 'n hedendaagse skoonstaal bedryf te bepaal, is monsters uit die gietvorms van die V1 en V2 stringgietmasjiene te ISCOR Vanderbijlpark versamel. Die invloed van hierdie aluminatoename op die viskositeit en kristallisasiegedrag van die gietslak is eksperimenteel bepaal. Viskositeitsmetings is met 'n roterendesilinderviskometer (in 'n vertikale buisoond) op twee kommersiële gietpoeiers gedoen (met toenemende Al_2O_3 inhoud). Modelle wat viskositeit voorspel, is beoordeel aan die hand van die gemete viskositeitwaardes. Kristallisasiemetings is gedoen deur afbluslopies met 'n warmtermokoppeltegniek. Die kristallisasiegedrag na 'n gespesifiseerde hittesiklus is gevolg deur die persentasie ondeursigtige materiaal (kristallyn) en die persentasie deursigtige materiaal (glas) met 'n optiese mikroskoop te bepaal.

Vir die sewe reeks giete waarvan daar monsters uit die gietvorm versamel is, is gevind dat die alumina-inhoud van die gietslak binne die eerste pan (eerste 40 minute) 'n plafonwaarde bereik van tussen 3 en 4 massa % toename. Die invloed van 4 massa % aluminatoename op gemete viskositeitswaardes is van so 'n aard dat funksionering van die poeier nie negatief beïnvloed sal word nie. Viskositeitsvoorspellingsmodelle varieer in hul akkuraatheid, en is slegs geldig oor beperkte bereike van gietpoeiersamestelling en temperatuur.

Die verhoogde alumina inhoud het 'n sterk invloed op die persentasie kristallyne materiaal. In 'n monster wat verhit is tot 1300°C, gehou is vir 10 sekondes, en afgeblus is, sal die kristallyne materiaal afneem van 60 % na 30 % as 5 massa % alumina toegevoeg word. Hierdie verlaagde kristallyne materiaal kan die hitte oordrag noemenswaardig verhoog. Totale kristallisasie vind

nie plaas by 'n enkele temperatuur nie, en kristallisasie kan plaasvind oor 'n temperatuur interval van tot 200°C. Hierdie bevinding beteken dat kristallisasie temperatuur waardes wat deur gietpoeier vervaardigers aangegee word, afhanklik moet wees van die hitte-siklus en die tegniek gebruik tydens die kristallisasiemetings. 'n Aantal kristalfases is teenwoordig in gestolde gietslakke en hierdie kristalfases word sterk beïnvloed deur die alumina-inhoud. Die gevolg is dat die stabiele kristalfases verander soos die alumina toeneem.

Vir hedendaagse alumina toename in gietslak is die effek op viskositeit klein, tewyl die effek op kristallisasiegedrag meer beduidend mag wees.

Sleutelterme: stringgieting, gietvorm, gietpoeier, alumina, viskositeit, viskositeitvoorspellingmodel, kristallisasie, warmtermokoppelmetode, smering, hitte-oordrag

Table of Contents

1. Introduction

Steel making technology and quality control of cast steel have improved greatly during the past decade. In continuous casting, mould powders gained a firm place in mould-related technology, due to their decisive effect on the surface quality of the continuously cast product. Casting powders are added on top of the molten steel surface in the mould where they melt and are drawn into the mould/strand gap during oscillation. Casting powders are used to: protect the steel from oxidation; provide thermal isolation to prevent partial solidification of the metal surface; absorb inclusions in the steel; lubricate the surface of the strand; and provide homogeneous heat transfer between the strand and the mould. It is imperative that the powder should perform satisfactory at each stage since failure to do so will result in inferior steel surface quality.

The chemical composition and physical properties of the in-mould slag are different from the starting mould powder owing to the reactions at the steel-slag interface (including the absorption of non-metallic inclusions rising from the steel). For aluminium killed carbon steel the casting powder especially enriches in Al_2O_3 (alumina), formed by the reaction of aluminium (added to the steel for the purpose of de-oxidation) with oxygen (dissolved in the steel or from the atmosphere). Alumina enrichment takes place both through the reaction of dissolved aluminium in the steel with reducible oxides in the casting slag, and by absorption of the alumina floating from the steel. During sequence casting, the alumina content of the casting slag increases, but reaches a steady state value during the first ladle in the sequence [Nakano et al, 1984].

The ability of casting powder to perform its functions should be evaluated at the increased alumina content during sequence casting. The reason for this is that especially two characteristics of the powder are affected as the alumina content increases – viscosity and crystallisation. The current study examined the influence of increased alumina content on viscosity and crystallisation behaviour of two commercial casting powders. The results of the separate studies were then broadly put in the context of the in-mould situation, since the viscosity and the crystallisation/solidification behaviour simultaneously influence lubrication capability of the slag. Heat transfer between the strand and the mould is strongly governed by the crystallisation/solidification behaviour of the slag layer. Viscosity and crystallisation were examined because they are experimentally measurable and quantifiable, **but** their combined influences on the related functions (lubrication and heat transfer) of the slag in the mould were not directly measured.

2. Background (Broad overview)

Function of mould powders

Mould powders perform a fivefold function during continuous casting [Branion, 1987] :

I) They provide chemical protection of the molten steel surface from oxidation

II) They provide thermal insulation to prevent solidification of the steel surface and of the sintered powder layer

III) They absorb inclusions in the molten slag pool

IV) They lubricate the strand through the mould

V) They control heat transfer by providing a uniform heat transfer across the infiltrated slag layer in the mould.

2.1. Chemical protection

The presence of (I) a liquid slag pool above the meniscus and (II) carbon particles in the sintered and powder layers prevent oxidation of the steel surface.

2.1.1. Slag layer above the meniscus

Powder is added continuously to the mould to form 3 layers: (I) a raw powder layer (II) a sintered layer (III) a pool of liquid slag (shown in Figure 2.1).

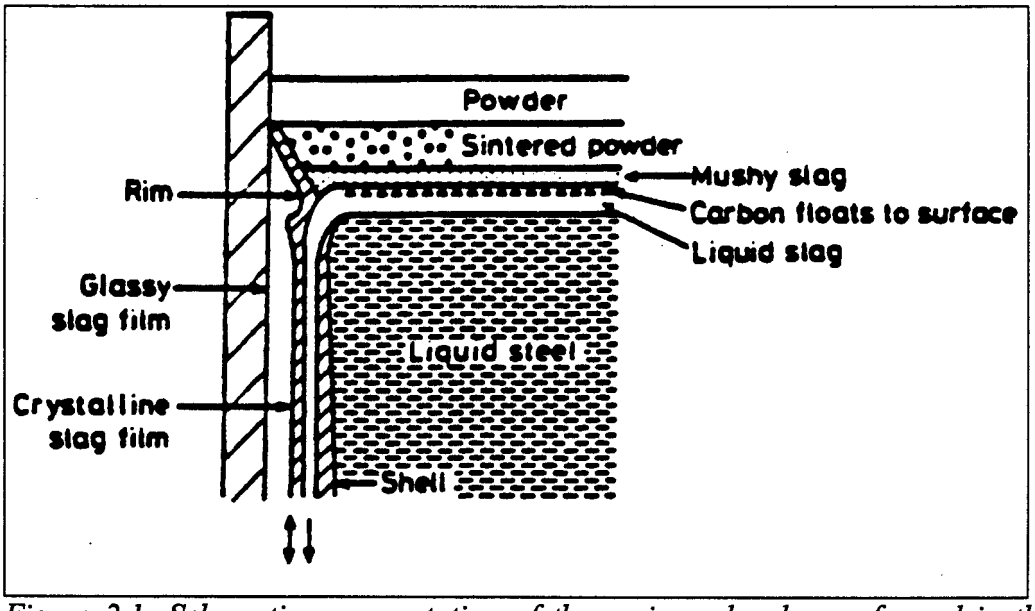

Figure 2.1: Schematic representation of the various slag layers formed in the mould [Mills, 1991a].

The thickness of these different layers will affect the degree to which the slag can protect the steel from oxidation. Thicker layers will provide more efficient chemical protection.

During operation, feed rates should be high enough to maintain a thick unmelted layer (at least 25mm) for protection of oxidation and especially thermal insulation by reducing vertical heat flux. A thicker unmelted layer will limit upward heat loss and provide a melted slag layer sufficient to provide lubrication of the strand. The melted layer should be maintained between at least 10 and 20mm thickness in order to assure slag infiltration throughout the entire oscillation stroke length that is typically close to 10mm. The reason for this can be seen from Figure 2.1. The slag rim shown closely follows the movement of the mould. It is necessary for the liquid slag to flow into the mould-strand gap during the entire oscillation cycle without being blocked in the lowest position by the slag rim.

Chemical protection is compromised by:

(i) excessive turbulence in the mould when there is a non-uniform flow through the submerged entry nozzle (henceforth referred to as the SEN)

(ii) the narrow face is disturbed by a standing wave (which arises because of steel flow through SEN); this standing wave tends to expose the molten steel.

Powder design can help to rectify this problem to a certain extent. If the powder consists of spherical particles, the particles can roll down the slope of the standing wave exposing molten slag or steel surface. Expanding granules on the other hand have reduced flowability and will keep the molten metal from being exposed to the atmosphere [Diehl et al, 1995]. A spherical granule with an expanding agent is reported to provide the best thermal isolation together with chemical control and minimum flowability.

Transport of oxygen from an oxidising atmosphere (in this case the atmosphere above the mould) through a slag is strongly dependent upon the iron oxide content of the slag. It is well understood

that the use of powders rich in iron oxide is detrimental to the quality. Most commercial casting powders contain less than 1% total iron. Therefore, a liquid layer of almost any of the casting powders available today is sufficient to protect the molten steel surface from oxidation [Riboud & Larrecq, 1979].

2.1.2. Carbon content and the form of carbon

Casting powders are a mixture of slag components and carbon (Typically 2 - 5 % of carbon). The carbon fulfils a twofold function: (I) it will protect the molten steel from oxidation by reacting with oxygen from the atmosphere to form CO gas (II) more importantly, it controls the melting rate of the powder.

Carbon in the form of carbon black, graphite or coke dust is added to the mould powder to control its melting rate and to provide insulation to both the steel and the liquid slag. The disadvantage of using carbon for this purpose is carbon pick-up that is experienced during the casting of steels (especially ultra-low carbon steels and stainless steels where very low carbon levels are needed).

Two aspects of the carbon source are of particular importance: the typical particle size and the temperature of ignition of the carbon source. A fine carbon black particle has high surface area, high reactivity and low ignition temperature so it can effectively protect the steel with CO gas. Simultaneously it is believed to coat each particle of the mould powder and delay coalescence of individual pools of molten flux, and thereby retards the melting rate of the powder. Fine carbon black is limited to between 1 and 2 percent of the total mould powder [Bommaraju, 1991].

An alternative to the use of carbon is the use of carbonates in the raw materials. The use of carbonates holds the advantage of an increased melting rate that is needed for higher casting speeds. Kawamoto [1994] found that melting rate increases as carbonate content increases due to the increased specific conductivity which is caused by the dissociation of the carbonates (evolution of CO_2 gas). The findings of Kawamoto [1994] are the opposite of what would be expected; that carbonates would retard the meting rate by the endothermic decomposition reaction at temperatures between 400 and 500°C.

When the melting rate is too high, more of the casting powder on top of the mould will melt. This in turn can bring about the formation of a larger slag rim and partial solidification of the molten steel surface if the powder on top of the steel surface cannot reduce vertical heat flux sufficiently. For this reason, carbonates are used together with other carbon sources. A second advantage to the use of carbonates is that carbon pick-up during casting cannot occur as is the case with carbon particles. A disadvantage of carbonates from the chemical protection viewpoint lies within the decomposition reaction that makes them otherwise favourable - Carbon dioxide is a product of this reaction that provides an oxidising atmosphere.

2.1.3. Chemical protection of volatile constituents of the casting powder

A sufficient thickness of unmelted powder layer will also provide chemical protection of the volatile constituents of the casting powder. The vaporised species from the hot, melted part of

the casting slag will cool down in the cooler powder layer, precipitate and not be lost as fluoride vapour. These volatile fluoride vapours are hazardous to health and often carry heavy restrictions on their allowable amounts in the atmosphere. The pure fluorides of calcium, potassium, sodium and lithium have significant vapour pressures at 1530°C [Zaitsev et al, 1994]. Thus, during melting of raw mixtures it is possible to evaporate significant amounts of these volatile fluorides.

Reactions such as:
$Na_2O + CaF_2 = 2NaF_{(g)} + CaO$

$K_2O + CaF_2 + 2KF_{(g)} + CaO$

$SiO_2 + 2CaF_2 = SiF_{4(g)} + 2CaO$

$Al_2O_3 + 3CaF_2 = 2AlF_{3(g)} + 3CaO$

$CaF_2 + H_2O = CaO + HF_{(g)}$

are thermodynamically feasible. As indicated above, humidity also increases the fluorine evaporation problem by reacting with the fluorine constituents of the slag phase and the gas phase to form HF. All liberated fluorides will react with water to form hydrogen fluoride in the atmosphere.

Zaitsev et al [1994] found that the evolution of fluorides is strongly related to the mineralogical constituents present in the mould powder formulation. Powders containing F in the form of cryolite (Na_3AlF_6) experienced F evaporation (as Sodium-Aluminium-Fluorides) at a rate a hundred times greater than if F were made up of CaF_2. Pre-fusion of mould slag and increasing the CaO/ SiO_2 ratio of the powder will reduce the overall evolution of fluorine containing gases. The reason for this is the formation of a solution in which the activity of F^- is low. The Fluoride is thus bonded to a greater extent.

2.2. Thermal insulation of the steel and molten powder

Thermal insulation is accomplished mainly by maintaining an unmelted powder layer of sufficient thickness above the molten powder layer. There are two ways to achieve this and thereby to minimise vertical heat flux in the mould. The first is to change the characteristics and the method of manufacture of the powder and the second is to change the melting behaviour of the powder.

2.2.1. Manufacturing method and characteristics of the powder

The principal factors affecting thermal flux through the powder are the bulk density of the powder and the shape of the particles.

Casting powders can be pre-treated in order to improve their uniformity of chemical composition, flowability, density and melting rates [Diehl et al, 1995]. The powders can be

mixed in water to form a slurry and then granulated or extruded to form spherical (granule size is around 400 microns) or tubular particles.

The insulating ability of different powder types (as well as other attributes) is shown in Table 2.1.

Table 2.1: Attributes of mould powder types [Diehl et al, 1995]

Item	**Powder**	**Extruded granule**	**Spherical granule with expanding agent**
Price	Good	Fair	Fair
Thermal insulation	Good	Poor	Fair
Cold Flowability (As pertaining to automatic feeding systems)	Poor	Fair	Good
Chemical Homogeneity	Fair	Good	Good
Environmental friendliness (Dust losses)	Poor	Good	Good

It is clear from Table 2.1 that the shape of the manufactured particles will determine the vertical heat flux. It must be noted that the thermal insulating ability of each type of flux will be improved by lowering the bulk density of the powder.

2.2.2. Melting behaviour of the powder

As discussed in section 2.1.1 a critical depth of unmelted layer is needed to provide thermal insulation so the molten steel surface will not freeze and to provide a sufficient liquid slag depth for lubrication throughout the stroke length.

This can be accomplished by increasing the carbon black content of the powder to reduce the melting rate, or more simply by increasing the depth of the powder layer added in the top of the mould. Carbon and its effect on melting behaviour have already been dealt with. The addition of a thicker unmelted powder layer in the mould is advantageous in every respect and should be standard practice if poor thermal insulation is a problem. About 25mm thickness appears to be a good measure. A thicker unmelted layer will reduce vertical heat flux to very low values and so assure high temperatures in the meniscus region of the molten steel. The meniscus region is suggested to be the most critical part to effectively control since it will determine how the steel shell forms and what form it will have. Heat control in the meniscus region will also determine the ease and the temperature of slag inflow into the gap.

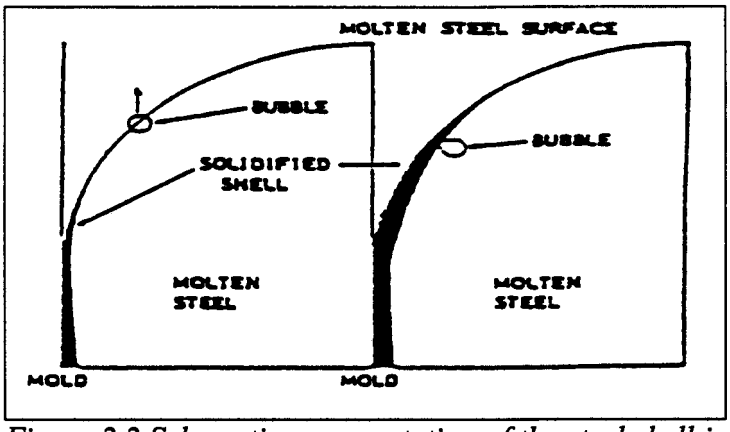

Figure 2.2 Schematic representation of the steel shell in the meniscus region during a) excellent vertical thermal insulation, b) poor vertical thermal insulation [Neumann et al, 1996].

Figure 2.2 shows that slag and gas bubble entrapment is easier during poor thermal insulation on top of the meniscus. Oscillation mark formation can also be pronounced under these conditions. The reason for this is found in the mechanism of oscillation mark formation that will be discussed briefly for the sake of completeness.

Riboud & Larrecq [1979] identified two mechanisms of oscillation mark formation. They used radioactive gold to monitor the solid shell formation. Traces of solid meniscus were visible in some of the samples, protruding into the liquid metal and corresponding to the oscillation marks. In other samples the solid overflow marks could not be noticed, and it is accepted that the meniscus shell could be bent backward against the mould wall in these instances.

The two mechanisms can be seen in Figure 2.3 (Marked as I and II respectively). The first occurs when a nail structure is produced under the surface of the steel meniscus when the mould level varies to a large extent (shown in Figure 2.3-I). Figure 2.3-I ^{bis} shows that the nail-like steel structure re-melts, but an oscillation mark is left behind as the new steel shell forms above it [Anzai et al, 1987]. The second mechanism occurs when a depression of the steel shell is formed as the solidifying steel shell is deformed under pressure at the meniscus with stable mould level conditions.

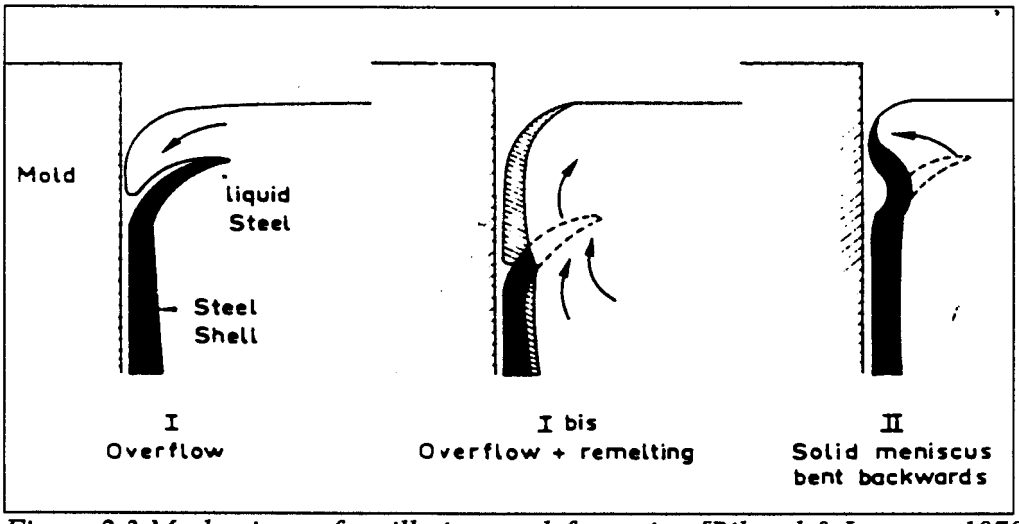

Figure 2.3 Mechanisms of oscillation mark formation [Riboud & Larrecq, 1979].

2.3. Absorption of inclusions

2.3.1. How inclusions are formed.

The principal non-metallic inclusion in continuous casting of aluminium-killed steel is Al_2O_3 (alumina). Alumina is formed during deoxidation of the steel by aluminium. It can also form as the result of the reaction between dissolved aluminium in the steel and reducible oxides (SiO_2, FeO and MnO) in the slag, or by contact with air.

$(Al)_{Fe} + M_xO_x = Al_2O_3 + x(M)_{Fe}$
with: M_xO_x = Oxide in slag

Under normal conditions about half of the alumina increase in the mould slag comes from dissolving alumina formed by oxidation of the aluminium in the metal by oxygen in the metal (during de-oxidation of the steel). The other half of alumina in the mould slag is formed by reaction with SiO_2, FeO and MnO in the slag [Skoczylas, 1996; Kyoden et al, 1987]. Alumina can also form during poor or unstable operation of the casting process where molten steel is exposed to air. Alumina forms a non-metallic highly refractory oxide that can build up in the SEN or on stopper rods and form agglomerates. When these agglomerates are released they can have detrimental effects on the steel performance or create problems during the casting process itself. It increases the mould slag viscosity greatly in two ways:

(i) Some of the alumina dissolves in the molten powder and increases the viscosity by acting as a network former (as discussed later in more detail)

(ii) The portion of the alumina that does not have time to dissolve in the molten powder will be present as a second solid phase in the molten powder and can even be trapped in the strand/metal gap resulting in poor lubrication.

Inclusions can be either solid or liquid. Liquid inclusions will just dilute themselves in the liquid slag. As for solid inclusions such as alumina clusters, the partly immersed position is always an intermediate step. (In general, the slag formed from casting powders wet alumina with a contact

angle of about 160°, suggesting almost complete wetting of the slag to alumina [Feldbauer et al, 1995]). Failure of the slag to dissolve these solid particles leads to a heterogeneous slag and the interface may become congested with solids. This will prevent further dissolution of inclusions into the slag and seriously hamper the flow of liquid slag into the mould/shell gap. The slag must dissolve these solid inclusions.

Mould powders should be so designed as to absorb the maximum amount of aluminates from the liquid steel in the mould, since the alumina inclusions in the steel matrix reduce cast steel quality. At higher casting speeds contact time between metal and slag reduces and a higher absorption rate into the mould slag is necessary.

2.3.2. Factors determining absorption rate.

For inclusions to be absorbed by the casting powder from the molten steel, the inclusions have to reach the meniscus area. Only after they arrive, can they be absorbed. Inclusion removal is essentially a mass transfer controlled process in the steel to the slag/metal interface. The possible action of the slag on inclusions concerns only those that have reached this slag/metal interface. The movement of the steel in the mould will determine the mass transfer kinetics. This will not be discussed in this section, and the discussion will centre on the ability of the casting powder slag to absorb inclusions that already reached the interface area.

Two factors seem to primarily determine the rate of alumina dissolution into the slag:
(i) slag viscosity and
(ii) basicity (Figure 2.4).
For higher casting speeds a more basic slag with a low viscosity will remove inclusions the fastest [Riboud & Larrecq, 1979; Nakano et al, 1984]. Viscosity of the slag is the most important parameter for the rate of dissolution of solid inclusions. In a more basic slag, and therefore a lower viscosity slag, complete dissolution of up to 15% alumina was measured [Riboud & Larrecq, 1979; Riboud et al, 1983]

The basicity of the flux is mostly and simply expressed as the V ratio:

$$Vratio = \frac{CaO}{SiO_2}$$

Or the Basicity index (B_i) that is based on the oxygen-ion attractive force as parameter for more detailed description and complex slags:

$$B_i = \frac{1.53(CaO + MgO + CaF_2) + 1.94Na_2O + 3.55Li_2O}{1.4SiO_2 + 0.1Al_2O_3}$$

Where: Oxides given in weight percentage

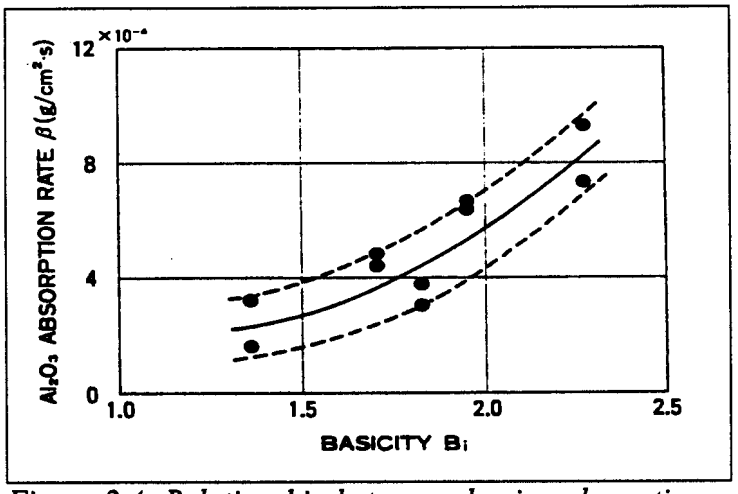

Figure 2.4: Relationship between alumina absorption rate of the molten powder and basicity B_1 [Nakano et al, 1984].

As can be seen from Figure 2.4 the rate of alumina absorption depends strongly on the basicity index of the molten powder, and rises exponentially as the basicity index rises.

The areas briefly discussed below affect inclusion absorption.

Alumina saturation

A rise in alumina increases the viscosity of the powder, provided that the alumina is absorbed and melted by the molten powder pool. When alumina exists suspended in the molten powder pool, the apparent viscosity of the powder greatly increases according to the volume fraction of suspended solid alumina clusters. [True viscosity measurements are not feasible, as a second phase (solid alumina phase) is present in the molten powder. As these solid alumina clusters pass by each other, as happens during flow, their shape, size, and cohesiveness will determine how much force is required to move them.] If alumina is present in very large clusters, it is not absorbed by the molten powder (due to insufficient time to dissolve the alumina, or less often saturation of the powder) and is entrapped by the steel during mould level fluctuations or the like to cause defects [Nakano et al, 1984]. Practical alumina saturation levels of industrial mould powders could not be found in literature, but is above 25 mass %, since this amount was added by various authors [Nakano et al, 1984; Kim et al, 1992; Koyama et al, 1987] without reaching saturation. Since alumina increase found in practice today is on the order of 3 mass percentage [Bommaraju, 1991] alumina saturation will not be achieved in the slag during casting and viscosity will not be affected by a second phase formed by saturation of the mould slag.

Start Al_2O_3 content

Mould powders contain some alumina in the start concentration, normally between 2 and 5 %, coming from the feed material. Nakano et al [1984] found that the amount of alumina absorbed by the molten powder pool depends on the alumina absorption rate and is not limited by alumina saturation of the molten slag (in line with the high saturation level, as indicated above). Higher start alumina content in the powder will not cause danger of alumina saturation of the liquid pool, but rather lower alumina dissolution by decreasing the dissolution rate.

Viscosity
The effect of alumina on the viscosity of the slag will be discussed in section 2.1. The paragraph below is only to provide a basis for the factors that influence absorption rate.

In slag, silica forms SiO_4^{-4} tetrahedrons. Alumina can fit into the silicate chain as for instance $NaAlO_4^{-4}$. When alumina is dissolved into a casting slag, AlO_4^{-5} is formed. AlO_4^{-5} requires a cation to be located near it (for instance Na) to provide a charge balance, form $NaAlO_4^{-4}$ and fit into the silicate chain. Because of the fact that alumina not only acts as a network former, but also requires a cation that would have acted as a network breaker, it is the most potent oxide in raising the viscosity of the mould slag. As alumina is absorbed, the viscosity rises and the absorption rate becomes lower. Proper design must allow for a viscosity and absorption rate change and still assure adequate lubrication and absorption as time progresses during the casting process.

In a good clean steel practice, the alumina rise in mould slag should not exceed about 3 mass % [Bommaraju, 1991]. For a 3 mass % rise in alumina a small viscosity increase will occur that is of no great concern and this ought not to alter the slag to a degree of endangering its proper function in the mould. In the early seventies alumina pick-up in the order of 10 mass % was still reported to be common [Mills & Bhat, 1973]. Operational problems however, like open pouring, clogging of the SEN that suddenly releases clusters, the ladle sliding gate that is burnt open and vortex formation in which tundish slag is drawn into the mould, will oxidise the steel to a similar extent and create more alumina inclusions that must be dissolved. Detrimental rises in viscosity may occur under these conditions.

Powder consumption
Powder consumption together with casting speed provides a crude measure of the time that the steel is in contact with the same liquid slag, and therefore the time that specific slag has to absorb inclusions. (High powder consumption means a greater throughput of slag in the mould and a shorter residence time of slag in the mould. Higher casting speeds on the other hand will decrease the residence time of steel in the mould and limit inclusion absorption.) This period that the steel is in contact with the slag and the amount of slag it is exposed to, will determine the final alumina content of the slag. Liquid flux consumption should be optimised to avoid excessive alumina content of the flux to restrict the rise in viscosity. Powder consumption can be expressed as kilogram of mould flux added per ton of steel cast (Q_t in kg/ton, useful for calculating running cost) or it can be expressed in terms of surface area dimensions of the strand (Q_s in kg/m^2, useful as a measure of lubrication). Typical reported values for Q_t (on slab casting machines) are between 0.3 and 0.7 kg/ton and the calculated consumption in kg/m^2 strand surface between 0.3 and 0.6 [Neumann et al, 1996; Wolf, 1987]. Since the consumption depends upon the size of the cast slab and is proportional to the strand surface, the amount of powder consumed in kg/m^2 strand surface is more suitable for evaluating the lubrication capability of the mould slag. (Since the mould powder consumption is related to mould surface area, the values of Q_s given above for slab casting machines are comparable or in the same range as both billet and bloom casting machines). Q_s can be related to Q_t in the following manner:

$$Q_s = \frac{7.6}{R} Q_t$$

$$R = \frac{2(w+t)}{wt}$$

Where: w = width of the mould (m)
t = thickness of the mould (m)

The trend today is to continually move towards higher casting speeds. For higher casting speeds, powder consumption decreases due to a thinner slag layer being dragged down the mould. This means greater alumina pick-up in less mould slag and places increasing pressure on the design, since the scenario described will work to sharply increase the viscosity. The designed viscosity has to be decreased to provide easier flow of slag down the mould and thereby to allow higher powder consumption rates.

Two papers illustrated that there is an optimum range of viscosity (η) and casting speed (V_c) which coincides with minimum heat transfer variations, frictional forces and surface defects. Ogibayashi et al [1987] found the uniformity of powder infiltration greatly varies with the powder viscosity while studying slab casting at casting speeds between 1.1 and 2 m/min. The optimum viscosity changes with the casting speed and these two variables can be arranged in an integrated manner by the term $\eta.V_c$, where η is the powder viscosity in poise at 1300°C and V_c is the casting speed in m/min. In the $\eta.V_c$ range of 2 to 3.5, the variations in the mould temperature, mould heat transfer and thickness of powder film at the mould exit are small, indicating uniform powder infiltration between the mould and the strand (Figure 2.5). He considered the optimum powder consumption (where fewest defects occur) to be given by:

$$Q_s = \frac{0.6}{\eta V_c}$$

Wolf [1987] defined the 'relative viscosity' of the slag in the mould with the term $\eta.V_c^2$ as he studied the influence of mould oscillation on lubrication (η is again the viscosity of the powder in Poise and V_c is the casting speed in m/min). The relative viscosity $\eta.V_c^2$ must be around 5 for the optimum powder consumption that is to be maintained around 0.3kg/m^2 for casting speeds between 1 and 2 m/min. Wolf aimed to show that ultra-low viscosity powders would be required for high-frequency mould oscillation in order to maintain the above consumption levels, by relating the higher casting speeds with the high mould speeds during higher-frequency mould oscillation. He considered the optimum powder consumption (where fewest defects occur) to be given by:

$$Q_s = \frac{0.7}{\eta^{0.5} V_c}$$

Wolf regarded the influence of the casting speed to be greater (squared) compared to Ogibayashi. The reason for this could have to do with his initial aim to show the effect of oscillation frequency on lubrication. None of these two authors studied casting speeds greater than 2m/min and the use of these equations is limited in this respect. Especially the 'relative viscosity' of Wolf predicts unrealistically low viscosities to be used in modern thin-slab casting that can cast at up to 5m/min. Typical values of viscosities of casting powders used for casting speeds of

5m/min are in the order of 0.8 Poise at 1300°C [Neumann et al, 1996]. In comparison, the parameter of Ogibayashi predicts around 0.5 Poise to be optimal and that of Wolf predicts around 0.2 Poise to be optimal.

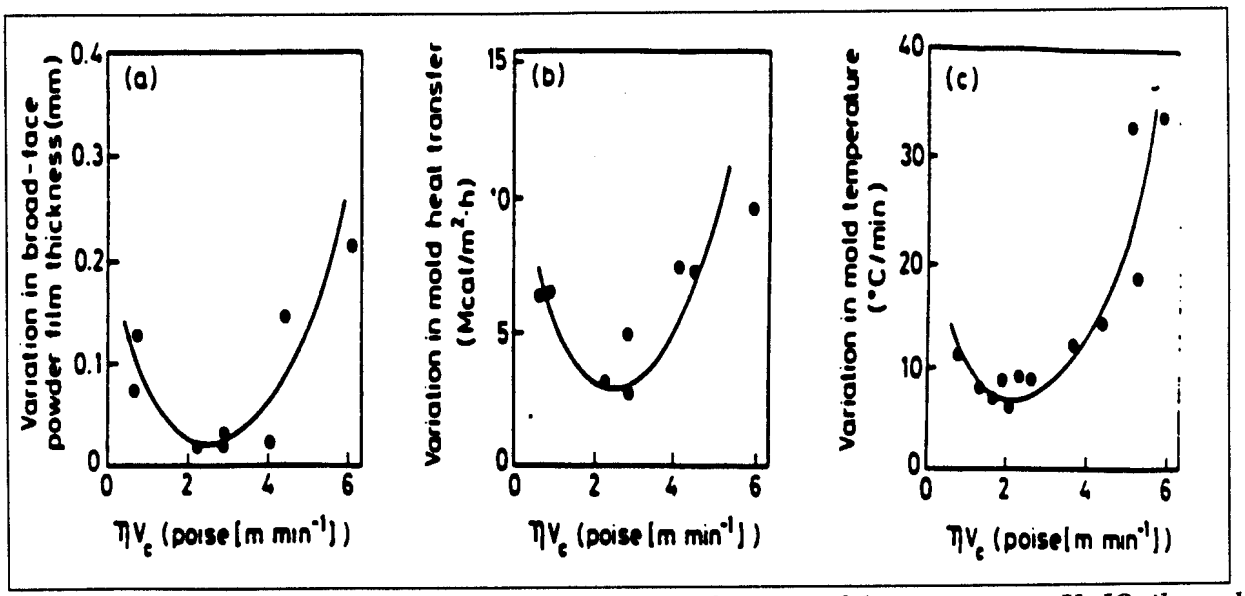

Figure 2.5: Frictional force and slag infiltration as a function of the parameter ηV_c [Ogibayashi et al, 1987].

2.4. Lubrication of the strand

Before this topic is discussed, it is necessary to go into some detail regarding the nomenclature about the solidification behaviour that will be used from here on forward.

Mould fluxes are very complicated oxyfluorides, which have a strong tendency towards glass formation upon cooling, even though the crystal phase is stable. As composition is varied, the fluxes can form either a glass or precipitate crystals upon cooling. Precipitation can result in a two-phase structure consisting of crystals surrounded by a residual glass phase. Glasses can be obtained by cooling a liquid below its equilibrium freezing point without the generation of a solid crystalline material. Most liquids can be supercooled below their equilibrium melting temperature before spontaneous nucleation and growth of their thermodynamically stable crystal form; however, glasses can be supercooled without crystallisation and are thus metastable. Time-Transformation diagrams are useful to provide insight into glass formation. Each Time-Transformation curve has a critical cooling rate for glass formation due to the competition with the driving force for crystallisation. Time-Transformation diagrams will be discussed later in more detail.

The temperature dependence of viscosity over a given temperature range is often represented by the Arrhenius equation:

$\eta = A \exp (E / RT)$

Or

$\ln \eta = \ln A + E/RT$
Where :
η = viscosity
A = Arrhenius constant
E = activation energy for viscous flow
R = gas constant
T = absolute temperature (K)

As such, by plotting 1/T versus ln η, a line with a constant slope E/R with intercept ln A can be expected over a given temperature range. Figure 2.6 shows a typical flux viscosity-versus-temperature curve [Branion, 1987]. There is no sudden slope change in this curve, but rather a temperature range where crystals and/or supercooled glass can start forming. The solidification temperature (T_s) for a powder like this will be defined as the temperature where the viscosity reaches 100 Poise. It is clear that this temperature has no significance at all to the crystallisation temperature (T_c or temperature at which the slag starts to form crystals) of the slag, since crystals could be precipitating over a temperature interval already.

The dashed line in Figure 2.6 shows a sudden change in the slope of the curve that will be called the Break Point Temperature (T_{bp}) of the slag. The break point temperature does not coincide with the temperature of the first crystals that formed. They can differ remarkably [Kim et al, 1992]. The viscosity breakpoint temperature (T_{bp}) does have practical significance since it gives the temperature at which the rate of viscosity rise markedly increases with decreasing temperature and it will have a large effect on the lubrication of the strand. The temperature marked as T_t (Transition temperature) in Figure 2.6 marks the temperature where the viscosity of the slag increases above the expected Arrhenius equation. This temperature is of no real significance, and is not generally noted, since it may markedly differ from the T_{bp}, T_s, and the T_c (as shown in Figure 2.6).

The term solidification temperature has little significance for the flux viscosity behaviour since it is not clearly reflected in the viscosity–temperature graphs. The solidification temperature (T_s) will henceforth be used to define that temperature at which the slag becomes solid (that being glass, crystalline or both). T_s cannot be related to T_c in any respect since it contains no information on where crystals start forming. T_{bp} and T_s on the other hand should be close in casting powders that exhibit a temperature where the viscosity will start to increase rapidly since the viscosity will reach 100 Poise near the sharp increase (T_{bp}) of the viscosity.

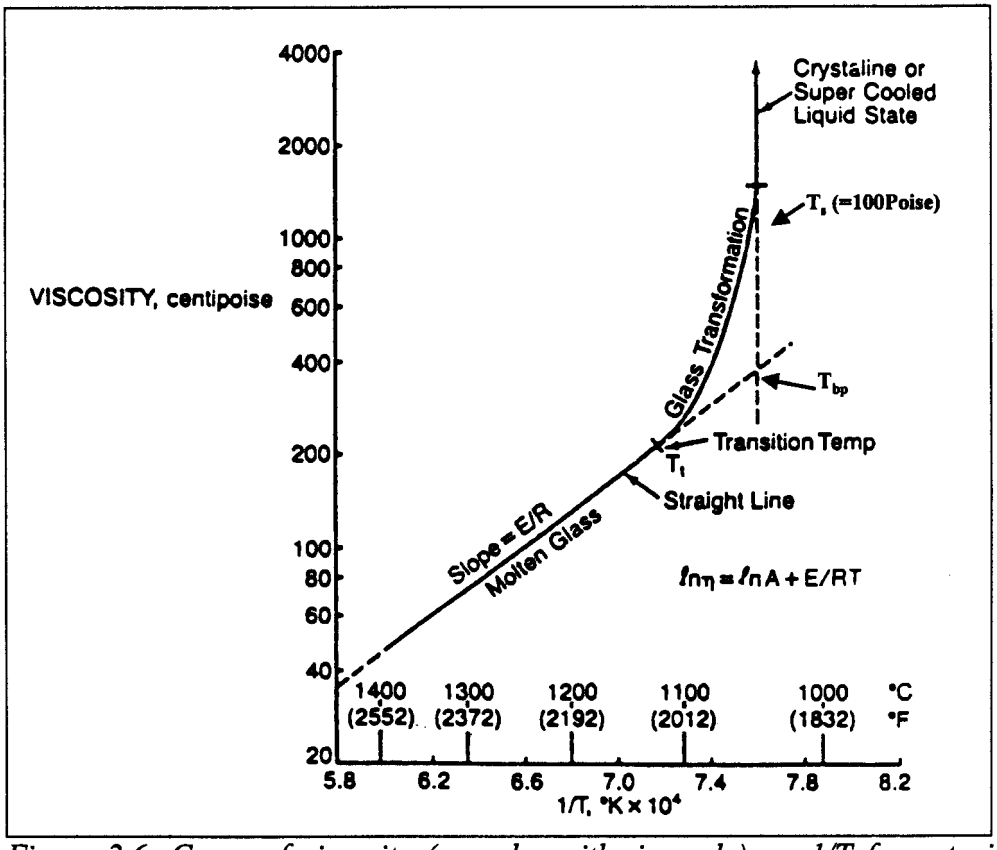

Figure 2.6: Curve of viscosity (on a logarithmic scale) vs. 1/T for a typical casting powder [Branion, 1987].

Friction force

The frictional force (F_{tot}) the steel strand experiences as it is drawn through the mould is a measure of the lubrication the strand enjoys. In the upper part of the mould, where the temperature is high, the frictional force is due to liquid slag lubrication (F_{liq}). If the temperature of the slag in contact with the steel shell in the lower part of the mould is below the temperature where the slag has solidified (either as glass, crystal or both), a solid slag layer will exist. This will cause solid slag / solid steel shell frictional forces (F_{sol}). During a poor slag feed situation, steel shell / copper mould friction can occur. The total frictional force consists of both the frictions due to liquid as well as solid lubrication.

$F_{tot} = F_{liq} + F_{sol}$

With: F_{tot} = Total friction force
F_{liq} = Liquid friction force
F_{sol} = Solid friction force

In work conducted by Nakato et al [1984] was concluded that over 90% of F_{tot} is contributed by F_{liq}, and the effect of F_{sol} is small for stable operation conditions. He also found that the frictional force measured increased gradually as the casting proceeded to a value of approximately 1.6 times the initial value after two hours of casting. He considered the change to be caused by the increase of the viscosity of the slag owing to enrichment of alumina.

This finding seems to be contradictory to that of work conducted by Hering et al [1992]; in that work, clear differences in terms of the amount of frictional force and of its dependence on alumina content have been established in the casting of various steel grades with casting powders of different origin. The simple explanation that the viscosity increases due to the increase in alumina content of the slag and that this leads to higher values of the liquid lubrication part of the frictional force proves inadequate. They found a sharp drop in the friction force of some powders at a certain increase in alumina that corresponds to a change in the mineral phase precipitating. The variation in friction force has therefore been attributed to the crystallisation of different mineral phases of the slag in the lubrication gap.

Figure 2.7 shows that the dominant mineral phase fractions of the casting powder changes as the percentage alumina increases. The conclusion of this study is shown in Figure 2.8 and shows that the increase in alumina influences both the viscosity and the crystallisation of the slag. If the desirable phase (gehlenite) is precipitated, the frictional force does not increase with the viscosity of the flux.

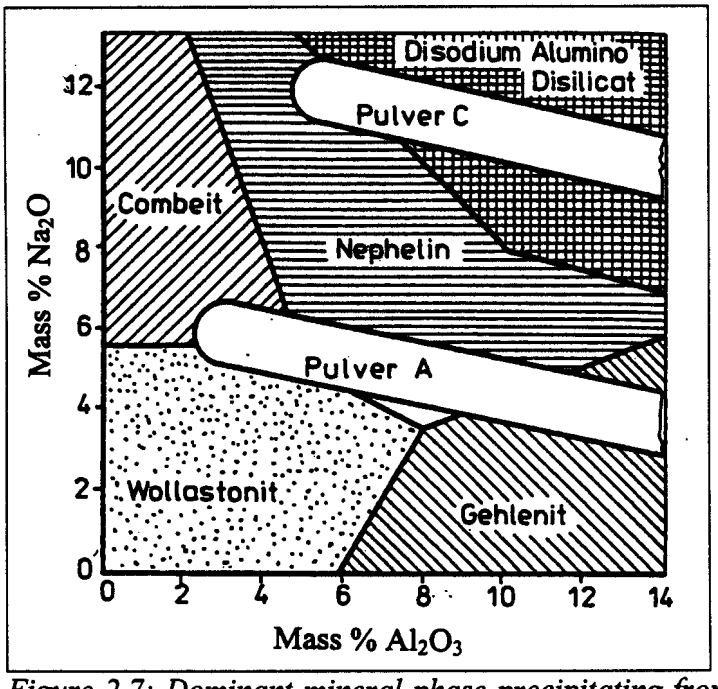

Figure 2.7: Dominant mineral phase precipitating from the slag vs. content of Al_2O_3 and Na_2O [Hering et al, 1992].

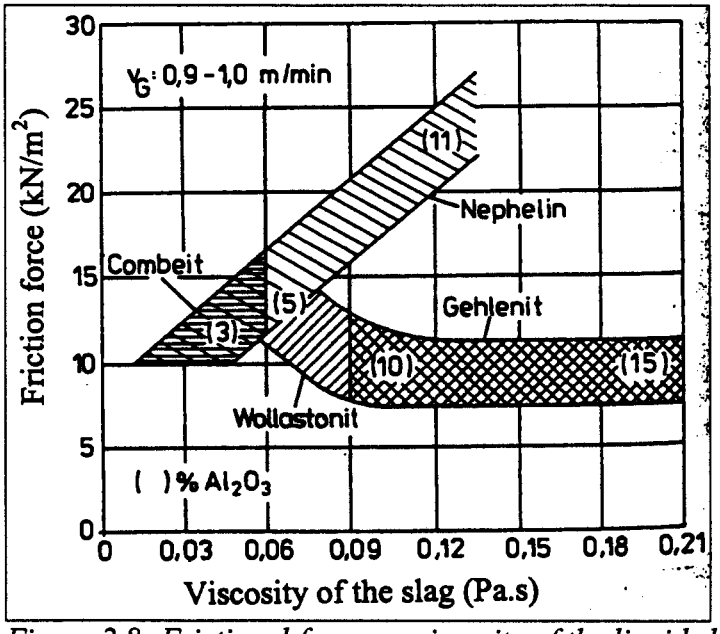

Figure 2.8: Frictional force vs. viscosity of the liquid slag and the mineral phase fractions of the slag [Hering et al, 1992].

Figures 2.7 and 2.8 show that alumina enrichment should so be controlled as to avoid the formation of nepheline crystals. Analysis of the crystalline composition [Fonseca et al, 1997] of solidified slag films indicates the presence of cuspidine, a calcium fluorosilicate with the formula $3CaO.\ 2SiO_2.\ CaF_2$. This phase is frequently present when the fluorine contents of slag is in the 4 % to 10% range. Some other crystalline phases capable of being developed through thermal treatment of films of casting slag are: wollastonite [$CaO\ .\ SiO_2$], gehlenite [$2CaO\ .\ Al_2O_3\ .\ SiO_2$], nepheline [$Na_2O\ .\ Al_2O_3\ .\ 2SiO_2$], and pectolite [$Na_2O\ .\ 4CaO\ .\ 6SiO_2\ .\ H_2O$].

Liquid and solid friction and what affects them will be discussed separately.

2.4.1. Liquid lubrication

The liquid frictional force F_{liq} is composed of the shear stress in the liquid slag film caused by relative motion between the shell and the mould.

$$F_{liq} = \frac{\eta(V_m - V_c)A}{d_l}$$

Where: η = viscosity of the slag film
V_m = velocity of the mould itself (at any given moment, positive or negative)
V_c = casting speed
A = area of the strand-mould contact
d_l = thickness of the slag film

Decreasing the viscosity of the slag and increasing the thickness of the slag film can therefore decrease the friction force due to liquid lubrication. As the casting speed is increased, the

increase of F_{liq} is mainly based on the increase in the relative velocity between shell and mould. The thickness of the slag film between the shell and the mould also gets thinner with increasing withdrawal speed. At the same time, the slab surface temperature in the mould rises and the viscosity of the slag decreases, so that the net effect is very small. Lowering viscosity will result in higher powder consumption, but lower slag film thickness. The above two requirements should therefore be simultaneously considered to obtain the optimum powder consumption rate related to a viscosity that also yields the lowest frictional force. As discussed earlier, Figure 2.5 shows that the viscosity and casting speed can be arranged as $\eta.V_c$ (η = viscosity; V_c = casting speed) in order to assure sufficient powder consumption that corresponds to a minimum in casting problems.

To minimise the liquid friction, it is desirable to use a casting powder that has a low melting temperature, since the viscosity decreases with increasing temperature above its melting temperature. A low melting temperature will also assure a liquid slag film at relative low temperatures lower in the mould, and so minimise solid friction.

According to Imai et al [1986] many types of gas bubbles such as argon and hydrogen are considered to pass through the powder pool until they are diffused toward the surface close to the meniscus. They found that the crystallisation of the mould powder is increased with an increasing amount of gas bubbles present in the slag (Figure 2.9). The index of crystallisation in a higher basicity (CaO/SiO_2 = 1) powder greatly increased. The index of crystallisation remained constant in a lower basicity (CaO/SiO_2 = 0.9) powder. The viscosity also sharply rises with increasing gas bubbles in the slag, which deteriorates the lubrication properties between the mould and shell (Figure 2.10). The use of an appropriate mould powder that is not so greatly affected by gas bubbles will maintain lubrication effective to prevent breakout caused by sticking.

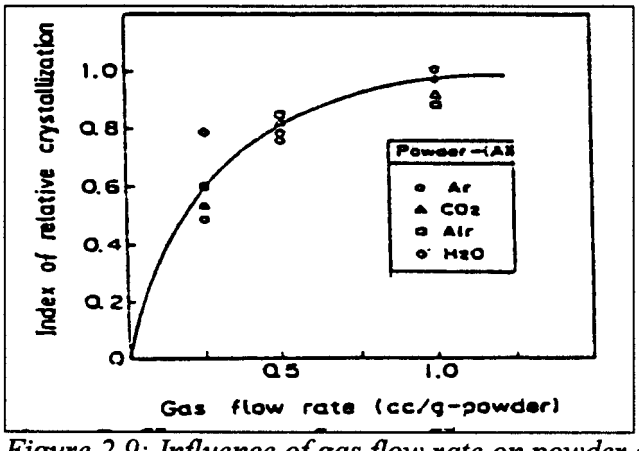

Figure 2.9: Influence of gas flow rate on powder crystallisation [Imai et al, 1986].

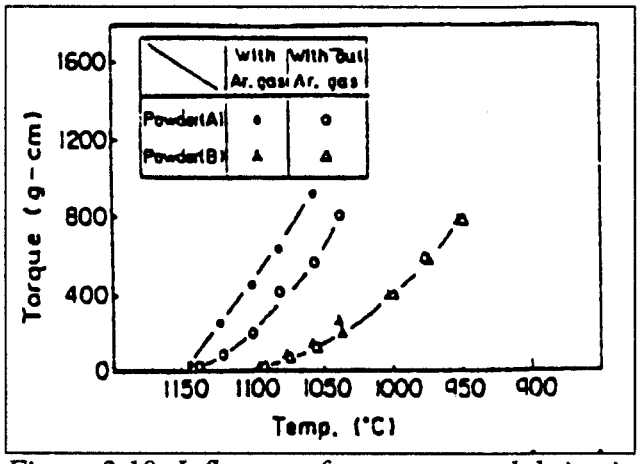

Figure 2.10: Influence of argon gas on lubrication of mould powder [Imai et al, 1986].

2.4.2. Solid lubrication (Friction)

When somewhere in the mould the entire gap between the copper mould and the steel shell is filled with solid slag, whether this solid is glass or crystalline, no viscous fluid lubrication can take place. Frictional forces at least ten times higher than that for a flux that maintains liquid lubrication can be expected to arise in this part of the mould [Branion, 1987]. The picture of assuring liquid lubrication throughout the mould is not as simple as it may seem; namely that only the melting temperature and the viscosity need to be lowered. The problem arises in peritectic steel grades (medium carbon between 0.08 and 0.15 %) where heat transfer across the slag layer has to be controlled in order to minimise heat flux fluctuations that cause longitudinal cracking in these grades. Two parameters need to be adjusted to achieve both lower heat transfer and maintain liquid lubrication. The first is to control heat transfer by increasing the temperature at which the flux solidifies, and to increase the T_c by increasing the CaO/SiO_2 ration to 1.2. The second is to maintain a low viscosity of the flux by adjusting the flux composition - increasing the Na_2O and F^- content [Kawamoto et al, 1997].

Heat transfer and fluctuations in the meniscus area are minimised by a thicker and more crystalline slag film in this area. The problem arises that a slag that has a crystallisation temperature high enough to start crystallising in the meniscus region can form a 100 % solid slag lower in the mould.

Work conducted by Brimacombe & Samarasekera [1979] has allowed calculation of the mould hot face temperature and strand surface temperature in the mould during casting (Illustrated in Figure 2.11).

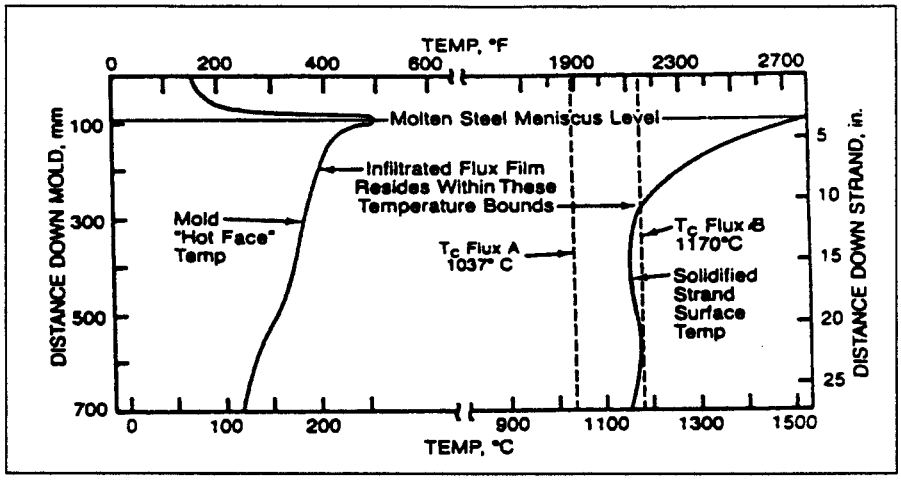

Figure 2.11: Thermal boundary conditions of infiltrated flux film between the strand and the mould [Brimacombe & Samarasekera, 1979].

The mould wall temperature for the conditions modelled for low carbon steels decreased from 260°C slightly below the meniscus to 110°C at the bottom of the mould. The shell temperature decreases from 1538°C at the meniscus to about 1150°C one third of the way down the mould and then stays relatively constant for the remaining two thirds of the way. The T_c of the flux will determine how much of the gap is filled with solid crystalline slag near the cold mould wall and the T_s will determine the liquid film thickness that is left for viscous fluid lubrication against the steel shell. If, for instance, for the above mentioned low carbon steel, the T_s is higher than the steel shell surface temperature at any point, liquid flux will not be present for lubrication, but the whole slag film will be solidified. Figure 2.11 shows flux B with T_s of 1170°C. For this situation, two-thirds of the mould length would enjoy a 100% solid slag layer and poor lubrication.

2.5. Heat transfer in the mould

In addition to controlling hydrodynamic lubrication, slag film conditions also affect heat transfer between the solidifying shell and the mould wall. Heat transfer is controlled in three steps :
(I) steel shell to slag layer
(II) through the slag layer
(III) slag to mould wall.

2.5.1. Heat transfer from steel shell to slag

A liquid slag film provides maximum heat flux in this area and temperature drop across this interface is small compared to the other two areas of heat transfer mentioned above. The moment a 100% solid layer slag forms against the steel shell frictional forces at least ten times higher than for viscous fluid lubrication can be expected according to Branion [1987]. The heat transfer from the steel shell to the slag becomes very low under these conditions due to air gaps that form and cannot be filled with liquid slag. The temperature drop across this interface then rises sharply. Investigations into the liquid slag contact resistance against the wall of a graphite crucible have been conducted by Jenkins [1995]. These measurements suggest that the liquid

slag contact resistance is at least one or two orders of magnitude smaller than the solid slag contact resistance.

Kyoden et al [1987] suggested that part of the effect of viscosity on heat transfer across this section is due to the ability or inability of the mould slag to eliminate air gaps in the shell/mould interface. Figure 2.12 shows an enlarged view of the film with calculated temperature profiles for a liquid-solid slag (50mm below meniscus) and a 100% solid slag (300mm below the meniscus).

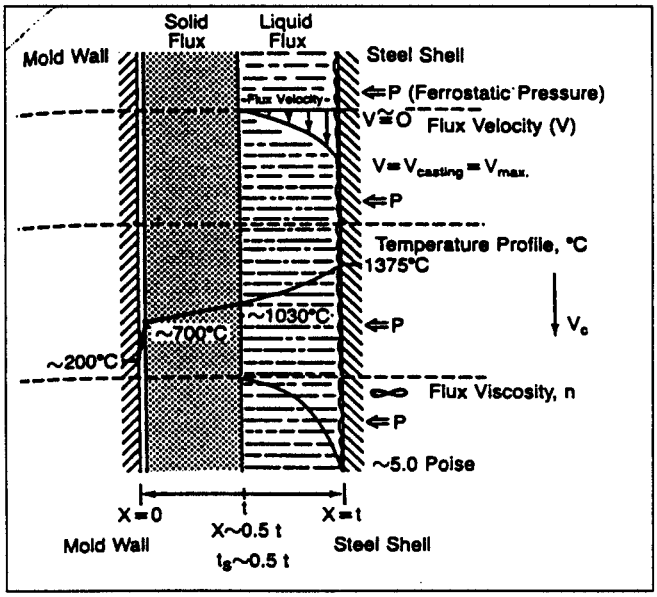

Figure 2.12A: Enlarged view of the flux film with temperature profiles for a liquid-solid slag (50mm below meniscus)[Branion, 1987].

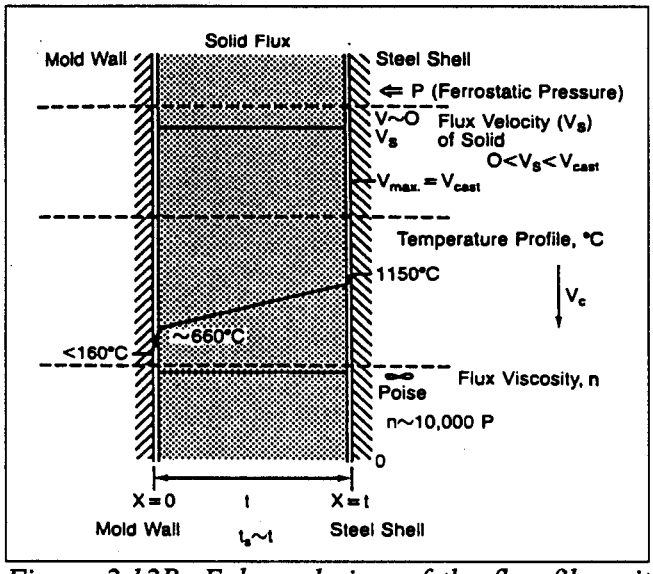

Figure 2.12B: Enlarged view of the flux film with temperature profiles for a 100% solid slag (300mm below the meniscus) [Branion, 1987].

2.5.2. Heat transfer through the slag layer

Taking into account that the slag layer consists of liquid part and of a solid part (or only a solid part), the heat flux through the slag layer will be separated into heat flux through the viscous liquid and through the solid part.

2.5.2.1. Heat transfer through the liquid slag layer

Viscosity seems to be the main parameter determining the heat flux through the liquid layer. This is especially true in the upper part of the mould were a very thin solid layer exists and the viscosity at 1500°C is very important. High viscosity slag will form thicker insulating layers and consumption will decrease. If the viscosity is low, the heat flux will be high through the thin layer [Riboud & Larrecq, 1979]. Furthermore, Branion [1987] referred to work conducted by Alberny et al who also showed that heat flux increases as slag viscosity decreases. It was suggested that the viscosity of the slag determine the flowability of the slag that is a measure of the ability of the liquid to eliminate air gaps between the steel shell and slag layer. (This will be discussed in more detail in the next section.)

Increasing hydrogen content in steel has been found to greatly reduce the heat transfer through the mould. Hydrogen solubility in steel is greatly reduced upon solidification in the steel shell. Some hydrogen diffuses to the casting slag/steel interface as the steel rejects it where it subsequently enters the liquid mould powder layer. Gaseous hydrogen is virtually insoluble in liquid slag, but the physical entrapment of H_2 bubbles is possible [Turkdogan, 1996]. An increasing volume of hydrogen being evolved from the steel should lead to a corresponding increase in hydrogen entrapment in the mould powder. This in turn will manifest itself as porosity and cause an increased resistance to heat transfer and therefore a reduction in the rate of heat removal. With increased crystallisation temperature, the effect of hydrogen on heat removal is much less pronounced than in the case of lower crystallisation temperature powders. This is likely due to the lower volume fraction of liquid powder into which the hydrogen can penetrate as the crystallisation temperature is increased [Zasowski & Sosinski, 1990].

2.5.2.2. Heat transfer through the solid slag layer

Steels that are continuously cast can be divided into two main groups according to operational difficulties. The first is 'crack sensitive' or peritectic steel grades (carbon content between 0.08 and 0.15%). For these steels the heat flux between strand and mould should be reduced by:
(i) developing a thicker solid layer and
(ii) developing a more crystalline layer.

The second group is 'sticker sensitive' steel grades with carbon content > 0.4%, or at higher casting speeds carbon content < 0.08 %. For these steels good lubrication must be achieved while creating a thinner and glassier slag layer between the shell and mould. The reason for this is that the thinner glassy layer allows a high heat flux for a thicker steel shell. This will lessen the possibility of sticker breakouts occurring in these grades.

Jablonka et al [1991] showed that mechanical stresses arise in peritectic steel grades with carbon

content between 0.08 to 0.15%, leading to longitudinal cracking. Figure 2.13 shows the difference in thermal contraction experienced when a peritectic steel grade cools and undergoes the delta-ferrite to austenite transformation.

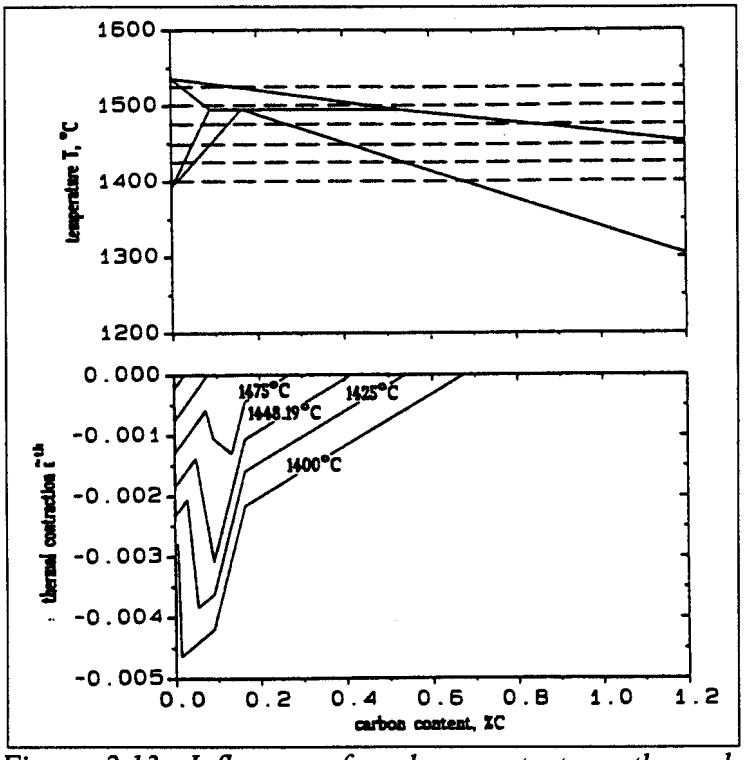

Figure 2.13: Influence of carbon content on thermal contraction of iron-carbon alloys at different temperatures [Jablonka et al, 1991].

Longitudinal cracking arises because of the difference in thermal contraction coefficients between delta ferrite and austenite. Strain can be developed when the steel cools through this high temperature delta ferrite region to austenite. This transformation takes place in the temperature area of the meniscus. Strain that develops in this meniscus area can be relieved by surface cracking (longitudinal cracks). In order to minimise these strains it is important that the shell in the meniscus region should be as thin and as uniform as possible. The heat transfer rate must be low to assure a thin shell. A slag layer in the mould/shell gap that has a sufficient solid thickness and/or crystallises more readily best does this.

A short discussion will now follow about the principles of heat transfer and the reason why a crystalline slag is more efficient to reduce the heat transfer:
Generally, conduction, radiation and convection transfer heat. The thickness of the flux film between the mould and the strand is generally estimated to be about 0.2mm. As convection cannot be developed in such a narrow space, the obtained effective thermal conductivity (k_{eff}) will be the sum of thermal conductivity by radiation (k_r) and lattice conduction (k_l).

$$k_{eff} = k_l + k_r$$

The effect that crystallisation has on the thermal conductivity is primarily by the scattering of

radiant heat by the crystals. The flow of heat due to radiation conductivity through a film of vitreous (glassy) slag present at the shell/mould interface may be twice the rate of flow established by lattice conduction. In a glassy slag, the primary heat transfer will therefore be through radiation conduction. However, scattering of radiant heat by the crystalline material in the slag film may reduce the radiation conduction contribution to between 0.1 and 0.2 times the lattice conductive flow [Fonseca et al, 1997]. Lattice conduction now becomes the principal mechanism controlling heat transfer.

Another reason is given by Pinheiro et al [1995] as an explanation for the reduced heat transfer through a crystalline slag. Small pores exist in the crystalline layer that present a great resistance to heat transfer. These small pores were noted in all the studied precipitated crystals, but their frequency and size varied in each crystalline phase. The authors concluded that these pores might be the result of some small contraction as crystals grow in the solid glassy layer.

Susa et al [1994] studied five different types of slag samples taken from a mould and obtained thermal conductivities in the order of 2 W/m.K at 600°C. This conductivity increases slightly as the temperature increases to about 2.5 W/m.K at 1000°C. These are typical values for partly crystalline and glassy phases, since slag films taken from the mould consist of both crystalline and glassy parts.

2.5.3. Heat transfer from slag layer to mould

An air gap forms due to the solidification of the slag being in contact with the mould. The interfacial thermal resistance in the mould was measured by Yamauchi et al [1992] and found to be around 0.4 - 0.8 m^2K/kW, corresponding to an air gap in the order of 30 μm, for the surface temperature of the copper mould to be approximately 300°C under usual casting conditions.

There is always a solid slag layer closest to the mould wall and this part of the slag remains more or less intact during the casting operation. Heat transfer from the slag to the copper mould is low and Branion [1987] calculated a temperature drop in the order of 500°C. This temperature drop corresponds to the value of the interface resistance determined by Yamauchi [1992], given above (for a typical heat flux of 1000 kW/m^2).

It has been proposed that the lower heat transfer caused by crystalline material are due to a larger air gap between the mould and the slag, formed by greater contraction of crystalline material.

The presence of different gases in the gap between the slag and the mould has an effect on heat transfer across this gap. Hydrogen gas formed by decomposition of the spray water on the strand just under the mould can fill this gap and increase heat transfer across the gap.

3. Research problem and objectives

The principal non-metallic inclusion in continuous casting of carbon steel is Al_2O_3 (alumina). Alumina is formed during deoxidation of the steel by aluminium. It can also form as the result of the reaction between dissolved aluminium in the steel and oxides in the slag. Alumina is a non-metallic highly refractory oxide that can build up in the SEN (submerged entry nozzle) or stopper rods and form agglomerates. When these agglomerates are released they can have detrimental effects on the steel quality or create problems during the casting process itself if they are not dissolved in the slag. Mould powders should be so designed as to absorb the maximum amount of aluminates from the liquid steel in the mould. When the alumina content of the casting slag rises, the in-mould characteristics change with respect to the viscosity and the crystallisation of the casting slag.

- A rise in the alumina content of the casting slag will cause the viscosity of the powder to increase through the following mechanism: In slag, silica forms SiO_4^{-4} tetrahedrons. Alumina can fit into the silicate chain as for instance $NaAlO_4^{-4}$. When alumina is dissolved into a casting slag, AlO_4^{-5} is formed. AlO_4^{-5} requires a cation to be located near it (for instance Na) to provide a charge balance, form $NaAlO_4^{-4}$, and fit into the silicate chain. Because of the fact that alumina not only acts as a network former, but also requires a cation that would have acted as a network breaker, it is the most potent oxide in raising the viscosity of the mould slag. (For further discussion, refer to section 3.1.2)
- Alumina will affect the crystallisation behaviour of the slag in two respects. Firstly, since it acts as a network former in the slag, it will suppress crystallisation and lower the temperature at which the slag starts to crystallise. Secondly, the equilibrium crystal phase that forms during cooling will also change.

As both the viscosity and the crystallisation change simultaneously, the slag will be affected in the way it is able to fulfil its functions during casting. The two functions that will be affected the severest are the ability of the slag to lubricate the strand during casting and to control the heat transfer in the mould area [Carli & Ghilardi, 1998].

- The lubrication depends both on the viscosity of the liquid slag during liquid lubrication in the upper part of the mould, and on the length of the mould that enjoys liquid lubrication (which will in turn be determined by the temperature that the slag solidifies as glass or crystal).
- Heat transfer of the powder is influenced through the fraction of solid to liquid slag in the gap (the T_s of the powder) and the amounts of crystals present (the T_c of the powder). Crystallisation restricts radiation conductivity to almost zero by the crystals scattering the radiant heat.

It is necessary to understand the exact thermal conditions for precipitation and growth of a crystalline phase from a slag to understand the heat flux encountered in the mould of a continuous caster. At the same time it is necessary to understand the crystal morphology and the temporal development of the fraction of solid to understand lubrication.

The following discussion on both the viscosity and the crystallisation behaviour of a mould slag will be based on some aspects that still await clarification in the literature, concerning the influence of alumina. This discussion is by no means exhaustive and acts only as a more detailed formulation to address some areas that were studied experimentally by the author.

3.1. Effect of alumina on viscosity

3.1.1. The pick-up during sequence casting

In the past when clean steel production was not practised as it is today, the increase of alumina in the casting powder during casting was in the order of 5 – 10%. In modern times alumina increases in the order of 3% are generally found, even during a sequence cast that can last several hours. Scenarios exist that can increase this amount of alumina absorbed by the casting powder by oxidation of more of the aluminium in the steel. Open pouring of the steel without a nozzle and slag carry over in the mould when the tundish is drained too low are examples of such scenarios. It is necessary to know what the actual magnitude of the alumina increase is in order to design the mould powder to function properly, especially concerning its viscosity and ability to absorb alumina.

It is empirically known that when aluminium-killed steel is continuously cast, the amount of alumina in the molten powder pool in the mould remains at an almost constant level during the casting operation. To illustrate this, the mass balance in the molten powder pool during casting can be considered as described below.

A powder with initial alumina concentration C_o is added to the mould and forms a molten powder pool. The molten powder pool absorbs alumina rising through the liquid steel or carried by the nozzle stream and reaches alumina concentration C. The molten powder with alumina concentration C flows out of the pool. The mass balance of alumina in the molten powder pool is given by:

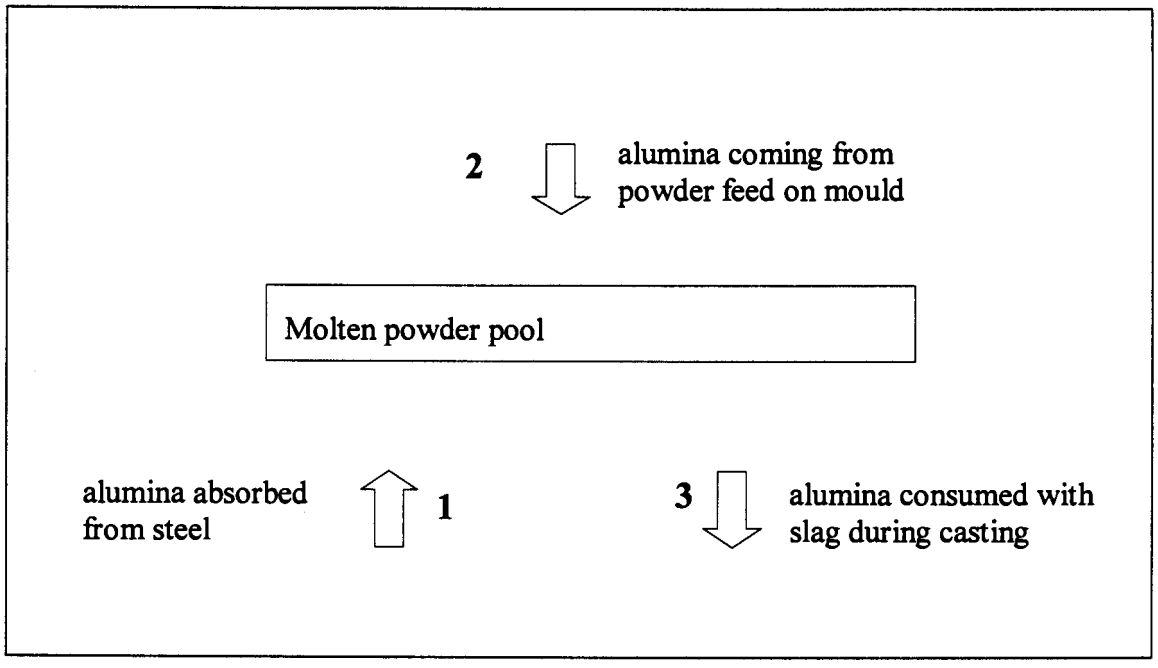

Change of mass in Al_2O_3 in powder = Mass flow of Al_2O_3 to slag (1+2) – Mass flow of Al_2O_3 out of slag (3)

$$\frac{dM_c}{dt} = 1 + 2 - 3$$

With:

$$\frac{dM_c}{dt} = \frac{w.m_t.d.\rho_c}{100}.\frac{dC}{dt}$$

$$1 = O_{ppm}.10^{-4}.\frac{M_{Al_2O_3}}{3M_o}.w.m_t.V_c.\rho_s.\frac{\alpha}{100}$$

$$2 = \frac{C_0}{100}.\frac{Q_t}{1000}.w.m_t.V_c.\rho_s$$

$$3 = \frac{C}{100}.\frac{Q_t}{1000}.w.m_t.V_c.\rho_s$$

Where: C = concentration of Al_2O_3 in the molten powder pool (mass %)
C_o = concentration of Al_2O_3 in the original powder (mass %)
t = time (min)
α = fraction (percentage) of O_{ppm} (as Al_2O_3) in steel that reports to mould slag
O_{ppm} = Oxygen content of the steel (ppm)
$M_{Al_2O_3}$ = Molar mass of Al_2O_3 (kg/mole)
M_o = Molar mass of oxygen (kg/mole)
V_c = casting speed (m/min)
Q_t = powder consumption rate (kg/ton of steel)
m_t = thickness of the casting mould (= thickness of molten powder pool) (m)
w = width of the casting mould (= width of molten powder pool) (m)
d = depth of the molten powder pool (m)
ρ_s = density of the steel (kg/m^3)
ρ_c = density of the molten powder (kg/m^3)

Figure 3.1 presents the change with time of the content of alumina in the molten powder, as calculated by equations given above. The values used in this calculation are as follows:

Mould size ($w.m_t$)	= 210*1200 (mm^2)
Casting speed (V_c)	= 1.5 (m/min)
Powder consumption (Q_t)	= 0.45 (kg/t)
Density of steel (ρ_s)	= 7800 (kg/m^3)
Thickness of molten powder pool (d)	= 10 (mm)
Density of casting powder (ρ_c)	= 2500 (kg/m^3)
Oxygen in steel (O_{ppm})	= 20 ppm
Original alumina concentration (C_0)	= 4.8 mass%

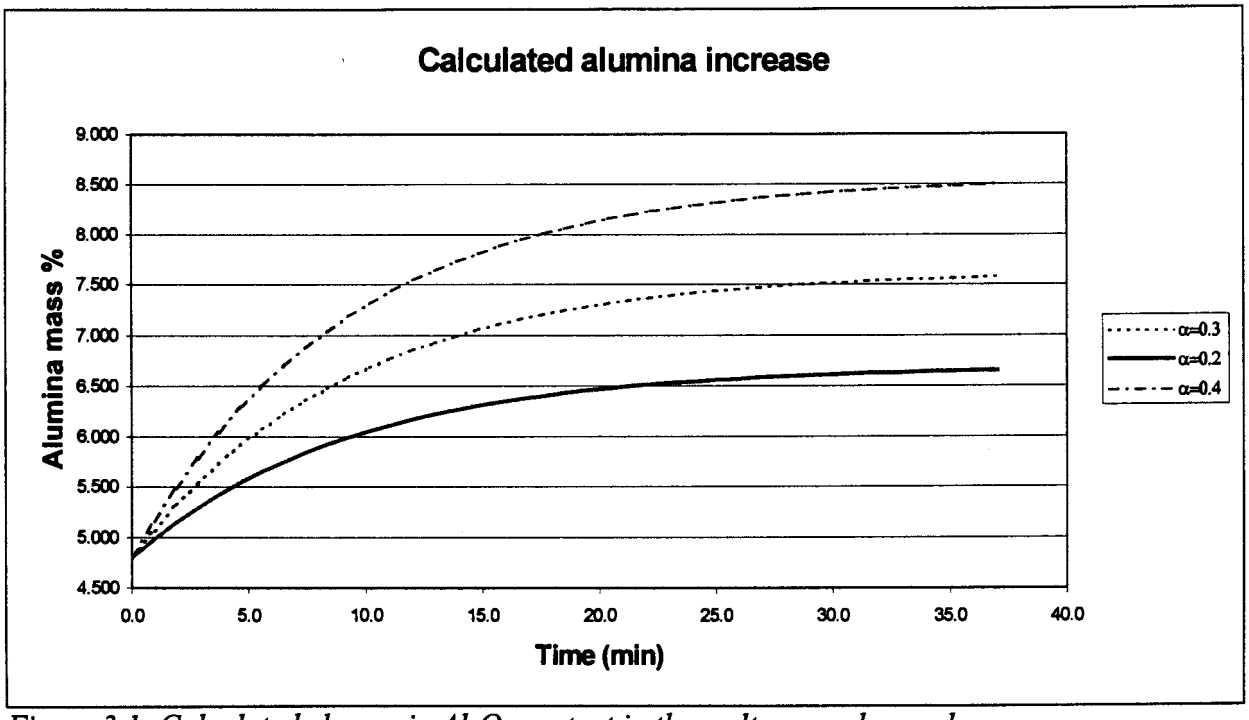

Figure 3.1: Calculated change in Al_2O_3 content in the molten powder pool.

Figure 3.1 shows that the alumina content in the molten powder pool increases with time and gradually approaches a steady-state value that depends on α (the fraction of the alumina in the liquid steel that reports to the mould slag). The alumina concentration in the molten powder pool is practically at steady state after 20 minutes of casting, according to this calculation. This agrees with the work conducted by Nakano et al [1984].

3.1.2. Mathematical modelling of the influence of slag composition

The ability of an oxide to form a network can be expressed in terms of its local field strength, given by:

$F = Z_c / a^2$
With:
F= the field strength,
Z_c = the valence of the cation and
a = the distance between the centres of the radii of the cation and oxygen ions (in Å).

A cation with a higher field strength (F= 1.5) is more able to attract oxygen anions to achieve a denser packing and become a glass former. Field strengths of 0.1 - 0.4 characterise network modifiers that tend to lose oxygen anions when dissolved in a slag, for example CaO and MgO. Network modifiers break up the silicate network by adding oxygen anions to the network of silicate tetrahedra. This causes the network of silica tetrahedra to separate as each tetrahedron has its own complement of oxygen ions. The cation will be accommodated at the breaks in the silicate structure. This results in the formation of discrete molecules that decrease steadily in size as more basic oxides are added to the melt. The addition of fluorine reduces viscosity very

effectively. As the radius of F^- (1.31 Å) is similar to that of O^{2-} (1.38 Å) in a tetrahedral bonded Si-O network structure, F^- can easily replace the divalent oxygen ion resulting in breakdown of the Si-O network [Johnston & Brooks, 1997].

In a multi-component slag, Al^{3+} (F=0.96) assumes a co-ordination number of 4 and forms tetrahedra of $[AlO_4]^{5-}$ which are similar in size to the silica tetrahedron $[SiO_4]^{4-}$, so that in such systems aluminium is a glass former. In order to substitute Al^{3+} for Si^{4+} in the silica chain and maintain electrical neutrality, the presence of monovalent or divalent cations such as Na^+ or Ca^{2+} is required. Thus the ability of alumina to increase the silica chain length is dependent upon the basic oxides. Alumina forms networks in the molten slag, increasing the molecular size and decreasing the molecular mobility. Johnston & Brooks [1997] found that a 6% increase in alumina increased the molar volume more than three times the original value. A 14% increase gave a 300-fold increase in molar volume. This increases the molecular size and the viscosity accordingly. Of all the elements that can be added to the slag, alumina is the element that increases the viscosity the strongest.

The dependency of viscosity (η) on temperature could be approximated by either an Arrhenius's relationship :

$$\eta = A_A \exp\left(\frac{E}{RT}\right)$$

With:
A_A = frequency factor
E = activation energy for viscous flow
R = gas constant
T = absolute temperature

or a Weymann's relationship:

$$\eta = A_w T \exp\left(\frac{E}{RT}\right)$$

It has become apparent from recent literature [Fox & Mills, 1999] that at least ten mathematical models are available for the prediction of the viscosity of slag from their chemical composition. The groups responsible for each of the models have pursued their own models, apparently independently of the others. Consequently, it is difficult for industrial laboratories to know which model best suits their needs without trying them first and even then, not knowing the probable uncertainty of the predicted values.

Viscosity measurements are an expensive and time-consuming exercise. It would be beneficial for both manufacturer and consumer if models would be available to provide reliable viscosity values from chemical composition, which could be determined for every batch, but are much quicker and easier to derive than viscosity measurements. For the purpose of this study, only three of the most widely used equations will be referred to for the basis of comparison. The three

models evaluated divide the components of the slag into different categories, (network breakers, network formers and amphoterics).

Kim et al [1992] carried out linear least square regression analyses on several chemical composition variables to predict the viscosity. The results were obtained as an Arrhenius relationship:

$\text{Log}(\eta) = \log A + B / T$
$\text{Log } A = -2.307 - 0.046\ SiO_2 - 0.07\ CaO - 0.041\ MgO - 0.185\ Al_2O_3 + 0.035\ CaF_2 - 0.095\ B_2O_3$
$B = 6807.2 + 70.68\ SiO_2 + 32.58\ CaO + 312.65\ Al_2O_3 - 34.77\ Na_2O - 176.1\ CaF_2 - 167.4\ Li_2O + 59.7\ B_2O_3$

Where all the components are accounted as **mole %**, T = temperature (K) and η = Viscosity (Pa.s).

Riboud & Larrecq [1979] measured viscosity for a number of compositions in the system CaO-SiO_2-Na_2O-CaF_2-Al_2O_3

For the range of composition:
$33 < SiO_2 < 56\%$
$12 < CaO < 45\%$
$0 < Al_2O_3 < 11\%$
$0 < Na_2O < 20\%$
$0 < CaF_2 < 20\%$

An interpolation formula has been derived for the parameters ln A and B as a function of the **mole fraction** of the constituents. They used a Weymann temperature relationship:

$\ln(\eta) = \ln A + \ln T + B / T$
$\ln A = -19.81 - 35.75\ Al_2O_3 + 1.73\ CaO + 5.82\ CaF_2 + 7.02\ Na_2O$
$B = 31140 + 68833\ Al_2O_3 - 23896\ CaO - 46351\ CaF_2 - 39519\ Na_2O.$

This formula can be extended to slag containing small amounts of MgO and MnO, by considering the sum (CaO + MgO + MnO) instead of CaO alone. It would appear that the major disadvantage of this model might be that it fails to differentiate between the various cations, e.g. MgO on a mole fraction basis is treated as if it were CaO.

Koyama et al [1987] measured viscosity in the SiO_2 - Al_2O_3 - CaO - CaF_2 - Na_2O - Li_2O system. A viscosity equation was derived from analysis of 483 data points relating the composition to the viscosity of the powder system.

$\ln \eta = \ln A + B / T$
$\ln A = -0.242\ Al_2O_3 - 0.061\ CaO - 0.121\ MgO + 0.063\ CaF_2 - 0.19\ Na_2O - 4.8160$
$B = -92.59\ SiO_2 + 283.186\ Al_2O_3 - 165.635\ CaO - 413.646\ CaF_2 - 455.103\ LiO_2 + 29012.564$
Where all the components are accounted as **mole %** and T = temperature (K).

For a discussion on the accuracy of the models (compared to actual measured values), refer to the discussion in section 5.2.3.

3.2. Effect of alumina on crystallisation

The following discussion will attempt to provide an overview of the situation of phase change of a casting powder upon cooling as it is currently found in the literature. The reason for this is to show what the latest experimental work in the world is aiming at in order to establish a sensible way of describing crystallisation, since at this time there is no standard technique for its evaluation. The result of this could be to present crystallisation data alongside solidification data in such a manner that it will give a clearer understanding of what the true slag characteristics is progressively down the mould length. After this the specific influence of alumina increase will be discussed as it affects crystallisation.

3.2.1. Presenting crystallisation in a usable form

Crystallisation in the mould occurs in a matter of tens of seconds as the slag moves through the mould. The cooling rate of a powder initially on top of the molten steel surface (at 1550°C) moving down the mould at 1m/min (with the steel shell) to the bottom of the mould (at 1150°C) is around 7°C/s. Kashiwaya et al [1998b] referred to work done by Ho & Thomas [1992] who estimated actual cooling rates between the steel shell and the mould of a continuous caster to range from less than 1°C per second to 20°C per second depending upon position in the mould. It is difficult to present crystallisation in a sensible manner for these high cooling rates. The most accurate way will be to present data in the form of a Continuous Cooling Transformation (CCT) diagram and/or with a Time Temperature Transformation (TTT) diagram. A short description of and motivation for the techniques to obtain these diagrams will now follow.

Quantification of mould slag solidification phenomena is normally conducted using differential thermal analysis (DTA) or slag casting in a chill mould: however, these techniques are limited as there is no direct observation of the solidification phenomena and only effects which liberate significant quantities of heat can be measured. The DTA technique records the temperature lag (or advance) when a specimen undergoes an endothermic (or exothermic) transformation upon being heated (or cooled) at a fixed rate. Crystallisation gives an exothermic peak. In DTA, the powder and alumina (reference) are placed in identical crucibles in a furnace. The temperature difference between the sample and the reference is monitored continuously, as the furnace is heated at a fixed rate. Any thermal event, such as a transformation, is revealed as a departure from the base line. The highest temperature associated with an exothermic peak gives the temperature of crystallisation (T_c). In general, a higher 'Crystallisation Temperature' is related to a higher fraction of crystalline phase in the mould slag layer between the mould and the strand. However, a unique criterion to establish the cooling rate of the sample has not been established in these studies and only a few studies have considered the effect of cooling rate on crystallisation behaviour [Watanabe et al, 1996; Sakai et al, 1997] and even fewer attempted to construct TTT or CCT diagrams [Sakai et al, 1997]. Furthermore, the term 'Crystallisation Temperature' is sometimes confused with the so-called 'Solidification Temperature' of the slag which is determined from viscosity tests where a rapid rate of viscosity increase with decreasing temperature is incorrectly used as an indication of the onset of crystallisation within the slag.

Another technique that is frequently employed to determine the crystallisation behaviour of a mould slag consists of melting the mould slag sample before quenching in a metallic mould [Hering et al, 1992; Sakai et al, 1997]. After quenching, the sample can be inspected at room temperature by different techniques. For example, the proportion of crystalline and glassy phases can be evaluated using microscopy, and X-Ray diffraction can determine the crystalline phase present. Another method consisted of fusion of the slag sample in a high temperature microscope and observation if its behaviour during cooling [Kishi et al, 1987]. The temperature at which the slag lost transparency was considered to be the crystallisation temperature. Obviously, these methods are useful to define a 'crystallisation index' which compares, qualitatively, the tendency of different slag to give glassy or crystalline phases; however, these indices do not provide a quantitative measurement that can characterise the slag behaviour in the mould.

To properly characterise the precipitation of a second solid phase from a liquid, it is necessary to define the thermal field, phase diagram and the nucleation and growth behaviour of the solid. In mould slags, that are liquid oxides and easily transform to a glass at high cooling rates, it is necessary to be able to describe the conditions under which glass transformation is possible. These include conditions for the initiation of solidification, the crystal morphology, chemistry and growth rate and the time evolution of the fraction of solid. Knowing these at different cooling rates are important in the determination of the effect of crystallisation of the slag on heat transfer and rheology. Thus a technique, whereby the thermal field can be determined as the solidification process is observed, was developed by Kashiwaya et al [1998a; 1998b]. This technique combines the hot thermocouple technique with video observation and image analysis that allows crystal growth rates, morphologies and solidification fractions to be determined under defined thermal conditions.

3.2.2. The influence of alumina on crystallisation

The absorption of alumina will tend to make the slag glassier since it increases the polymerisation and commandeers cations for charge balancing (As discussed in Section 3.1.2). Thus the increase in alumina content during the casting sequence results in the formation of glassier slag toward the end of the cast.

Kim et al [1992] found that an increase of 10 mass percentage alumina decreased the crystallisation temperature of the studied slag by approximately 60°C. It must be noted that what he termed 'Crystallisation Temperature' has been defined as the solidification temperature of the slag in this discussion. However, it is expected that an increase in alumina content will work to decrease both the solidification temperature (as Kim et al [1992] found) and the crystallisation temperature. No information could be found in literature about the effect of increasing alumina content at different cooling rates on the crystallisation temperature.

4. Experimental Procedure

Three separate areas of the behaviour of casting powders were experimentally investigated in order to evaluate their performance in practice when their alumina content increases.

4.1. Measurement of Alumina increase

The aim of the data collected was to clarify two areas of alumina increase in practical continuous casting:

I) To determine true practical levels of alumina increase in modern clean steel manufacture. Put more distinctly, what alumina values different powders attain under different casting conditions.

II) To investigate the time taken to reach this upper alumina value.

Samples of different commercial casting powders were gathered. The names of the powders and the chemical analyses as provided by the manufacturers are given in table 4.1. The analyses provided were normalised to a carbon-free basis.

Table 4.1: Chemical analyses of casting powders studied (Mass percentages).

Powder name	**SiO_2**	**CaO**	**MgO**	**Al_2O_3**	**Na_2O**	**K_2O**	**Li_2O**	**Fe_2O_3**	**F**
Scorliat SPH-401/PS2	40.1	33	1.49	5.7	9.39	0.82	-	1.88	7.23
Teemix HS 15G	41.48	37.3	6.5	1.96	3.48	-	-	0.42	8.83
Teemix CNS-15NE	41.4	41.2	-	6.82	7.87	-	-	2.7	5.37
Accutherm STC 89	34.9	30.8	1.78	5.36	12.7	0.9	-	2	10
Accutherm STSP-232-BA	37.6	37.6	0.72	5.88	8.04	0.12	0.96	1.32	6.24

4.1.1. Sample collection

Samples were collected from the moulds of the V2 and V1 continuous casting machines at ISCOR Vanderbijlpark. At timed intervals of between 5 and 10 minutes during a sequence cast, small samples were collected from the same position in the mould (Between the SEN and the narrow face of the mould). Sampling continued across ladle changes as long as circumstances allowed safety and continuity. Casting conditions and possible irregularities were noted to aid data interpretation.

Sampling was done by means of a small (6mm outside diameter * 150mm length) silica tube that was designed with a thin part at the bottom. The tube was under vacuum and was therefore able

to aspirate some of the molten powder as soon as the thinner bottom part melted. The tube was held in position for sampling with a simple steel arm that held the tube at the end by means of an elastic. The thin bottom part of the tube was pushed through the unmelted and sintered powder layers into the molten powder layer where melting of the thin part of the tube occurred within a second or two.

4.1.2. Sample analyses

Energy Dispersive X-Ray analyses (EDX), also called Energy Dispersive Spectrometry (EDS) was performed on all the samples for chemical analyses by means of a JEOL 5800 LV scanning electron microscope fitted with a NOKAN EDS Voyager 4 detector. An acceleration voltage of 25 kV and an analysis time of 100 seconds were used throughout the experiments.

To establish the validity and accuracy of this technique to obtain chemical analyses of the samples from the mould, the following questions need to be addressed.

- Does the silica in the tube used for measurements react with the molten powder during sampling?

To test this, the silicon content was monitored over the width of a cross section of the tube with powder inside. The silicon content analysed assumed the value of silicon in the bulk of the casting slag directly next to the silica tube surface. No reaction of the silica tube with the casting slag was found. The reason for this is due to the quenching of the powder as it enters the tube. All of the slag that was aspirated into the tube quenched as glass. Since glass breaks into smooth surfaces, samples were not polished, but only mounted and coated with carbon by means of an E6000 BIO RAD Carbon-damper machine. Carbon coating was performed to ensure electrical conductivity of the sample and prevent it from charging, due to the electrons it was bombarded with in the electron microscope when the sample was visually assessed with secondary electrons.

- Is EDX representative of the true analysis of the sample?

As already mentioned, the powder samples obtained quenched as glass and not as the stable crystalline phases. This implies that the composition will not vary with crystal phases and will be more homogeneous. Furthermore, five measurements were made at different positions in the sample to test for homogeneity and a confidence interval was obtained to evaluate the data gathered. The lowest possible magnification was used (100*) in order to analyse as large a surface as possible.

- What is the effect of the different oxidation states that elements may be present in?

Since the aim of this experiment was only to monitor the alumina contents of the casting slag (the molten casting powder can also be referred to as the casting slag or slag) as it changes with time, oxidation states of minor elements (like Fe and Ti) do not play a role in the results obtained. The chemical analyses retrieved from EDX were compared to the initial constitution of the powder (as provided by the manufacturers) to check validity. Table 4.2 gives a comparison of the manufacturer-supplied analysis and the EDX analysis of the casting powder STC 89 after 40 minutes of casting. The results from EDX compared quite favourably, with lower Fluorine and Sodium values; as would be expected due to vaporisation of especially NaF. Higher alumina values were measured due to alumina inclusion removal by the powder. ISCOR Vanderbijlpark

does not add calcium to modify and facilitate alumina inclusion removal, and hence the CaO value is not expected to increase with that of alumina.

Table 4.2: Chemical analyses determined by EDX and given by manufacturers.

Accutherm STC 89	SiO_2	CaO	MgO	Al_2O_3	Na_2O	K_2O	Fe_2O_3	F
Manufacture details	34.9	30.8	1.78	5.36	12.7	0.9	2	10
EDX analysis	36.7	35.8	1.69	6.2	9.3	0.9	2.2	4.2

4.2. Viscosity measurements

High temperature viscosity measurements are performed with commercial viscometers normally employed for room temperature measurements. These viscometers are mounted on top of a furnace and employ a modified extended "arm" to position the spindle used by the viscosity meter within the furnace where the specimen is heated. High temperature viscosity measurements are well established and quite common around the world, but remain in lack of a standardisation or calibration technique. There are many laboratories measuring viscosity, but results differ greatly from one to another (as is evident from Figure 4.1). Values of viscosity at high temperatures (1400°C to 1200°C) provided with casting powders are often a function of the laboratory where it is tested.

4.2.1. Apparatus employed

4.2.1.1. Viscometer

A Brookfield Programmable DVII+ Viscometer with electronic display was utilised in the determining of the casting powder viscosity. The concentric cylinder method was employed where a fluid (molten casting powder) is contained in the annular gap between the two cylinders (sample crucible and the spindle). The spindle is rotated at constant speed, the fluid rotates and a torque is transmitted to the spindle. Viscosity is calculated from the measured torsional resistance. (Viscosity is the measure of the internal friction of a fluid. The friction becomes apparent when a layer of liquid is made to move in relation to another layer. The greater the friction, the greater the amount of force required to cause this movement). The following equations apply to cylindrical spindles only:

Shear rate (sec^{-1}): $$S = \frac{2\omega R_c^2 R_b^2}{X^2(R_c^2 - R_b^2)} \qquad \mathbf{1}$$

Shear stress ($dyne/cm^2$): $$F = \frac{M}{2\pi R_b^2 L} \qquad \mathbf{2}$$

Viscosity (Poise): $$\eta = \frac{F}{S} \qquad \mathbf{3}$$

The integrated version of equations 1 - 3, with the torque as constant, gives the viscosity relationship as follows:

$$\eta = \left(\frac{M}{8\pi^2 \omega L}\right) * \left(\frac{1}{R_b^{\,2}} - \frac{1}{R_c^{\,2}}\right) \qquad 4$$

The above equation applies to infinitely long cylinders and it is normal practice to calibrate viscometers with viscosity reference materials. Viscosities are usually calculated by the equation given below:

$$\eta = \frac{D}{G} \qquad 5$$

Where: ω = angular velocity of spindle
R_c = radius of crucible
R_b = radius of spindle
X = radius at which shear rate is being calculated
M = torque input by instrument
L = effective length of spindle
D = scale deflection of the viscometer
G = apparatus constant determined by calibration experiments

Calibration of the meter using the special molybdenum spindle can be performed at room temperature with the aid of standard viscosity oils that have viscosities in the range of typical casting powders. In order to use the spindle in the tube furnace used to heat the sample, the spindle must be made of carbon, molybdenum or platinum. Molybdenum was employed since platinum is too expensive and carbon proves to yield vastly varying results from run to run [Mills & Machingawata, 1991]. During a study conducted by NPL (National Physics Laboratory in England) on a global scale, it was found that carbon that reacts with the melt was responsible for the data variation.

In order to establish the accuracy of the viscosity data obtained at high temperatures in the furnace, a program launched by NPL was joined to evaluate the same slag data with some of the most respected laboratories in the world. Viscosities of two synthetic reference slags were measured one year apart and sent away for comparison to the other laboratories. The results received appear to be valid and consistent, as shown in Figure 4.1.

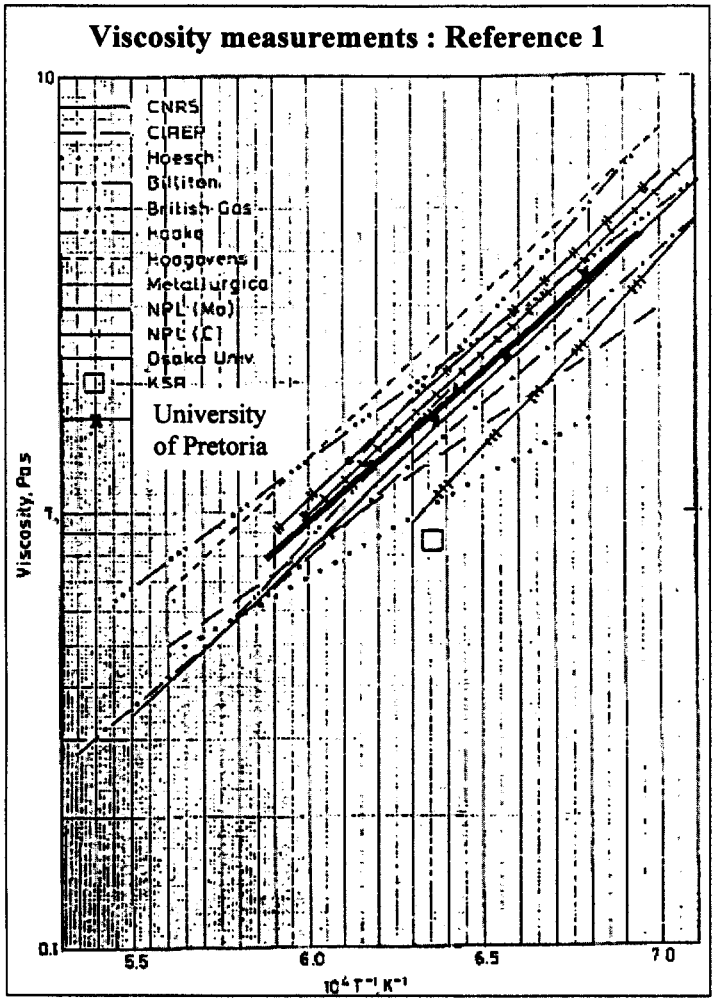

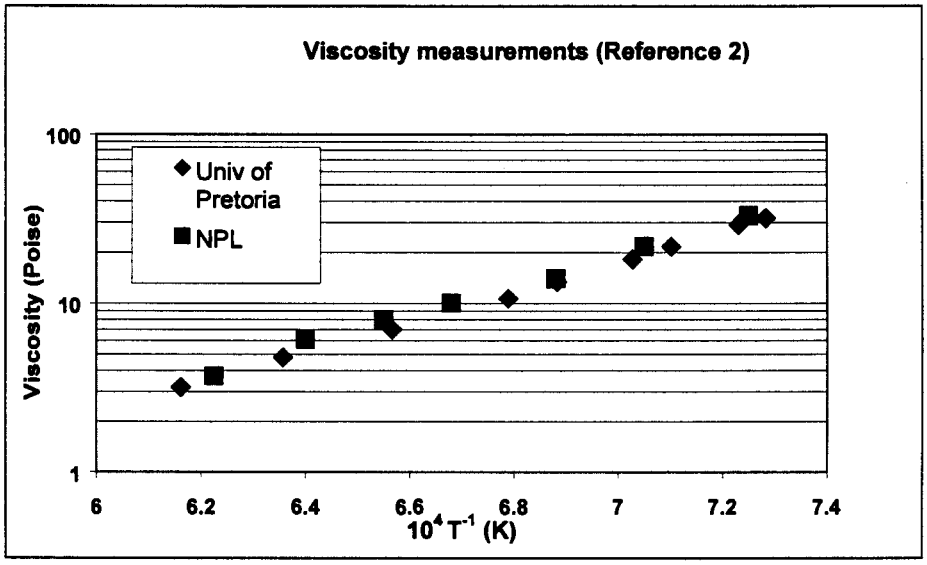

Figure 4.1: Results from two global round robins launched a year apart indicating accuracy of the calibrated viscosity meter [Mills, 1991b].

4.2.1.2. Furnace

A vertical tube furnace with fourteen silicon carbide elements (that can heat the furnace to 1500°C) and an alumina tube with an outside diameter of 70mm that fits through the furnace were used to heat the sample. Figure 4.2 shows a photo of the viscosity meter mounted on top of the furnace. Figure 4.3 shows a sectional drawing of the furnace to illustrate the mounting of the sample and the position of the spindle and thermocouple.

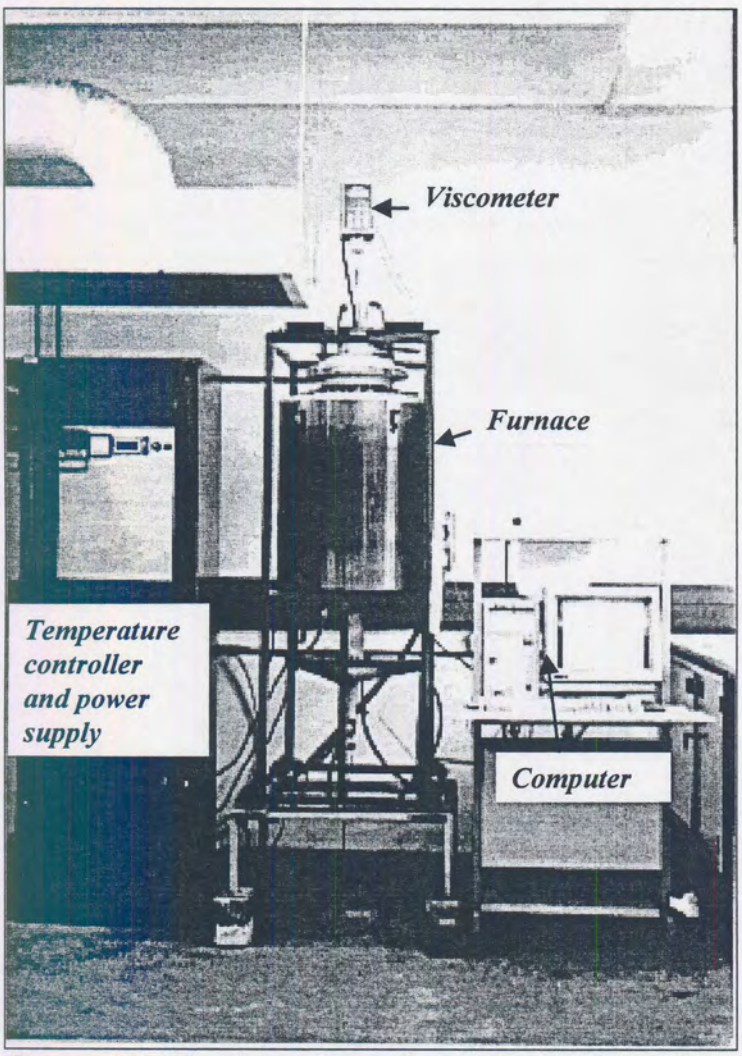

Figure 4.2: The photo shows the viscometer (on top) and the furnace employed in the viscosity measurements.

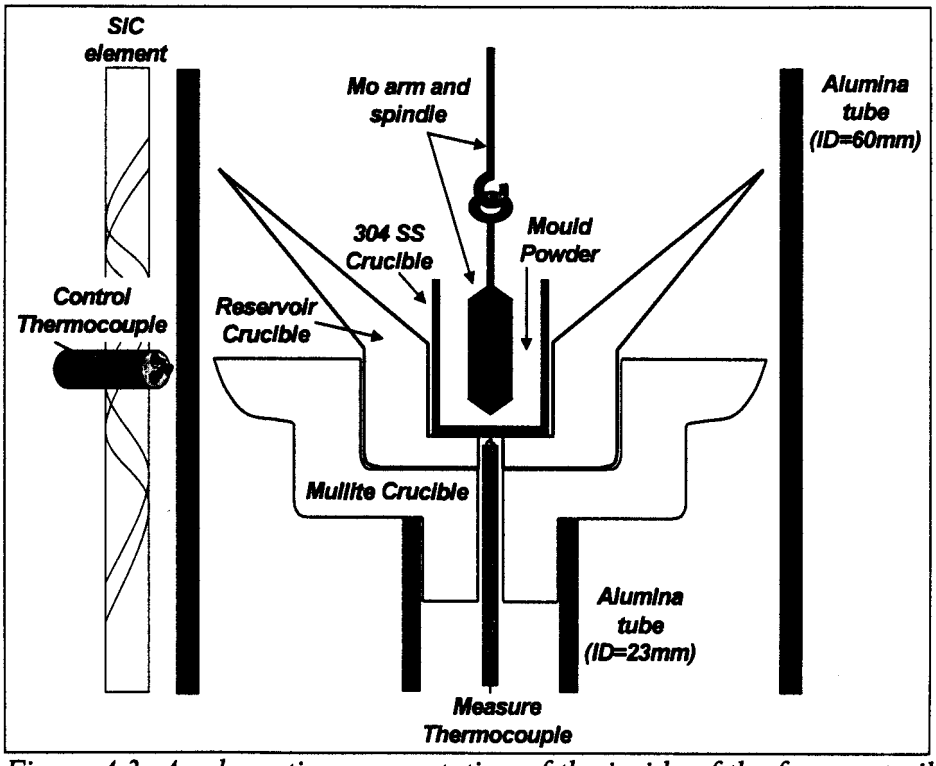

Figure 4.3: A schematic representation of the inside of the furnace to illustrate the mounting of the sample and position of the spindle and thermocouple.

Simple description of constituents of furnace

The ends of the alumina tube fitting through the furnace were sealed with water-cooled copper heads. Through a small hole in the top copper head the spindle extension hung and the crucible support extended through the bottom copper head.

The crucible used to contain the casting slag sample was machined out of 304 stainless steel. The crucible had an outside diameter of 32mm, an inside diameter of 28mm and was 60mm high. This crucible was supported on an alumina tube (with outside diameter of 26 mm) passing through the bottom copper head. Fitting into this tube was placed a mullite crucible holder. Fitting into this again was a calcium oxide – alumina based crucible holder for the purpose of acting as a reservoir for slag that crept out of the stainless steel crucible. On occasion slag crept out of the stainless steel crucible due to surface tension effects during the final cooling of the sample. It was discovered that the slag crept during the final cooling at low temperatures just before freezing during a run in which the reservoir crucible had not yet been employed. In this case, the thermocouple was exposed to the slag that crept out of the sample crucible and ceased working properly.

Temperature measurements

The furnace is controlled by an S-type thermocouple that is situated between the elements. This temperature will not be representative of the true temperature of the sample at a given moment. For this reason another S-type thermocouple was situated right beneath the crucible that contained the sample. The thermocouple was enclosed in an alumina sheath (outside diameter of 4 mm) that fitted in the smaller alumina tube sticking through the bottom copper head. The

thermocouple tip passed through both the crucible holders and was situated right under the stainless steel crucible (as shown in Figure 4.3). In this way the time for the crucible to reach a steady-state temperature could be determined more precisely. The steady-state temperature of the crucible was measured at 33°C lower than the temperature of the furnace at the furnace thermocouple position for the entire temperature range studied. During the cooling intervals this temperature difference was smaller depending on the rate of cooling. The hot zone length of the furnace was defined as the length in which the temperature was measured within ± 1°C of the set control temperature and was determined beforehand as 6 centimetres.

Gas atmosphere

Since the spindle and its extension from the viscosity meter were made of molybdenum, and the sample crucible was made from 304 stainless steel, the oxygen partial pressure in the furnace had to be kept at low levels. Above the top copper head was a small chamber with an argon gas feed (shown in Figure 4.4). Gas flow rates for the small gas compartment above the top copper head was in the order of 0.02 litres per minute. This design prevented air from entering the furnace through the hole for the spindle in the top copper head.

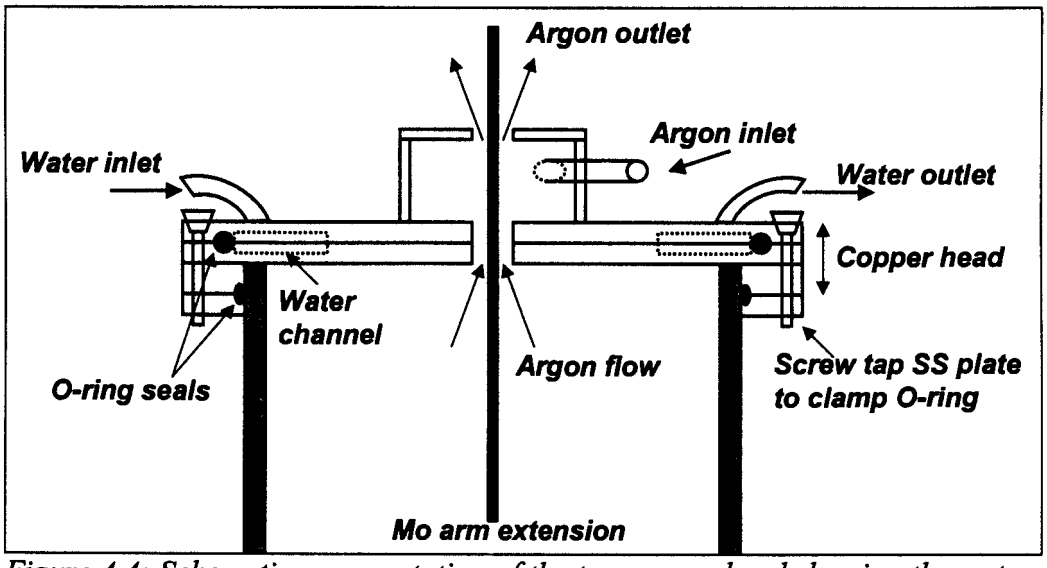

Figure 4.4: Schematic representation of the top copper head showing the water cooling channel and the gas compartment on top.

Argon gas was also blown through the furnace tube at rates of 2 litres per minute. The gas entered at two places in the lower copper head and escaped through the hole for the spindle in the top copper head (shown in figure 4.5).

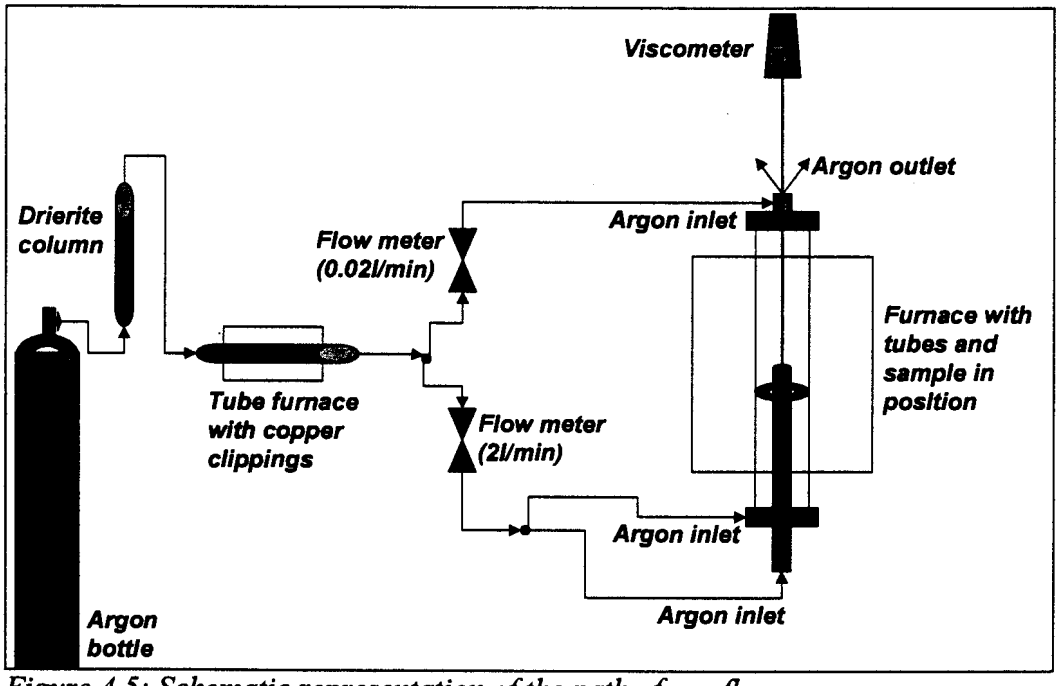

Figure 4.5: Schematic representation of the path of gas flow.

The argon gas was purified in respect to oxygen and water content to aid in keeping the oxygen partial pressure low. The argon gas passed through a Drierite tube (outside diameter 35mm, length 350mm filled with drierite) at room temperature to strip the gas of water before it entered the furnace. The drierite used was self-indicating by changing colour from blue to pink when it did react with water.
The argon gas then passed through a tube furnace that contained copper fillings in a silica tube (outside diameter 40mm, length 300mm in the tube furnace) at 600°C. At 600°C any oxygen in the argon gas passing through the tube will react with the copper to form CuO. The copper that oxidised to CuO can easily be observed by its dull appearance in contrast to the metallic lustre of the copper fillings. The CuO can be regenerated (reduced) to copper by hydrogen gas passing through the silica tube at 200°C.

4.2.2. Sample preparation

Samples used in viscosity experiments were prepared by mixing different amounts of pure Al_2O_3 powder with a commercial casting powder. Only two powders were chosen to perform the study on. Stollberg in Germany produces them both; Accutherm STC 89 is designed for casting low carbon steels, and Accutherm STSP-232-BA is designed for casting medium carbon steels. The manufacturer's analyses are given in table 3.3. The analysis for powder CNS-10b-2E is included since its viscosity-temperature relationship is given in Figure 5.8 to demonstrate the breakpoint temperature effect.

Table 4.3: Chemical analysis of casting powders used in viscosity measurements.

Powder name	*SiO_2*	*CaO*	*MgO*	*Al_2O_3*	*Na_2O*	*K_2O*	*Li_2O*	*Fe_2O_3*	*F*
CNS-10b-2E	33	36.6	0.88	6.57	12.9	0.3	-	2.18	7.3
Accutherm STC 89	34.9	30.8	1.78	5.36	12.7	0.9	-	2	10
Accutherm STSP-232-BA	37.57	37.57	0.72	5.88	8.04	0.12	0.96	1.32	6.24

About 70 grams of the casting powder was heated in a muffle furnace to 600°C and left for 10 hours to burn off all the carbon that is contained in the powder. This practice of decarburisation is performed before viscosity measurements in order to allow the carbon sufficient time to oxidise, ensuring that the carbon will not be entrapped in the powder during melting and influence measurements. After decarburisation the powder had a white appearance, whereas it was black/grey before. The decarburised powder was then milled in a "rock and roll" machine in order to allow effective compacting of the powder in the stainless steel crucible.
Between 1 and 15 mass percentage Al_2O_3 powder was added to the decarburised casting powder sample. After thorough mixing 60 gram of the sample was compacted into the 304 stainless steel crucible.

After viscosity measurements were taken in the furnace, the crucible was sectioned longitudinally. One half was removed as a solid chunk and glued unto a flat rod of Perspex with quick set resin. After this it was coated with carbon in order to ensure electric conductivity as EDX analyses were performed in an electron microscope (refer to section 4.2.4.1). The other half of the sample was removed from the piece of crucible and crushed in a "rock and roll" mill in order to perform X-Ray analyses on the sample (refer to section 4.2.4.2).

4.2.3. Description of test performed

The furnace was heated at the rate of 100°C per hour from room temperature to 1400°C and controlled there for two hours. The viscosity of the sample was measured at this temperature and re-measured after ten minutes in order to test for attainment of steady-state temperature within the sample. After this the furnace was cooled at 50°C per half an hour and left for 20 minutes after each 50°C decrease to reach steady-state. The viscosity was measured for three different spindle rotation speeds (within the viscosity range) at temperature decrements of 50°C until 1200°C were reached. (Experimental tests together with data from the thermocouple at the base of the sample crucible confirmed a stable and even temperature of the sample in the crucible after fifteen minutes at the specific temperature.) As the slag was cooled down further, the 50°C measurements were continually made at three different spindle speeds, but only together with a continuous monitoring of the sample at a single spindle rotation speed as it cooled down. By these continuous measurements the viscosity of the sample could be tracked more carefully (along with the thermocouple situated at the base of the 304 crucible) for any abrupt slope change in the viscosity to temperature data, which would be indicative of a breakpoint temperature or possible crystallisation.

Newtonian behaviour of a liquid means that the viscosity of a liquid is not a function of the shear rate (speed at which the spindle in the liquid rotates). A non-Newtonian fluid is broadly defined

as one for which the relationship F/S (described in equation 3, section 4.2.1.1) is not a constant. For a non-Newtonian fluid the experimental parameters of viscometer model, spindle and speed all have an effect on the measured viscosity. This measured viscosity is called the "apparent viscosity" of the fluid and is accurate only when explicit experimental parameters are furnished and adhered to. Non-Newtonian flow is probably of mechanical origin [Brookfield, 1996]. As solid objects pass by each other, as happens during flow, their shape, size, and cohesiveness will determine how much force is required to move them. At another rate of shear, the alignment of the objects may be different and more or less force may be required to maintain motion. The solid objects can be large molecules, colloidal particles or suspended materials such as crystals. This behaviour is common to some slags, especially when partial solidification starts in the sample and crystals are present in the sample [Brookfield, 1996]. Dilatant non-Newtonian behaviour means an increase in viscosity with an increase in shear rate. The casting slags studied displayed dilatant behaviour at lower temperatures. This is commonly observed in fluids containing high levels of solids.

The first temperature (encountered during one of the 50°C decrements) where the slag displayed non-Newtonian behaviour was sought, if such a definite point existed. This was done to test the idea that the temperature where non-Newtonian behaviour of the slag begins to be noticed might be an indication of the temperature where crystals start to form in the sample. This of course will only hold if crystals form in a narrow temperature range. Obtaining such a temperature proved to be ineffective due to a gradual change in the flow behaviour.

Viscosity measurements were stopped when the viscosity of the sample reached 30 Poise. The spindle was then lifted out of the crucible. Two experimental viscosity runs were performed up to 120 Poise to check for non-Newtonian behaviour and possibly a break point temperature. Where these higher viscosity measurements were done (lower temperatures), the sample had to be heated again to 1350°C in order to lift the spindle from the sample. After the spindle was lifted from the sample, the furnace was programmed to cool down at 100°C per hour to room temperature.

During the cooling of a single run, the temperature that the thermocouple at the bottom of the sample crucible measures, was plotted against time for a fixed furnace cooling rate of 80°C per hour from 1400°C to room temperature. The idea was to test whether the crystallisation of the sample would register as an arrest in the cooling curve. Due to the size and thermal inertia of the system no such observation could be made.

4.2.4. True sample analyses

Due to high temperatures in the furnace during viscosity measurements, fluoride evaporation takes place, especially in the form of NaF. In addition, nominal analyses provided by the powder manufacturers are not necessarily accurate due to variations from batch to batch of the casting powder. For these reasons the true sample analyses of the slag in the crucible were essential to efficiently test the viscosity models that use the actual composition of the slag, and to know the true amount of alumina increase in the casting slag. Actual sample composition was also needed to evaluate the stable crystal phases forming during cooling to room temperature, since the Na_2O and Al_2O_3 contents of the slag primarily control crystallisation.

4.2.4.1. Energy dispersive X-Ray analyses

Energy Dispersive X-Ray analysis (EDX), also called Energy Dispersive Spectrometry (EDS) was performed by means of a JEOL 5800 LV scanning electron microscope fitted with a NOKAN EDS Voyager 4 detector. The acceleration voltage was 25kV and the analysis time was 100 seconds. The same composition analysis method was employed as with the mould samples, but with some adaptations, which are justified below.

The casting slag from the furnace cools slowly enough for the stable mineral phase(s) to precipitate. The result is that areas of different composition exist within the sample.

- Is EDX representative of the true analyses of the sample?

Eight measurements were made at different positions in the sample to calculate a confidence interval over the areas analysed. The lowest possible magnification was used (100*) in order to analyse as large as surface as possible. Crystals appeared to have a very fine grain size (in the order of 60 μm) when imaged with back-scattered electrons. The confidence interval (as %) of the data for calcium (the element that analysed with the least consistency – refer to section 5.2.1.1) was typically ± 5%.

X-Ray Fluorescence Analysis (XRF) was performed with an ARL8420 XRF model on two of the samples from the furnace to compare with data from the EDX. Fluorine was regarded as the unanalysed element required summing the XRF analyses to a hundred percent, as well as accounting for the loss on ignition (since no other volatile specie was present and fluorine cannot be analysed by the XRF). Data obtained from the XRF fell within the range of the confidence interval from EDX data, supporting the accuracy of the EDX analyses.

4.2.4.2. X-Ray diffraction (XRD) analyses

As the alumina content of the slag increases during casting, it is expected that the equilibrium mineral phase that precipitates will also change. This in turn can have implications for the temperature at which crystals precipitate and on lubrication in the mould, as suggested in a paper by Hering et al [1992]. In order to test the suitability and relevance of data published by Hering et al [1992] on the stable mineral phase (as the stable phase is influenced by Al_2O_3 and Na_2O content), mineral phase analyses were performed by XRD. Half of every sample coming from the furnace after viscosity measurements was crushed in a "rock and roll" mill and subsequently taken for XRD analyses. XRD tests were done on a SIEMENS D501 X-Ray Diffractometer with a secondary monocromator. $Cu_{k\alpha}$ radiation was used with a 2θ of 3 – 70°, a step width of 0.05° (2θ) at 1.5 seconds/ step.

4.3. Crystallisation

The hot thermocouple technique was evaluated to study the temperature of crystallisation. A thermocouple heater was developed with some unique modifications to measure the exothermic crystallisation reaction temperature. The data obtained from these original experiments provided

useful information that highlights the idea that studying crystallisation behaviour of mould powders relies on both thermal and visual information.

Chapter 5 (Results and Discussion) provides the reason for using quench data experiments together with the hot thermocouple technique. The experimental procedure discussion will first elaborate on the hot thermocouple technique employed (section 4.3.1). Following this, quench data experiments will be discussed (section 4.3.2).

4.3.1. Hot Thermocouple Technique and apparatus used

A unique technique was developed in this study for the rapid determination of the temperature of crystallisation of casting powders. The technique used in this study utilises some of the features of the Hot Thermocouple Technique (as discussed in Chapter 3, section 3.1.1) to determine crystallisation temperatures, but is distinctly different in some ways.

4.3.1.1. Apparatus employed

Apparatus: Hot Thermocouple Driver
The hot thermocouple driver is a system that enables simultaneous measurement of temperature while a thermocouple is heated. Figure 4.6 illustrates the principle of the hot thermocouple controller. The electric current is rectified into a chopped direct current (DC) signal so that the heating cycle occurs for a time as to keep the desired temperature at the thermocouple. After the heating cycle occurs, there follows a period with no current input when the thermal EMF of the thermocouple can be sampled using a measure-and-hold circuit.

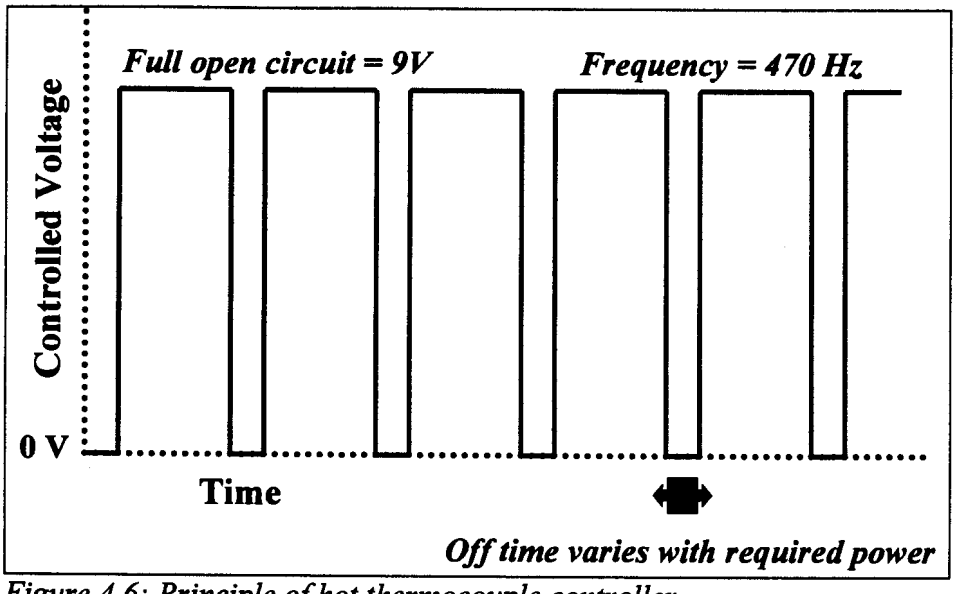

Figure 4.6: Principle of hot thermocouple controller.

The chopped DC signal is supplied to the thermocouple at a frequency of 470 Hz. An analogue PID controller controlled the width of each pulse. The PID controller served to maintain the thermal EMF signal from the control thermocouple at a set value, which was supplied by the computer. The maximum open circuit voltage was 9 Volt and the minimum off time was 0.5 ms.

Electrical noise experienced by the circuit was in the order of 4°C on the control thermocouple (that also manifested in the temperatures measured by the measure thermocouple). Heating and cooling rates in excess of 300°C/s could easily be achieved. The casting powders were heated at 250°C/s and cooled at between 0.5°C/s and 30°C/s for crystallisation measurements.

Apparatus: Thermocouples

In essence, the technique makes use of two thermocouples simultaneously. One thermocouple controls the temperature of the wire through the hot thermocouple driver circuit discussed above. The other measures the true temperature of the sample, as shown in Figure 4.7.

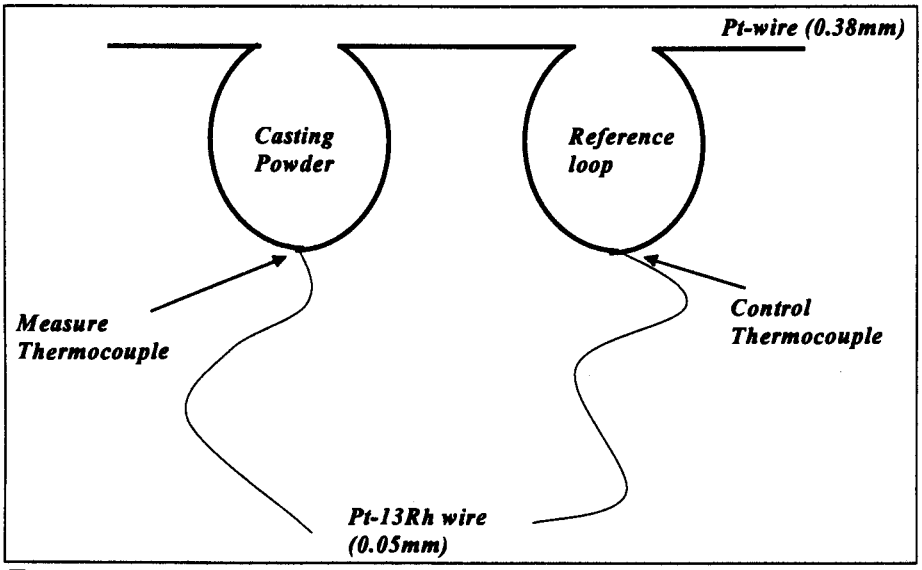

Figure 4.7: Schematic representation of the two thermocouples used in the heating wire of the sample.

The thermocouples shown in Figure 4.7 are of type R and consist of a 0.38 mm diameter pure platinum wire to contain the sample (represented by the thicker wire) and a 0.05 mm diameter platinum-13 rhodium wire (represented by the thinner wire). The loop indicated by 'casting powder' represents the area where the casting powder sample is melted and its true temperature is measured by the 'measure thermocouple'. The control thermocouple is situated in a loop represented by 'Reference' to give similar radiative heat loss to the casting powder loop. This allows the temperature measured by the measure thermocouple to be close to that of the control thermocouple. Nonetheless, the temperature is controlled only at the position in the control thermocouple where the wires touch, while the temperature along the rest of the wire has a gradient relative to the cooled contact points. The practical implication of this is that the temperature measured in the measure thermocouple may be up to 200°C less, due to the radiation and thermal inertia of the casting powder in the measure thermocouple loop. For this reason it is difficult to program the control thermocouple temperature in order to obtain the desired temperature for the casting slag in the measure thermocouple loop. To restrict the temperature difference between the loops and promote predictability of the measure thermocouple temperature, both loops need to be similarly (consistently) positioned between the water-cooled contact points (see Figure 4.8) and have a similar geometry.

The open ends of the thermocouples had to be controlled at room temperature. In the case of the thin Pt-13Rh wire this was easily achieved because of the small heat conduction capacity of the wire. The connection of the wire to the circuit was simply placed at least 5cm from the thermocouple's closed end. In the case of the thicker Pt wire that can transfer more heat, 5cm Pt wire length was allowed after which compensation wire for platinum was used to assure the cold connection was sufficiently removed from the closed thermocouple end to be at room temperature. The connection of the Pt-wire to the circuit was done by two crocodile clamps which were water cooled by a continuous water flow through a thin copper tube to which the clamps were soldered (The system is shown in Figure 4.8).

Figure 4.8 is a photo of the two thermocouples as employed in the experiments. It also shows a Perspex box covering the system to minimise airflow over the thermocouples and avoid sudden temperature disturbances.

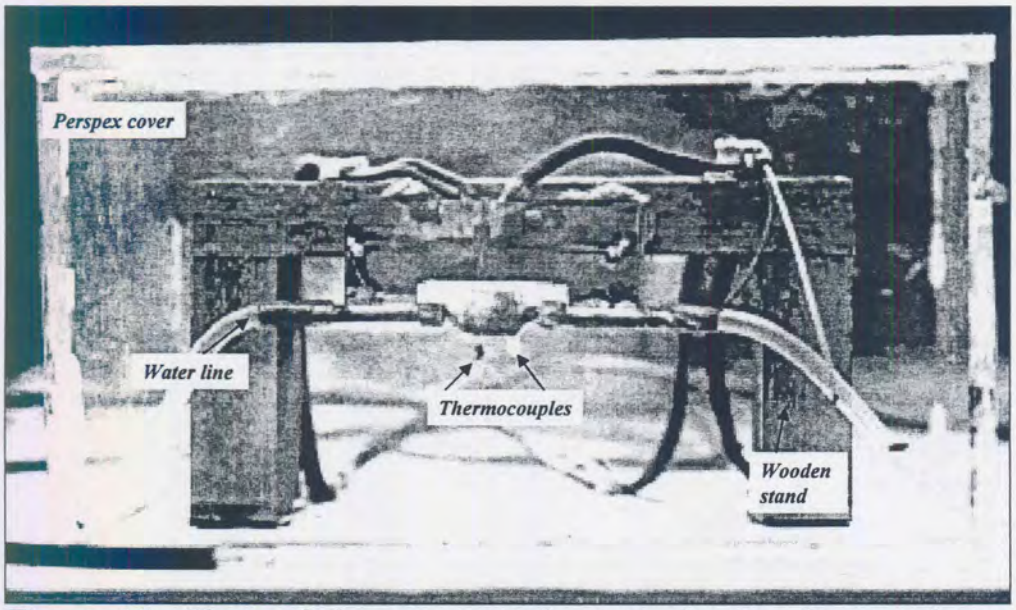

Figure 4.8: Photo of the experimental set-up showing the two thermocouples used for determining the crystallisation temperatures.

Apparatus: Computer

A computer was run with a program written in Turbo Pascal to supply the set value of the sample temperature to the PID controller. In this way the heating and cooling rate of the sample could be specified before each run. The computer both supplied the voltage needed by the hot thermocouple driver and recorded the thermal EMF from the two thermocouples.

Test of accuracy

The technique was tested for accuracy by measuring the crystallisation temperature of a pure component with known thermo-physical properties, such as calcium fluoride (CaF_2). Pure CaF_2 crystallises at 1418°C. Accuracy was determined to be in the order of ± 10°C, as illustrated by the results shown in Figures 4.9 and 4.10. Figure 4.10 shows the influence of the cooling rate on the measured crystallisation temperature of pure CaF_2.

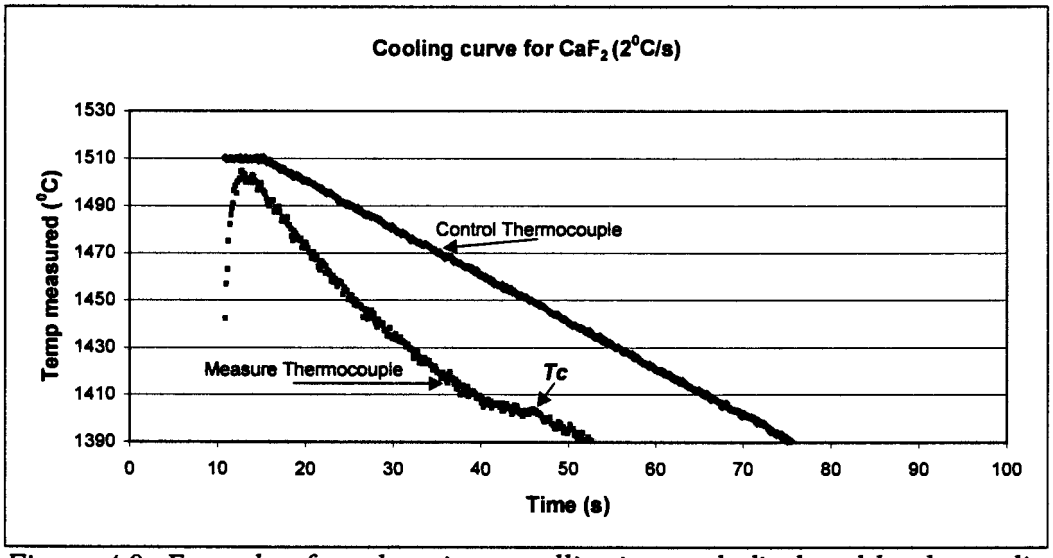

Figure 4.9: Example of exothermic crystallisation peak displayed by the cooling of chemically pure CaF_2 (2°C/s).

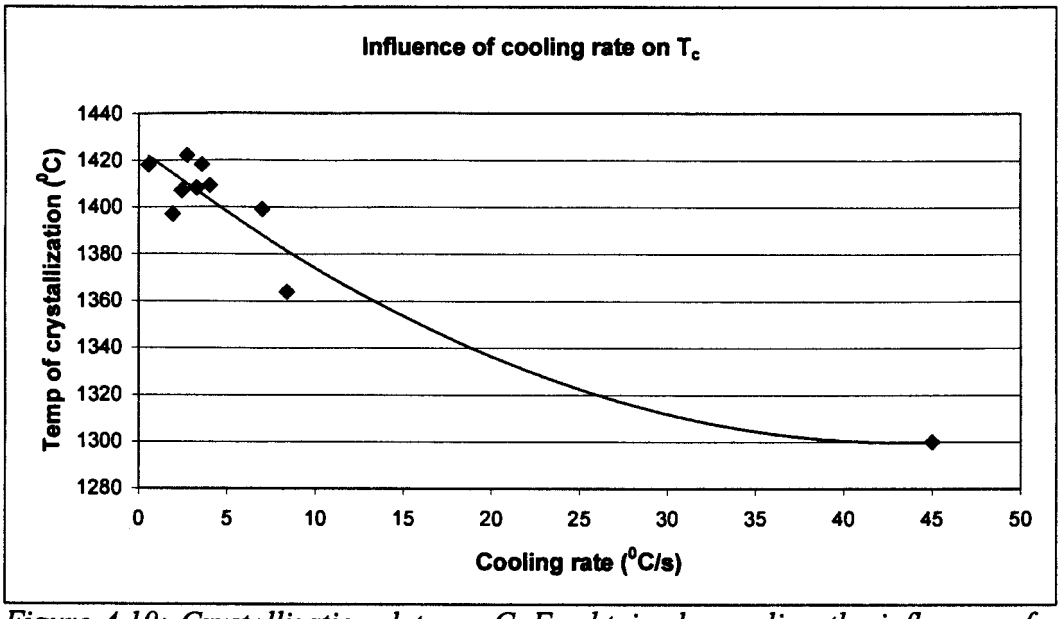

Figure 4.10: Crystallisation data on CaF_2 obtained revealing the influence of cooling rate on crystallisation temperature.

4.3.1.2. Sample preparation

The casting powder was decarburised in a muffle furnace at 600°C for a period of 10 hours. Additions were made to the powder in the form of sodium oxide (Na_2O) and alumina (Al_2O_3). As discussed in chapter 2, section 2.1.3, NaF has a significant vapour pressure at the temperatures attained during the heat cycle, with the result that only trace amounts of Na and F were analysed after a heat cycle was undergone. Na_2O was added to the powder in order to compensate for the sodium (Na) losses as sodium fluoride (NaF) during the thermal cycle in the measure thermocouple loop. The extent of Na and F losses during the heat cycle and the implication for

results obtained are discussed in chapter 5, section 5.3.1. Since Na_2O (together with Al_2O_3) are the principal constituents determining the crystallisation of the sample, Na_2O was added in order to simulate the original composition of the powder and alumina powder was added to simulate the effect of alumina pick-up during casting. Following these additions, the powder was pressed into a pellet and sintered in a muffle furnace at 900°C for 24 hours. The sintering step was done to achieve a more homogeneous composition of the powder since very small samples (2 – 4 milligrams) were loaded into the platinum wire loop for the crystallisation temperature determination. The sintered pill was then crushed in a "rock and roll" mill. After thorough mixing of the powder, acetone was added to a small amount of the powder. Acetone wets the powder enough to keep it in position when the powder is applied to the loop in the thermocouple wire. Acetone quickly evaporates and leaves the powder suspended in the loop. Water is not used because it would bind with the powder and cause the formation of HF during heating.

After the completion of the experiment the small piece of crystallised slag was removed from the thermocouple wire mechanically. First, this crystallised slag was mounted on an aluminium support to be carbon coated and analysed for its composition with EDX. Secondly, this small sample was crushed and XRD was performed on it in order to know the mineral phases present (refer to section 5.3.1).

4.3.1.3. True sample analyses

4.3.1.3.1. Energy Dispersive X-Ray analyses

The samples coming from the thermocouple were exposed to temperatures in the range of 1400°C. Losses of Na, K, Ca, F, occur during the heat cycle. In order to establish the influence of these losses and the true Al_2O_3 and Na_2O content of the sample, EDX analyses were performed on the sample. A sample of the size as was studied with the thermocouple technique, is complex to analyse accurately, due to its limited surface area. The danger exists that the portion of the surface analysed may not be representative of the true average composition, when for instance an area is analysed that crystallised a mineral phase with a fixed composition. It must be noted that the EDX analyses technique (especially given the small size of the sample and the crystalline nature of the sample) provides at best only a rough idea of the true composition of the sample. The small area available for analyses does not provide the opportunity for a better average composition, while several crystal phases may be present in the sample and manifest as a definite composition.

4.3.1.3.1. X-Ray diffraction

X-ray diffraction analyses give an idea of the main crystalline phases present in the sample as the composition changes and different cooling rates are experienced by the same composition. The size of the sample made X-Ray diffraction difficult and sensible data was obtained on only some of the samples.

4.3.2. Quench experiments

This leg of the experimental work was added due to the lack of accurate data obtained from the hot thermocouple technique (because of the wide crystallisation range).

4.3.2.2. Apparatus employed

Hot Thermocouple driver
The thermocouple driver discussed in section 4.3.1.1 was used to simulate classic quenching experiments to visually determine the true extent of crystallisation. Using the thermocouple driver enables the high heating and cooling rates (about 300°C/s) to be utilised for rapid quenching data determination.

Optical microscope
Due to the opaque nature of the crystalline material opposed to the transparent nature of glassy material, visual assessment of the percentage crystalline material present in the sample could be made with the aid of an optical microscope. An optical stereo microscope with a magnification of 16* was used for this purpose.

4.3.2.1. Description of tests performed

The samples used were similar in weight and dimensions as with the hot thermocouple technique for crystallisation temperature determination (refer to section 4.3.1.2). Approximately 2 – 4 milligrams of powder was loaded into the Pt-wire loop and heated within 10 seconds to the Peak Temperature. The peak temperature referred to is defined as the maximum temperature to which the sample is heated and left to require uniformity for different lengths of time (referred to as Time at Peak Temperature). After maintaining the sample at peak temperature for the specified time, it was continuously cooled at a fixed rate to the quench temperature of the experiment. At the quench temperature the electric current was terminated and the sample was allowed to cool. Measurements of the sample-temperature in the Pt-wire loop after the current was cut showed that cooling rates of the order of 300 °C/s were achieved.

Quench data results are affected by a number of experimental variables. Especially four variables in the current experiment affect the results. They are:
i) composition – in this instance only alumina content was varied
ii) Peak Temperature
iii) Time at Peak Temperature
iv) Cooling rate from peak temperature to quench temperature.

Each of these variables was studied separately (while maintaining the other three at constant values).

4.3.2.3. Sample preparation

The same powder was used that was prepared for the experiments in the hot thermocouple driver in section 4.3.1.

After charging the powder in the Pt-wire loop, the sample was allowed to completely crystallise by allowing it to cool at 3°C/s from 1300°C to 800°C. Different heat treatments were performed on the sample only after this step. The initial condition of the sample was therefore 100% crystalline, and the formation of the % glass could be distinguished by the % transparent material

noted under the optical microscope. Each sample was used in only one sequence of cooling treatments, from the lower to the higher temperatures, while the % glass increased accordingly (For example, all things being constant, the quench temperature would be increased at 50°C intervals causing the % crystalline material to decrease). Figure 4.11 schematically shows the heat treatment cycle that the samples were exposed to. After the sample was subjected to the quench temperature equal to the peak temperature, it was removed from the measure thermocouple loop in the wire. The loop in the Pt wire was then loaded with fresh powder, heat treated to obtain 100% crystalline material, and the sequence of heat cycles was repeated. One such a sequence yielded around 5 data points. Every sequence was repeated three times to obtain reproducibility. The % crystalline and glassy material was determined by the optical microscope observation of the ratio of opaque to vitreous area at room temperature, with the sample still suspended in the thermocouple loop.

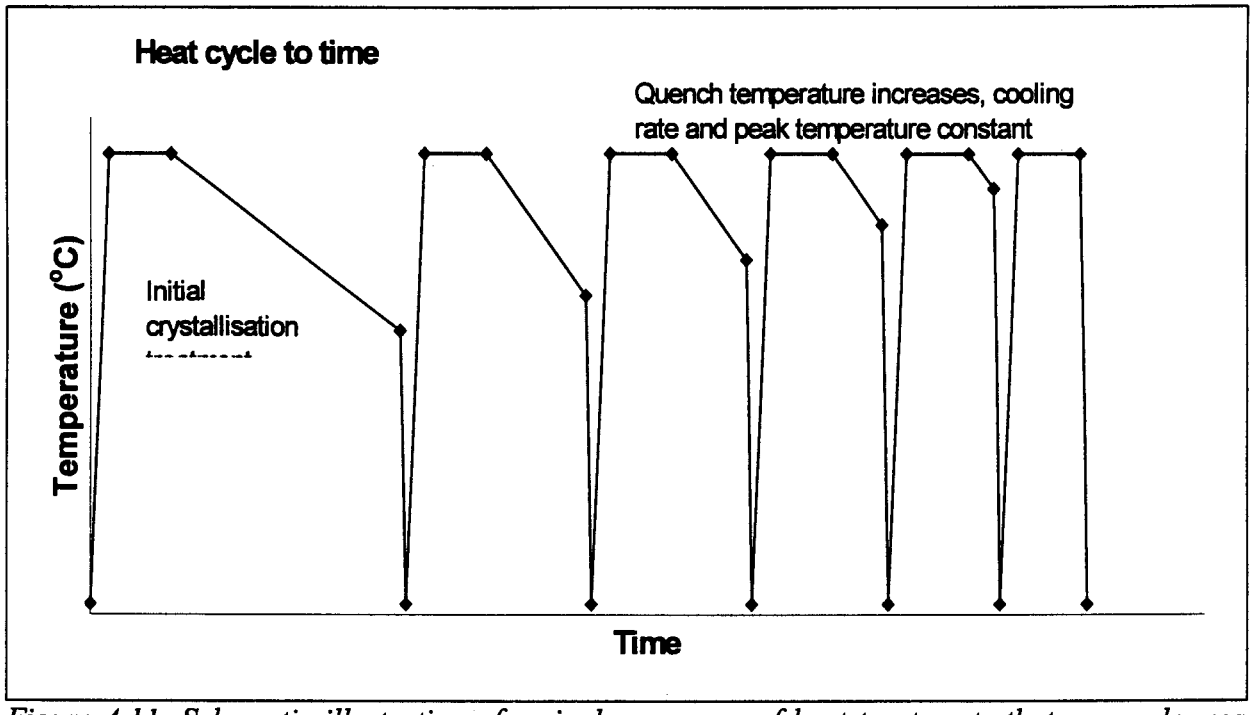

Figure 4.11: Schematic illustration of a single sequence of heat treatments that a sample was exposed to.

4.3.2.4. Sample analyses

Similar analysis techniques as in section 4.3.1.4 were used.

5. Results and discussion

5.1. True increase of alumina

Figure 5.1 is a summary of the alumina increase versus the time for a whole range of different powder types studied (each during a sequence cast). The data shows the trend of reaching a steady state alumina concentration after a certain period of time in accordance with theoretical calculations (see Figure 3.1 in section 3.1.1). With the current casting process under normal operating conditions at ISCOR-Vanderbijlpark, between 2 and 4 mass percentage of alumina is absorbed by the casting powder when casting different grades of aluminium killed steel. The alumina content of the different powders reaches the steady-state value within the first ladle of the sequence (the first 40 minutes of casting) and remains constant for the rest of the casting process. The efficiency of casting powder operation in fulfilling its functions must be evaluated at these increased alumina levels.

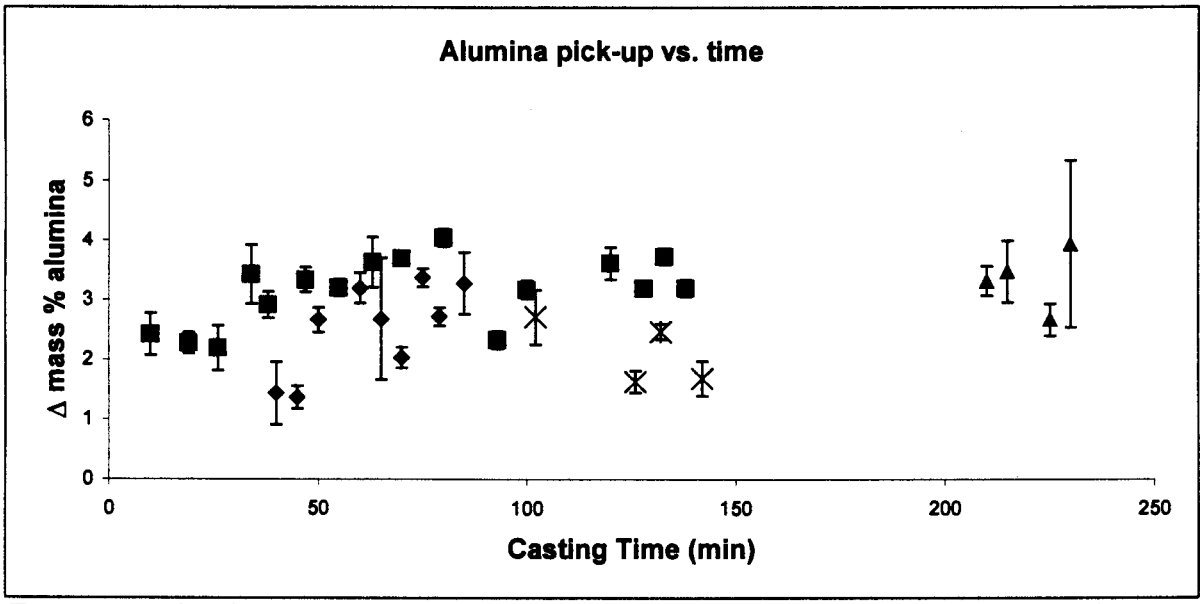

*Figure 5.1: Combined data on the **increase** in alumina content of the powder in four casting sequences (data from each sequence presented by different symbols, with the confidence interval of analyses presented with vertical error bars).*

Figure 5.2 and 5.3 each show data obtained for a single casting sequence. The casting powder STC-89 was used in the current study of the effect of alumina on viscosity. It appears from Figure 5.2 that about 3.5 mass % alumina was absorbed by the casting powder. The effect of this increase will be discussed with the aid of measured viscosity data in section 5.2.

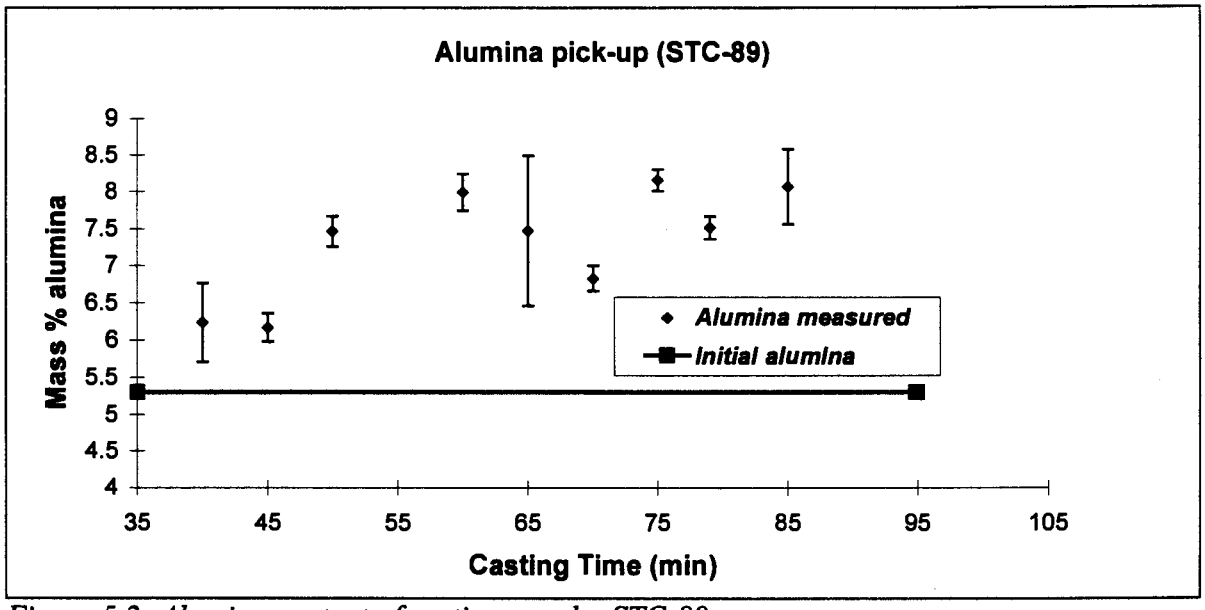

Figure 5.2: Alumina content of casting powder STC-89.

Figure 5.3 shows the decrease in alumina content of the powder as a new powder type was used for the casting of a different steel grade during a sequence cast. In order to keep the continuity of the casting sequence, medium carbon steel was cast directly after the low carbon steel; this being the reason for the powder change. During this powder change most of the "old" casting slag was scooped out of the mould prior to replacement with the new powder that was used. (It is not necessary to scoop off the old casting powder, and in some cases the new powder is simply added to the old one, since this causes less disturbance at the meniscus area and assures continuous molten powder supply since there is no delay in waiting for the fresh powder to melt). The effect is clearly seen where the new casting powder with low alumina content is added. As can be seen, the new powder absorbs almost 5% alumina during the twenty minutes recorded. The reasons for this may include:

- the dilution with the previous powder that was left with higher alumina level
- the fact that this change followed in the sixth ladle in the sequence. The question is whether the tundish slag is still removing inclusions at the same rate as on the earlier ladles.
- Since a large amount of fresh powder is added to the mould that still need time to melt, there might be less molten powder available in the meniscus area that could cause poor lubrication and higher alumina levels in the smaller volume of molten flux.

Just before the last sample was taken from the mould, the SEN started clogging. This is indicative of alumina passing through the SEN; in other words before it reaches the casting slag. The source of this alumina might be the poorer function of the tundish slag in absorbing the alumina, a 'dirtier' ladle, alumina clusters coming loose from the shoot nozzle in the tundish, or a combination of all of the above. The only deduction to be made from this observation is the possible dangerous situation resulting from a fresh casting slag with insufficient molten powder to absorb this alumina, and if it can absorb it, to posses adequate viscosity to assure inflow for lubrication.

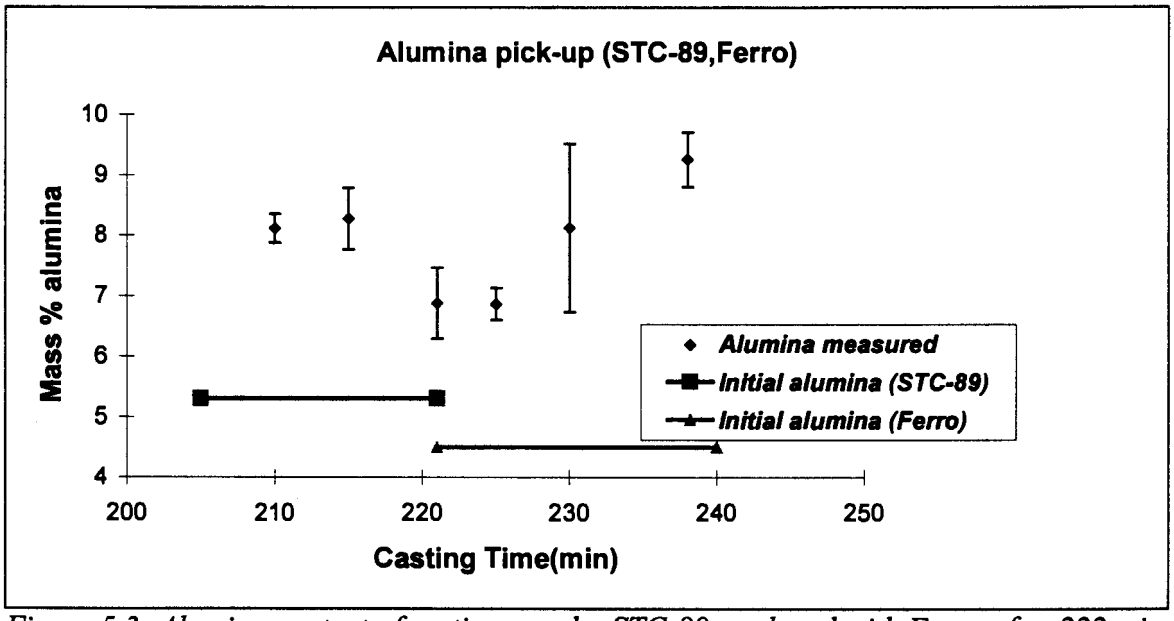

Figure 5.3: Alumina content of casting powder STC-89, replaced with Ferro after 222 minutes of casting.

5.2. Viscosity of mould powders

5.2.1. Composition

5.2.1.1. Composition of samples used in viscosity experiments

Models used for the prediction of viscosity are very sensitive to the composition of the slag. Figure 5.4 and 5.5 graphically show the major constituents (with the confidence interval of analyses) of the two powders used in this study - as analysed by EDX after viscosity measurements. The composition provided by the manufacturer and the alumina additions made to the powder are also shown – composition normalised to 100 mass % (excluding carbon). Table 5.1 and 5.2 provide all the components analysed as used in the evaluation of the viscosity models. Analyses of the casting slag after viscosity measurements revealed that on average about 1.1 mass % of chromium oxide (regarded as Cr_2O_3) and less than 0.1 mass % of nickel oxide (regarded as NiO) was present in the slag due to absorption of these elements from the 304 stainless steel sample crucible. Chromium and Nickel could not be included in the viscosity models since no provision was made for them.
Figure 5.4 and 5.5 show that constituents analysed close to the expected values according to the manufacturers specifications, except CaO for both powder types. (CaO values from the same batch of powder coming from different crucibles after viscosity measurements varied over a 10% range, and were on average considerably higher than manufacture specifications.) CaO values of the same order as reported here were analysed for identical powder types obtained from the mould in section 5.1. Higher CaO values used in the equations will have a noticeable impact on their predicted viscosity. No apparent reason for the somewhat higher CaO values was found, but the analysed values were used in preference in order to compare the predicted viscosity values.

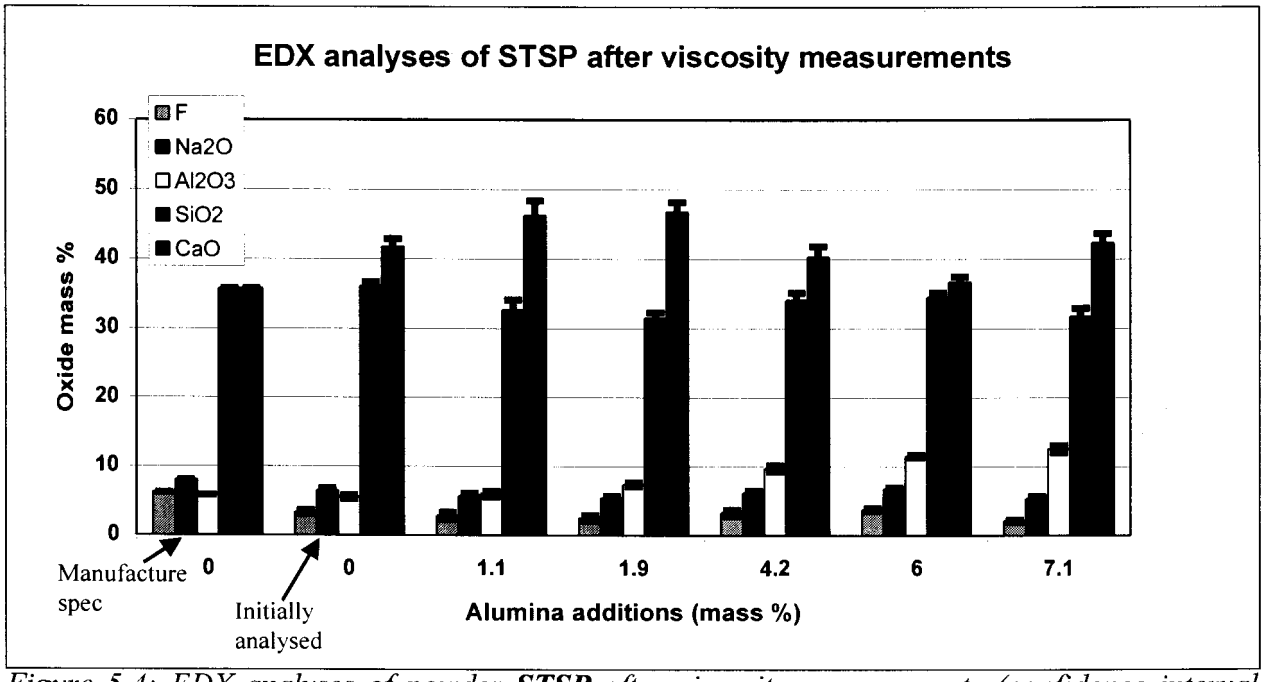

*Figure 5.4: EDX analyses of powder **STSP** after viscosity measurements (confidence interval presented by vertical error bars).*

Table 5.1: EDX analyses of powder STSP after viscosity measurements (mass % alumina added)

	Manufacture spec	**Initial powder**	**0.5%**	**1.9%**	**4.2%**	**6%**	**7.1%**
F	6.24	3.39	2.87	2.52	3.34	3.79	2.17
Na_2O	8.04	6.45	5.70	5.46	6.24	6.78	5.42
MgO	0.72	1.32	0.99	1.01	1.14	1.22	0.88
Al_2O_3	5.88	5.55	6.02	7.42	9.74	11.56	12.60
SiO_2	37.57	36.05	32.66	31.48	34.07	34.52	31.72
K_2O	0.12	0.22	0.24	0.19	0.19	0.27	0.15
CaO	37.57	41.75	46.19	46.74	40.26	36.68	42.26
TiO_2	0	0.21	0.17	0.24	0.19	0.23	0.27
Cr_2O_3	0	1.86	1.83	1.65	1.73	1.18	1.39
MnO	0	0.45	0.59	0.55	0.47	0.23	0.53
Fe_2O_3	1.32	0.47	0.38	0.55	0.36	0.73	0.49
NiO	0	0.05	0.10	0.03	0.11	0.05	0.02
B_2O_3	1.56	1.27	1.28	1.28	1.26	1.26	1.26
Li_2O	0.96	0.78	0.79	0.79	0.78	0.78	0.77

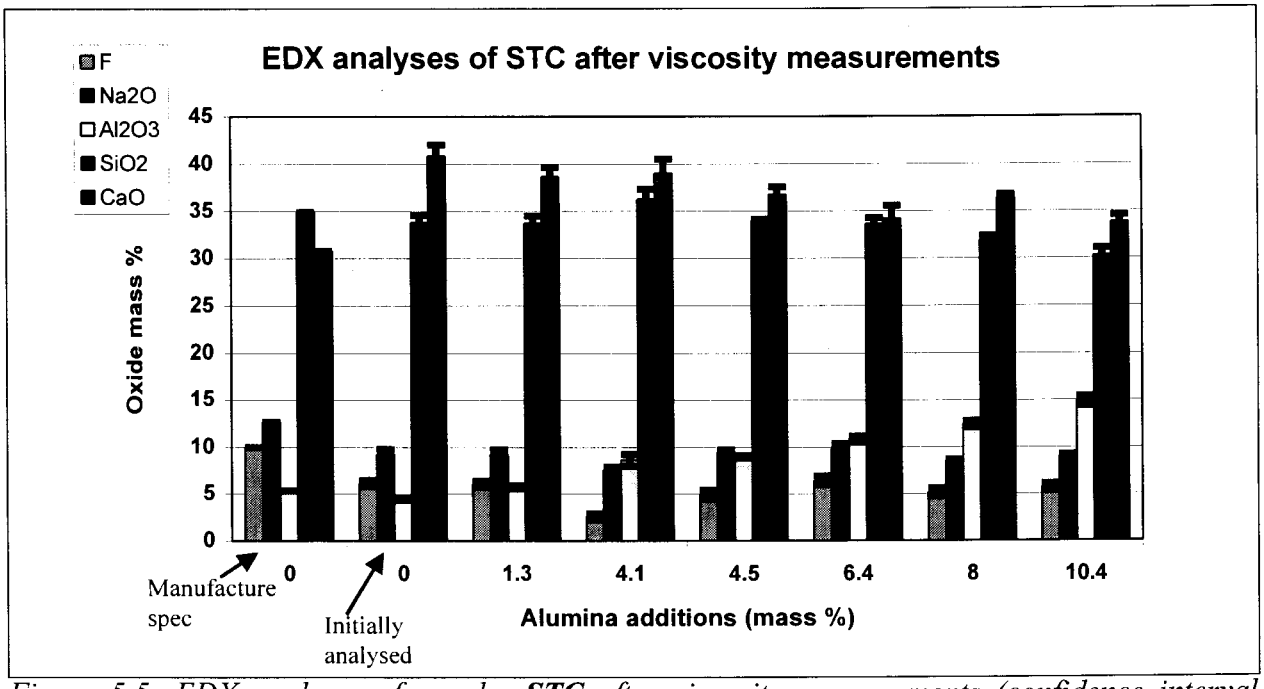

*Figure 5.5: EDX analyses of powder **STC** after viscosity measurements (confidence interval presented by vertical error bars).*

Table 5.2: EDX analyses of powder STC after viscosity measurements (mass % alumina added)

	Manufacture spec	**Initial powder**	**1.3%**	**4.1%**	**4.5%**	**6.4%**	**8%**	**10.4%**
F	10	6.15	6.10	2.60	4.93	6.45	5.16	5.74
Na_2O	12.7	9.28	9.22	7.58	9.44	9.82	8.48	9.01
MgO	1.78	1.55	1.34	1.32	1.55	1.35	1.28	2.78
Al_2O_3	5.36	4.47	5.76	8.60	8.99	10.85	12.46	14.91
SiO_2	34.9	33.82	33.75	36.29	33.97	33.64	31.93	30.23
K_2O	0.9	0.75	0.72	0.82	0.73	0.68	0.66	0.55
CaO	30.8	40.84	38.65	39.01	36.76	34.16	36.39	33.79
TiO_2	0.2	0.43	0.41	0.31	0.38	0.36	0.29	0.48
Cr_2O_3	0	1.71	2.37	1.72	1.87	1.51	1.81	0.96
MnO	0	0.49	0.31	0.24	0.29	0.27	0.52	0.26
Fe_2O_3	2	0.32	0.98	1.30	0.88	0.65	0.80	1.00
NiO	0	0.11	0.22	0.09	0.06	0.08	0.10	0.11

It is necessary to convert the weight fraction of fluorine (as obtained from EDX analysis) to calcium fluoride so that the models can be applied. The method selected here was to:

- Multiply the wt % F by $\left(\frac{78}{38}\right)$ - which is the molar mass of $\left(\frac{CaF_2}{F_2}\right)$
- Subtract 1.47 (wt % F) from the wt % of CaO

5.2.1.2. Composition of samples used in crystallisation experiments

Initially hot thermocouple experiments were performed on the commercial casting powder with only alumina added. EDX analyses of these experimental runs brought to light that all the components report in the analyses in the expected values, but lower values of F and Na were found, since NaF evaporates at the temperatures noted in Table 5.3. EDX analyses of commercial casting powder STSP + 5% alumina added are given in Table 5.3 (the columns with a temperature heading represent the peak temperature the sample experienced during the heat cycle). The analyses of the same powder, coming from viscosity measurements are included for the sake of completeness. The fluorine evaporating from the furnace during viscosity measurements is less than with the hot thermocouple technique. The reason for the high rate of fluoride evaporation measured during experimental runs with the hot thermocouple technique is due to the extremely high area to volume ratio of the sample in the thermocouple loop. EDX analysis of samples from the mould (in section 5.1) showed losses from the viscosity furnace to be of the same order as fluorine losses in the mould (with a smaller area relative to the volume of the sample than the hot thermocouple experiments). After this observation, Na_2O was synthetically added to the powder used in the heated thermocouple runs to compensate for these losses. It is not possible to rectify the loss of F. Loss of K was regarded as negligible, due to the small percentage present in the powder. Quench experiments (shown in Figure 5.23 through Figure 5.26) were all performed with the added Na_2O.

Table 5.3: EDX analyses of powder STSP + 5% alumina added, but no Na_2O added, after both viscosity measurements and hot thermocouple experiments (Indicated temperatures are the peak temperatures experienced by the sample during hot thermocouple experiments)

	Manufacture spec	**Analyses after viscosity experiment**	**1180°C**	**1230°C**	**1420°C**
F	6.24	3.79	0.00	0.08	0.05
Na_2O	8.04	6.78	4.81	4.61	2.39
MgO	0.72	1.22	1.29	1.23	1.14
Al_2O_3	5.88	10.56	11.33	10.78	10.72
SiO_2	35.75	34.52	37.02	38.35	37.88
K_2O	0.12	0.27	0.26	0.12	0.04
CaO	35.75	36.68	41.84	41.65	44.85
Fe_2O_3	1.32	0.73	0.71	0.71	0.85

Due to the small size of the samples used in thermocouple technique and the accompanying difficulty of chemical analyses, EDX analyses were not performed as extensively as with the viscosity samples, but was rather only performed on one sequence of powder coming from the thermocouple loop to ascertain the consistency of the sample chemistry. The Al_2O_3 and Na_2O that had been added to the sample reported reliably in the analysis, while virtually no F was analysed.

5.2.2. Viscosity – experimentally measured

Figure 5.6 and 5.7 show the effect of temperature on viscosity with increasing alumina content for respectively STSP and STC (the two commercial casting powders used in this study – their analyses is given in Table 4.3, section 4.2.2). Alumina increase shows a similar effect on both powder types.

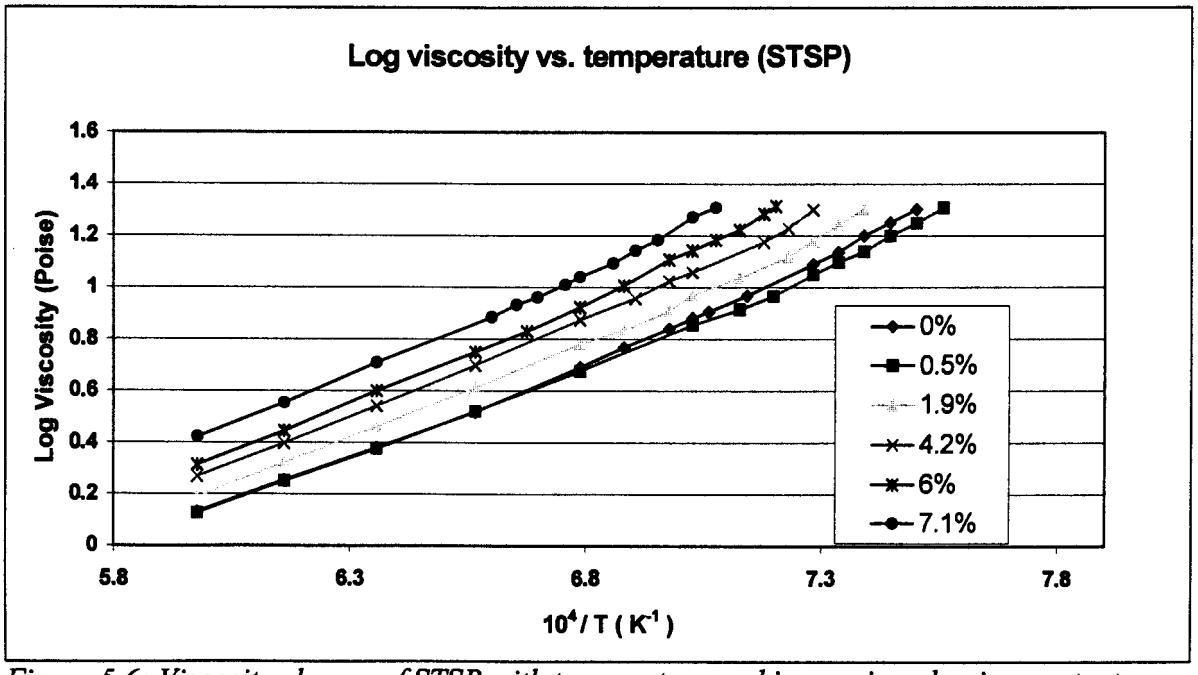

Figure 5.6: Viscosity change of STSP with temperature and increasing alumina content.

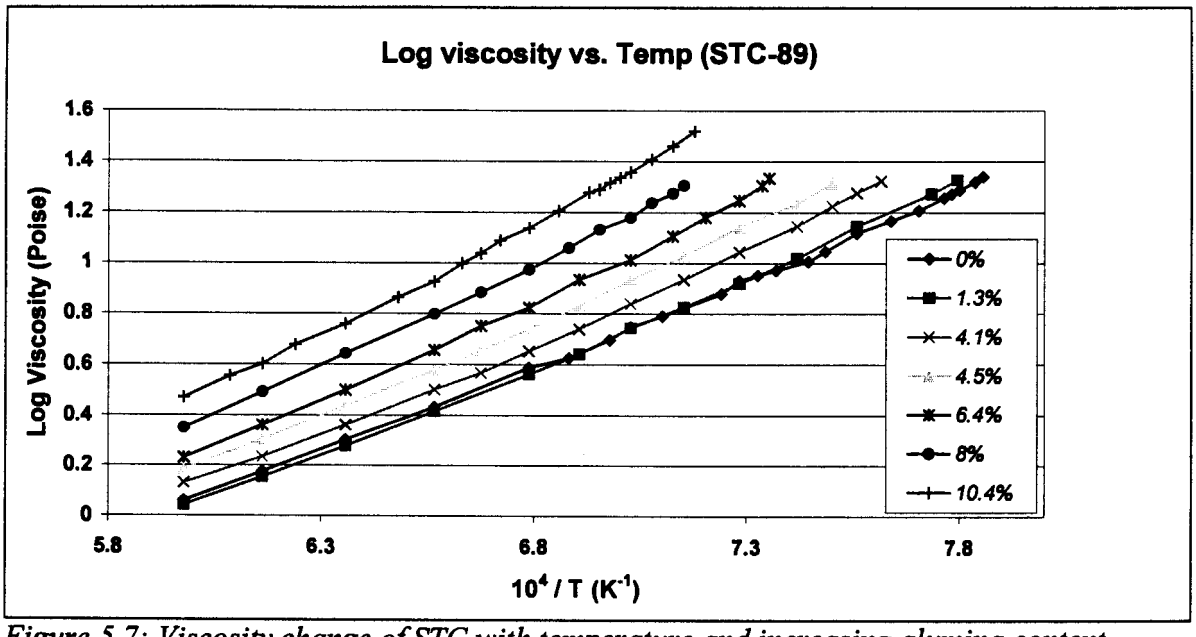

Figure 5.7: Viscosity change of STC with temperature and increasing alumina content.

Non-Newtonian behaviour

When the shear rate is varied in a non-Newtonian fluid, the shear stress does not vary in the same proportion. The viscosity of such fluids will therefore change as the shear rate is varied. The shear rate can be simplified as a function of the rotation speed of the spindle (Equation 1 in section 4.2.1.1).

Some indication of possible non-Newtonian behaviour is visible in Figure 5.8, which shows the temperature dependence of the viscosity to depart from the expected Weymann and Arrhenius relationships, showing positive deviations at lower temperatures (to the right in the graph). The equation coefficients were calculated to give a good fit at the high temperatures by using the least squares technique. With this fitting technique there is no visible difference between the calculated Arrhenius and Weymann equations.

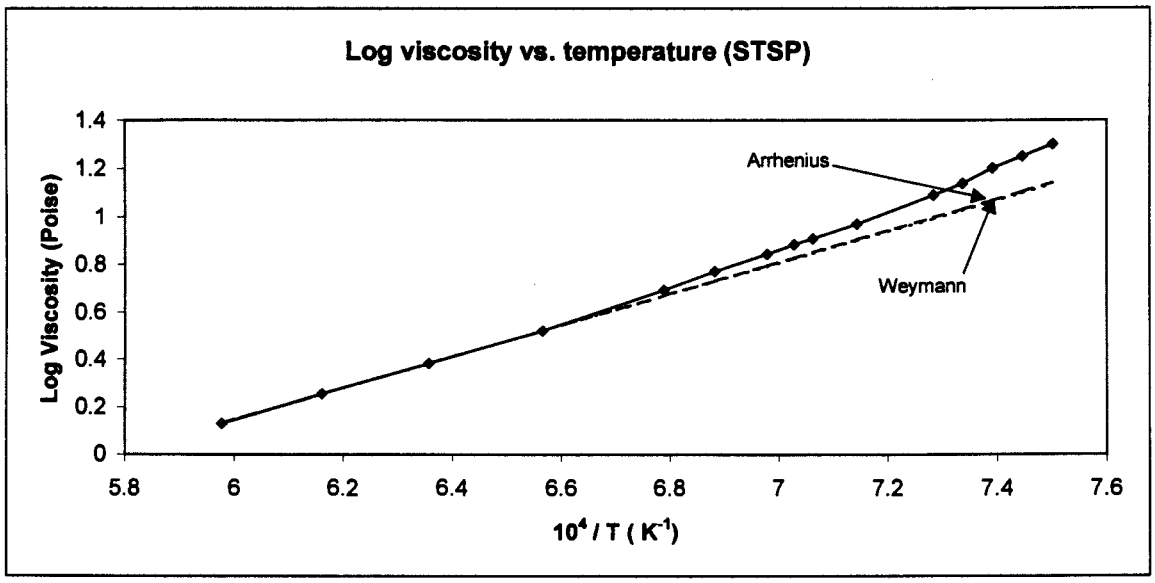

Figure 5.8: Log viscosity (η) vs. 1/T for the powder STSP (with no alumina added). The dotted lines show the results of fitting the higher-temperature data to the Arrhenius and Weymann relationships.

A common method for characterising and quantifying non-Newtonian flow is to calculate the ratio of the fluid viscosity as measured at two different spindle speeds. In constructing the ratio, the viscosity value at the lower speed should be placed as the numerator, the one at the higher speed as the denominator. These measurements are usually made at speeds that differ by a constant factor (for example, 2 and 20 RPM, 10 and 100 RPM, etc.). For dilatant (shear thickening) fluids, the ratio will be less than 1 as the degree of dilatancy increases. Figure 5.9 shows this tendency for the casting powder STSP at low temperatures.

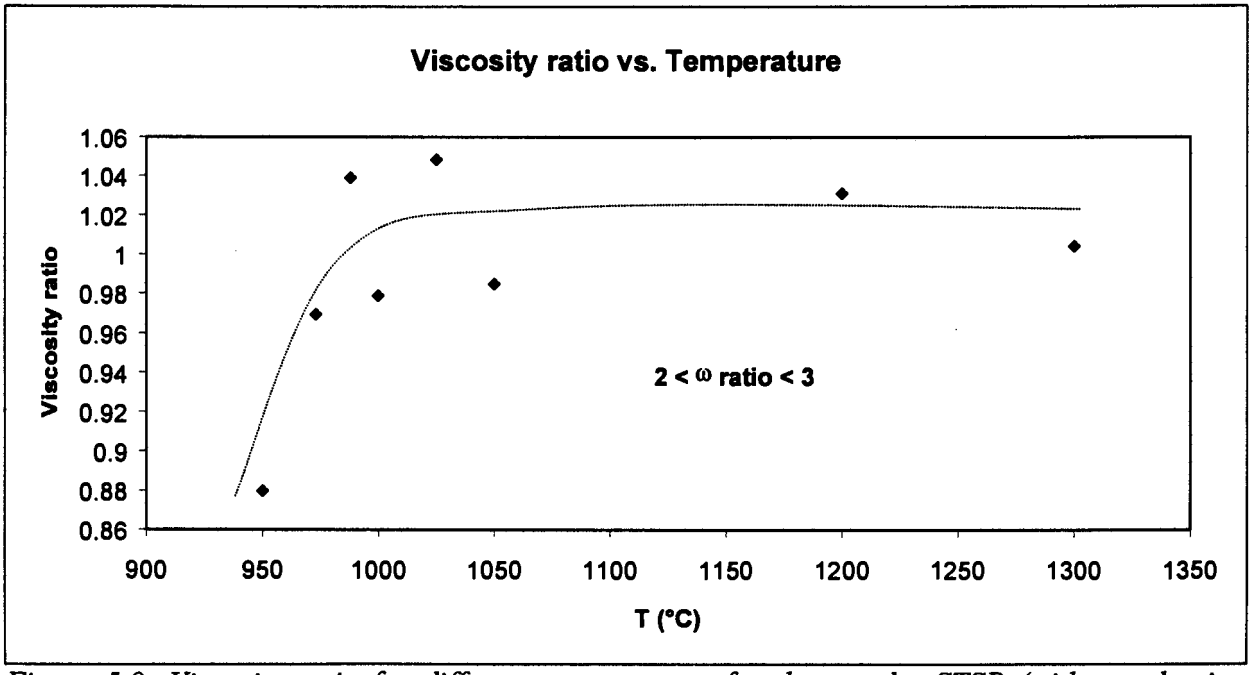

Figure 5.9: Viscosity ratio for different temperatures for the powder STSP (with no alumina added). The dotted line shows the trend of the data at lower temperatures. The ratio of rotation speeds (ω) is between 2 and 3.

The most basic graphic method of analysing non-Newtonian flow is constructing a plot of viscosity vs. spindle rotation speed. Figure 5.10 shows an example of the apparent viscosity increase as the spindle rotation speed increases. This kind of data should preferably be used together with Figure 5.9 (since it does not prove non-Newtonian behaviour by itself; the confidence interval band of viscosity measurements must be taken into account).

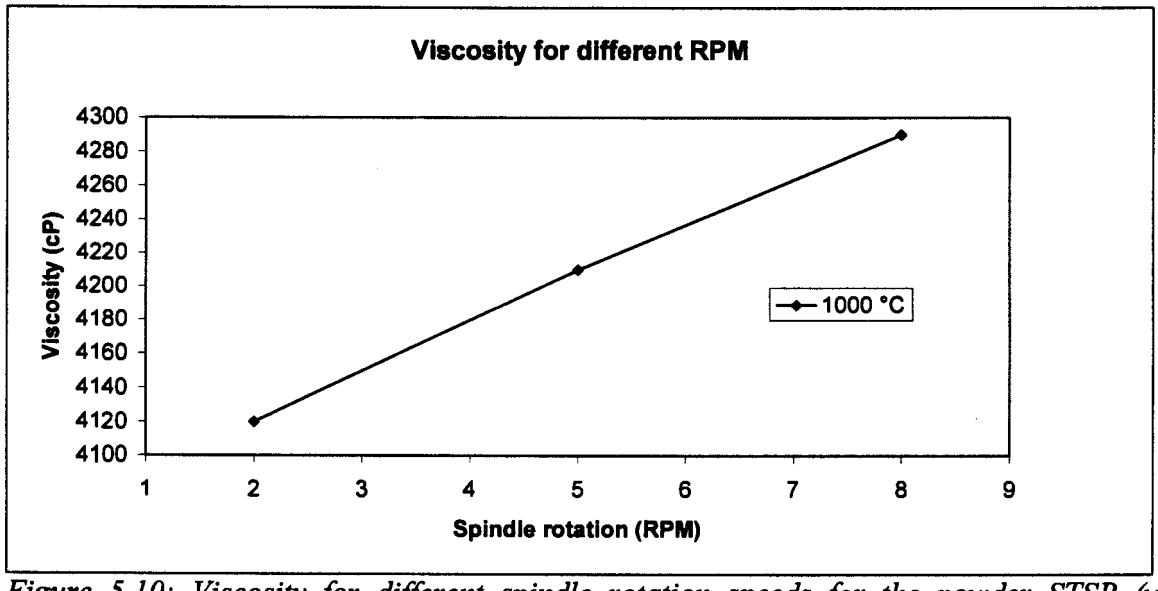

Figure 5.10: Viscosity for different spindle rotation speeds for the powder STSP (with no alumina added). Dilatancy is clearly seen in this single data series, but is not as clear at all temperatures.

The phenomenon of a sharp increase of the viscosity at a certain temperature (Break point temperature) was not found in powder STSP, even for viscosity of up to 100 Poise, as shown in Figure 5.11. STSP is a medium carbon steel grade powder and is designed to crystallise at high temperatures near the meniscus area in the mould (CaO/SiO_2 ratio of 1). CNS has a higher CaO/SiO_2 ratio of 1.11, which favours crystallisation and should yield a highly crystalline slag in the mould area. The existence of a Break point temperature appears to be as variable as viscosity test results and is a function of the laboratory studying the slag. Viscosity measurements were done on three other commercial powder types, of which only one displayed this phenomenon. Figure 5.11 is included only for an example of the phenomenon. Note that powder CNS-10b-2E has an average viscosity lower than that of STSP before this breakpoint temperature is reached at about 1090°C. (The manufacturers quoted this value to be 1140°C).

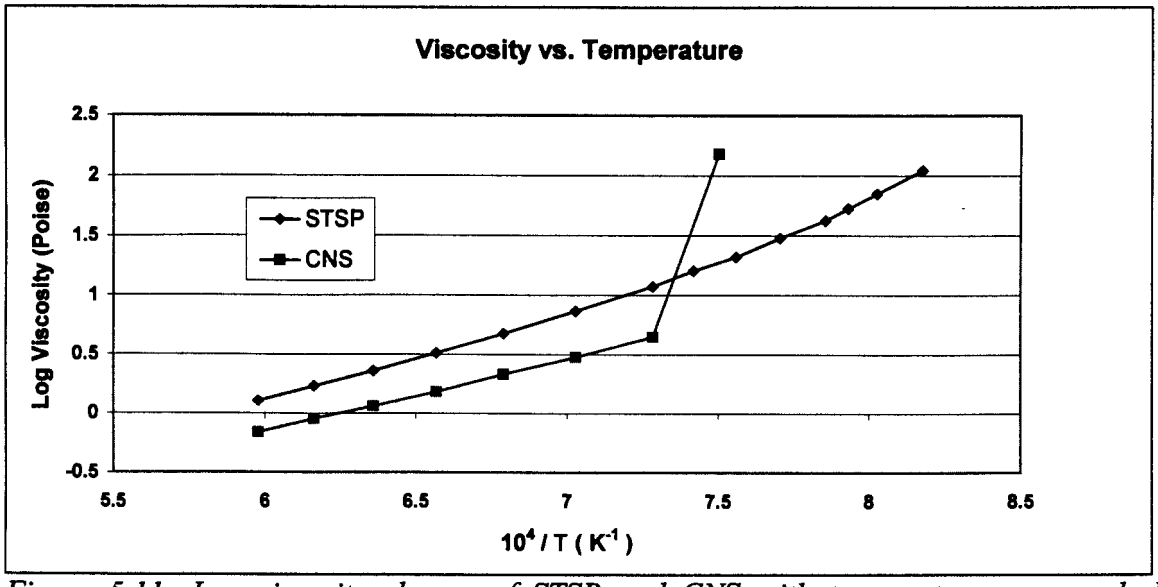

Figure 5.11: Log viscosity change of STSP and CNS with temperature measured showing breakpoint behaviour of powder CNS.

Implication of a 4 mass % increase in alumina content of STC-89

If, as shown in Figure 5.2, a 4 mass % alumina increase occurs during casting, the viscosity of the powder STC-89 at 1300°C will be affected by about 0.3 Poise, a 15 % viscosity increase, and even less at higher temperatures. Anzai et al [1987] conducted a study on the relationship of the pressure and flow rate of the powder film 20mm below the meniscus during the oscillation cycle. They found that, when the powder viscosity reaches around 4 Poise, the pressure distribution reverses and the molten powder flows not down, but up in the mould-strand gap. There is thus a maximum limit to the viscosity of the powder at the meniscus temperature so that the slag can stably infiltrate the mould-strand gap. STC-89 has a viscosity of 2 Poise at 1300°C, which can be regarded as a low viscosity powder, according to present manufacturing practice. If the viscosity is raised to 2.3 Poise by 4 % alumina increase, infiltration will not be affected if the 4 Poise limit of Anzai et al [1987] is taken as measure (The temperature 20mm below the meniscus should be higher than 1300°C, and the viscosity therefore lower. Only at low temperatures less than 1200°C will the viscosity be raised to above 4 Poise with 4 % alumina increase). It is concluded that the

rise in alumina content of the slag will not affect the ability of the casting slag to flow into the mould-strand gap (at around 1500°C).

In the same study, Anzai et al [1987] plotted the effect of viscosity at 1300°C on the oscillation mark depth, as shown in Figure 5.12. If the viscosity rises from 2 Poise to 2.3 Poise, the depth of the oscillation mark increases from 0.9mm to 0.92 mm. If the viscosity is raised to 4 Poise, the oscillation mark depth will be increased from 0.9mm to 1.1mm.

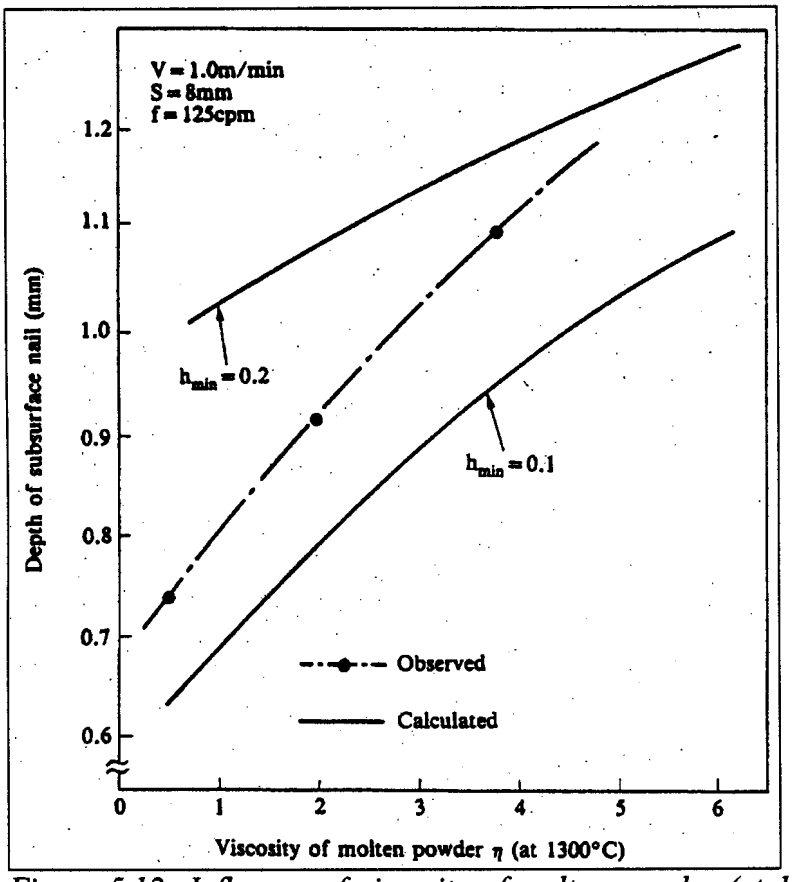

Figure 5.12: Influence of viscosity of molten powder (at 1300°C) on the observed oscillation mark depth [Anzai et al, 1987].

The surface of the steel strand that is in contact with the powder at the bottom of the mould, according to Branion [1987], is calculated to be at around 1150°C. Note that there is no breakpoint temperature measured for powder STC-89, as low as 1025°C, therefore no sudden rise in viscosity is expected in the mould. A viscosity of about 7 Poise is expected at the bottom of the mould at 1150°C if 4% alumina is absorbed (23 % viscosity increase from 5.6 Poise for initial powder at 1150°C), and the bottom of the mould should enjoy liquid lubrication. The impact on the lubrication in the mould due to the viscosity increase can be quantified through the influence on the liquid friction force. If the viscosity is 7 Poise at the bottom of the mould, it is not expected that there would be a partly crystalline mushy zone extending up to the steel strand surface, and by implication no possible solid friction with the steel strand is expected. (The force due to solid friction will be at least an order of magnitude greater than that of liquid friction, according to Branion [1987]). As discussed in section 2.4.1 the liquid frictional force F_{liq} is

composed of the shear stress in the liquid slag film caused by relative motion between the shell and the mould.

$$F_{liq} = \frac{\eta(V_m - V_c)A}{d_l}$$

Where: η = viscosity of the slag film
V_m = velocity of the mould itself (at any given moment, positive or negative)
V_c = casting speed
A = area of the strand mould contact
d_l = thickness of the slag film

It can be seen that viscosity has a linear first order influence, and the liquid friction force experienced at a definite position in the mould will double if the viscosity doubles. This simplification is by no means absolute in its prediction capability and serves only for illustrative purposes since it does not take into account that the thickness of the slag film should increase along with an increase in viscosity. The viscosity increases if 4 mass % alumina is absorbed by between 10% and 25% (as the temperature changes) throughout the mould. If an assumption is made that an average increase in viscosity of 20% exist through the mould when 4% alumina is absorbed, a 20% rise in liquid friction force will be experienced (which should even be less due to the thicker slag film). Since this increase in liquid friction is not expected to be coupled with solid lubrication, the total impact on friction should be of no concern.

Hering & Fenzke [1992] plotted the influence of the viscosity of different casting powders at 1300°C on the integral heat flow density across the broad face of a slab caster (shown in Figure 5.13, for a casting speed of 1 m/min). Figure 5.13 must be understood in the light of the entire slag behaviour in the mould area. The higher heat flux with lower viscosities can be expected from a slag that solidifies (as glass or crystal) at a lower temperature and is not merely the effect of the heat transfer in the mould area where there is only liquid slag present at 1300°C.

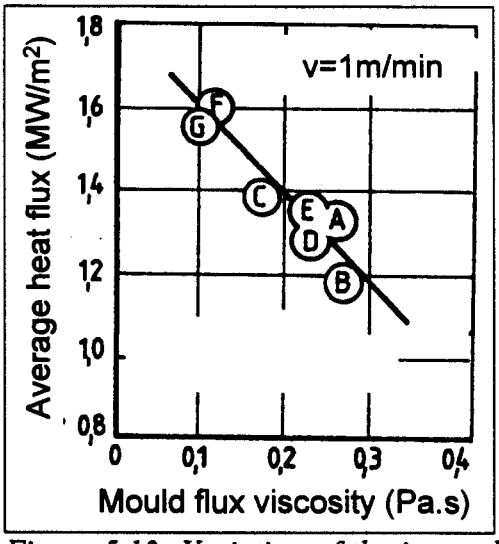

Figure 5.13: Variation of the integral heat flow density in the mould of a slab caster with the viscosity of the casting powder slag. Viscosities were measured with a rotating spindle viscometer at 1300°C and the letters A to G refer to different casting powders [Hering & Fenzke, 1992].

For a 4 mass % alumina increase, the viscosity will be raised from 0.2 to 0.23 Pa.s, and the heat flux (according to Figure 5.13) will only be lowered marginally (by less than 0.1MW/m^2).

Implication of a 10 mass % increase in alumina content of STC-89

Before clean steel practice became as paramount as it is today, alumina increase in casting powders of up to ten percent was common, since alumina was not removed at secondary metallurgy or in the tundish as effectively as today. When problems occur in current casting practice, this same scenario may be encountered; whether it be the aluminium in the steel that re-oxidises, or the alumina formed during de-oxidation that is not effectively removed. An alumina increase of 10% for powder STC-89 at 1300°C will cause a viscosity increase from 2 Poise to 5.7 Poise, a 185% increase. A viscosity of 5.7 Poise at 1300°C is higher than any commercial powder displays today (typical 1300°C viscosity range from 1 to 3 Poise) and poor feeding (especially at higher casting speeds) can be expected, especially if the 4 Poise limit of Anzai et al [1987] is used as measure. STC-89 is a low carbon-steel casting powder and is designed to accommodate sticker-sensitive steel grades by its lowered viscosity with associated excellent infiltration and lubrication. It is clear that the infiltration ability will be severely hampered if 10% alumina is absorbed, and sticking of the steel shell to the mould wall can be expected.

The oscillation mark depth according to the study of Anzai et al [1987] will increase from 0.9mm to 1.2mm, a 33% depth increase, for the viscosity increase from 2 Poise to 5.7 Poise.

At 1150°C the viscosity will have increased from 5.6 Poise to 22.7 Poise, a 305% viscosity increase. The effect on friction experienced by the steel strand may at the same time look completely different than that of a 4% alumina increase. With the slag's viscosity being 22.7 Poise near the exit of the mould next to the steel strand surface, a partly crystalline mushy zone may be present in the slow moving viscous slag. It is even possible that solid lubrication may be

experienced at the bottom of the mould, depending on the heat cycle in that area. To effectively evaluate the extent on the total friction (solid friction + liquid friction) force experience by the steel strand, the effect of the higher viscosity near the bottom of the mould must be considered together with the effect of crystal growth in the slower moving, thin liquid layer.

An alumina increase of 10% for powder STC-89 at 1300°C will cause a viscosity increase from 0.2 Pa.s to 0.57 Pa.s. According to Figure 5.13, the heat flux will be drastically lowered to less than 0.8MW/m^2). It must be noted that alumina that is responsible for the increase in viscosity, undermines crystallisation, which in turn will raise the heat transfer relative to a more crystalline slag. Nevertheless, it is expected that the slag will increase the solid to liquid ratio (lower in the mould area) for the higher viscosities, and the heat transfer will decrease because of this.

It is concluded that a 10 mass % alumina increase can be expected to seriously hamper stable operation of the casting slag, and surface slab defects (or even a breakout due to poor lubrication) may occur.

5.2.3. Test of model accuracy

For a more complete description of the models mentioned here, refer to section 3.1.2, Chapter 3. Models predicting the viscosity with the temperature and the composition of the slag as variables have developed to the extent of approximating the influence of a constituent or temperature change in the system. As Figure 5.14 and 5.15 show, their accuracy may vary from highly accurate to yielding a 10 Poise under-prediction. Several models should be applied to a powder type in order to evaluate them and to choose one that predicts the trend for the specified situation the best, since there are a multitude of variables changing and influencing each other as chemical analyses or temperatures change. One model may approximate the influence of a certain element more accurately than another model, but may prove less accurate for a different element. This is also true for temperature changes.

The most extensive evaluation of viscosity prediction models yet was done in a recent paper by Fox & Mills [1999], based on a round robin study in which 22 laboratories from around the world participated. Five models were evaluated on their predicting accuracy, compared to the measurement values of the laboratories. The models evaluated were those of Kim, Koyama, Riboud, Iida and NPL. The findings are summarised below, since they bear direct impact on the current study.
In the overall rankings, the model of Riboud performed the best while the model of Kim was rated fourth out of five, and Koyama last (least accurate). A short discussion of the shortcomings and weaknesses of each model will follow:

Riboud
A disadvantage of this model might be that it fails to differentiate between the various cations, e.g. MgO on a mole fraction is treated as if it were CaO. Furthermore, the Riboud model does not account for MnO or Li_2O. If the slag composition contains significant amounts of these oxides, the actual viscosity may change markedly, while the value of the predicted viscosity remains the same. In practice, the mole fractions of MnO should be added to CaO and the mole fraction of Li_2O to Na_2O. The powder STSP that was used in the current study contains 0.8%

Li_2O, but the model predicted the viscosity more accurately for this powder than STC, that does not contain Li_2O at all (as shown in Figure 5.14 and 5.15).

Koyama

Koyama makes no allowance for B_2O_3, FeO or MnO, and only partially for Li_2O. Again, it might be expected that slag compositions that contain significant quantities of these components would result in the model prediction having a poor fit to experimental values. Fox & Mills [1999] found that the Koyama model consistently overestimates the viscosity, and corrections can be made to compensate for this. In the current study, Koyama consistently predicted the highest viscosity of the three models, but the predicted viscosity was not greater than the measured viscosity (as shown in Figure 5.14 and 5.15).

Kim

This model also excludes some components, namely FeO, MnO and TiO_2, and only partially accounts (contains terms in only one constant) for Li_2O, Na_2O and MgO. The Kim model proved inconsistent in its prediction ability, while generally underestimating viscosity, so no correction was attempted. In the current study, Kim was indeed found to consistently underestimate the viscosity (shown in Figures 5.14 and 5.15).

The Riboud model is based on a Weymann relation, and it is thought that this is partly the reason for its greater accuracy in predicting slag viscosity. The Kim and Koyama models make use of an Arrhenius relation, that was felt to be less accurate with respect to temperature changes and may reflect the poorer performance of these models relative to the Riboud model (refer to section 3.1.2 for the definitions of the relations). Furthermore, if those slag compositions containing components that are not considered by some models, are removed, it is likely that these model predictions would fit the experimental values better. This would be fairer for these models as they do not claim to be able to predict the viscosity of slag compositions containing these components. This recognises the limited range of compositions over which these models can accurately predict.

Figure 5.14 shows how three models predict the viscosity of STSP, a more crystalline powder than STC-89. Both Riboud and Koyama predict the viscosity within 2 Poise of the measured values over the whole alumina range at 1200°C, 1300°C and 1400°C. Koyama proves closer at the lower alumina values, up to about 5% alumina added. At the higher alumina values, Riboud is closer. Kim should not be used to predict the viscosity with powder STSP, since it under-predicts the viscosity, even with 0% alumina added. Note again that a model cannot be evaluated for only one casting powder type, or a limited temperature range. Furthermore, this study considered only the influence of alumina – the accuracy of the models cannot be judged for variations in other constituents. At lower temperatures than 1200°C, all three models lose accuracy by under-predicting the viscosity. The reason for this appears to be that these models do not take crystallisation or solid particles in the liquid (that will raise the apparent viscosity) into account. Their use is restricted to temperature ranges where a pure liquid is present. Viscosity measurements themselves could not provide evidence of the existence of solid phase particles in the melt, and the above statement is aided by data obtained from quench data experiments when crystallisation was studied separately. Since neither the heat cycle nor the experimental technique was the same during the viscosity and crystallisation measurements, the only

conclusive deduction to be made is the possibility of the existence of crystals at temperatures as high as 1200°C (according to the consistency of a crystal fraction present at 1300°C in Figure 5.23 to Figure 5.28). Another contribution to the possibility of the presence of crystals in the liquid is the time duration of the viscosity measurements. Altogether 50 minutes passed during every 50°C temperature interval that provided adequate time for crystal growth.

Figure 5.15 shows how the three models predict the viscosity of STC, a low carbon steel casting powder with an aimed low viscosity. Koyama proves overall closest, but under-predicts the viscosity at alumina levels higher than 5% added. The varying ability of these equations can be seen by the fact that Kim performs best at 1300°C at the more than 5% alumina added, while proving altogether unsatisfactory at the other temperatures. To successfully predict the viscosity of the powder STC, other models must be evaluated in addition to the three mentioned here, to find a more suitable one.

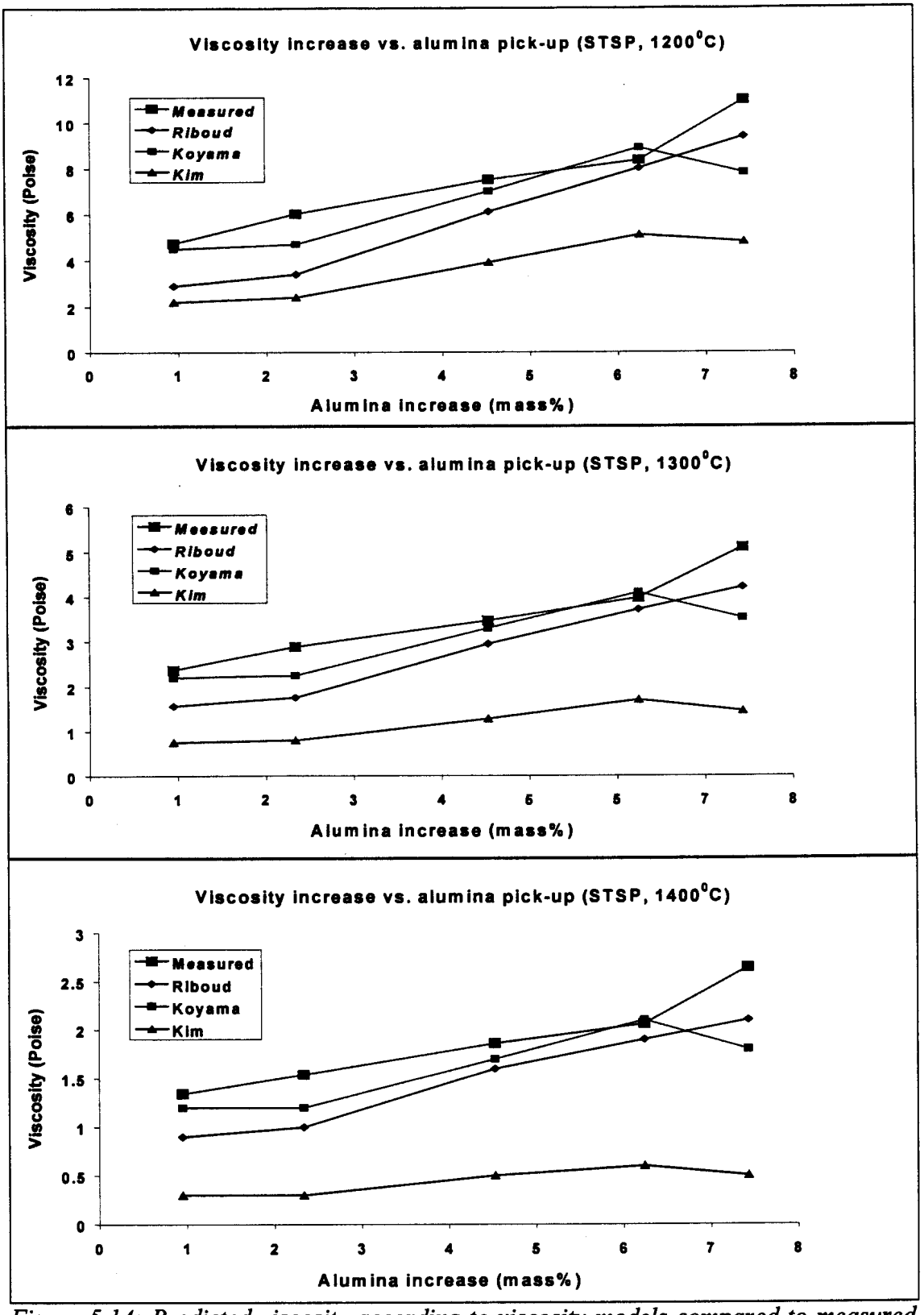

Figure 5.14: Predicted viscosity according to viscosity models compared to measured viscosity of powder STSP at 1200°C, 1300°C, 1400°C.

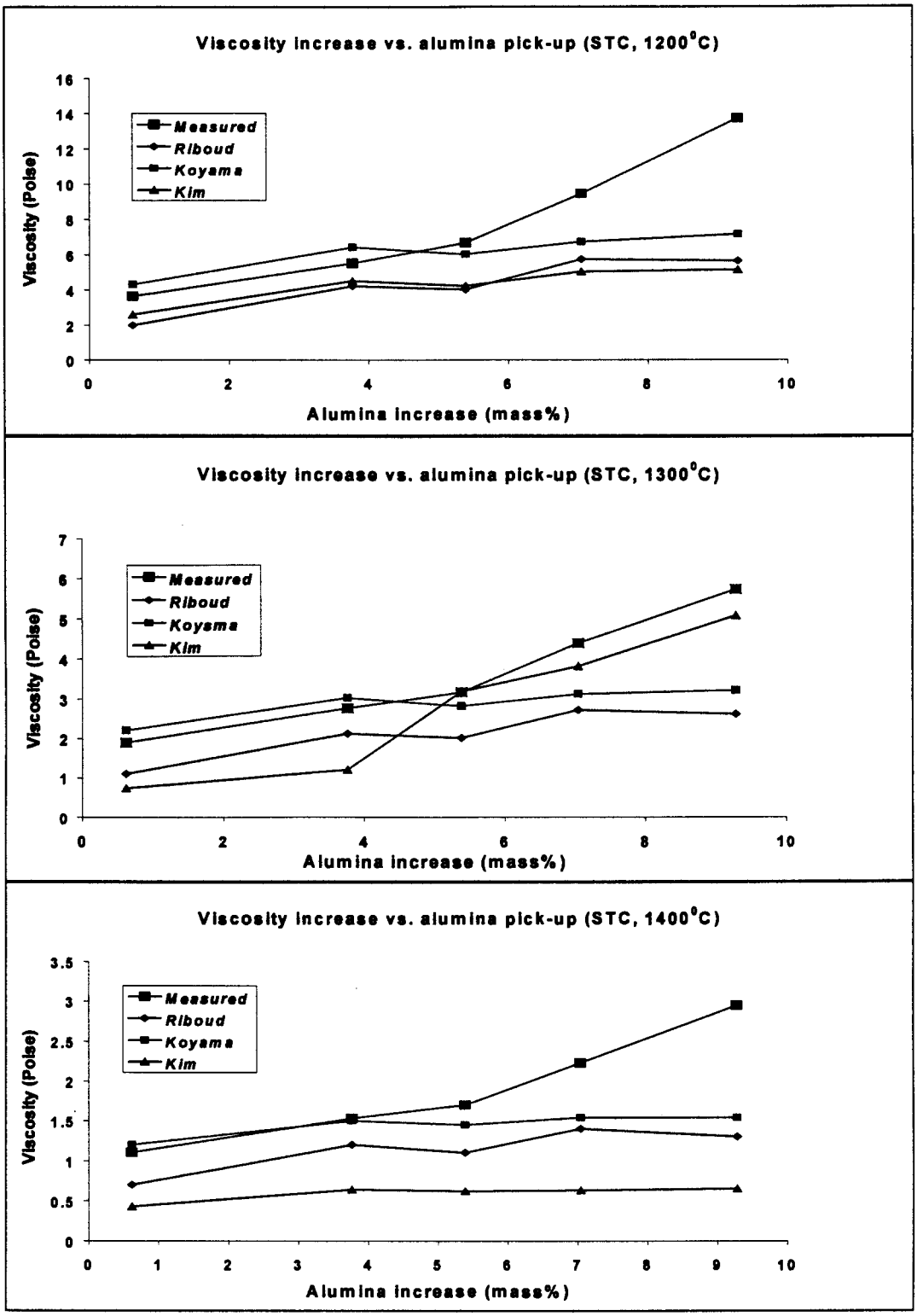

Figure 5.15: Predicted viscosity according to viscosity models compared to measured viscosity of powder STC at 1200°C, 1300°C, 1400°C.

5.2.4. Stable mineral phase precipitating

Section 2.4 in chapter 2 refers to work conducted by Hering et al [1992] that shows how the dominant mineral phase fractions of the casting powder change as the percentage alumina increases. Figure 5.16 shows the compositions of both STC and STSP superimposed unto this predicted mineral phase map. Figure 5.17 and 5.18 respectively show the mineral phases of STSP and STC as analysed with XRD – Cuspidine being always present as the most prominent mineral phase. Figure 5.17 and 5.18 were combined by taking the value of the strongest Cuspidine peak as 100% intensity. The value of the strongest peak analysed of the other phases where then presented as a relative intensity to that of Cuspidine. The findings of these figures compare quite favourably with Figure 5.16. From the viscosity measurements it is clear that increasing alumina content of both powders steadily increases the viscosity. STSP is a medium carbon steel powder with enhanced crystallisation behaviour. The result of the crystallisation of the powder may result in poorer lubrication (due to the liquid slag crystallising) and cause solid-solid friction between the mould and the strand. If the findings of Hering et al [1992] in Figure 2.8 prove accurate, the friction force of STSP will not increase in the mould as about 10% alumina is absorbed, despite the viscosity increase. The reason for this according to Figure 2.8 is the precipitation of the mineral phase Gehlenite. This phenomenon can be viewed with the aid of the following observation:
It may be possible that one mineral phase crystallises over a narrower temperature range than another. This in turn will influence the liquid arrangement in respect to the amount of solids (crystals) it contains and their morphology – the size and form of the mushy zone. To evaluate the above observation, both friction force data and crystal growth data need to be collected. Friction force was not studied by the author (this would require load cells beneath the mould or equivalent laboratory tests). Section 5.3 will discuss why only the use of the hot thermocouple technique **together with high temperature microscope** analyses can give an accurate description of the crystal growth and temperature dependence of crystallisation.

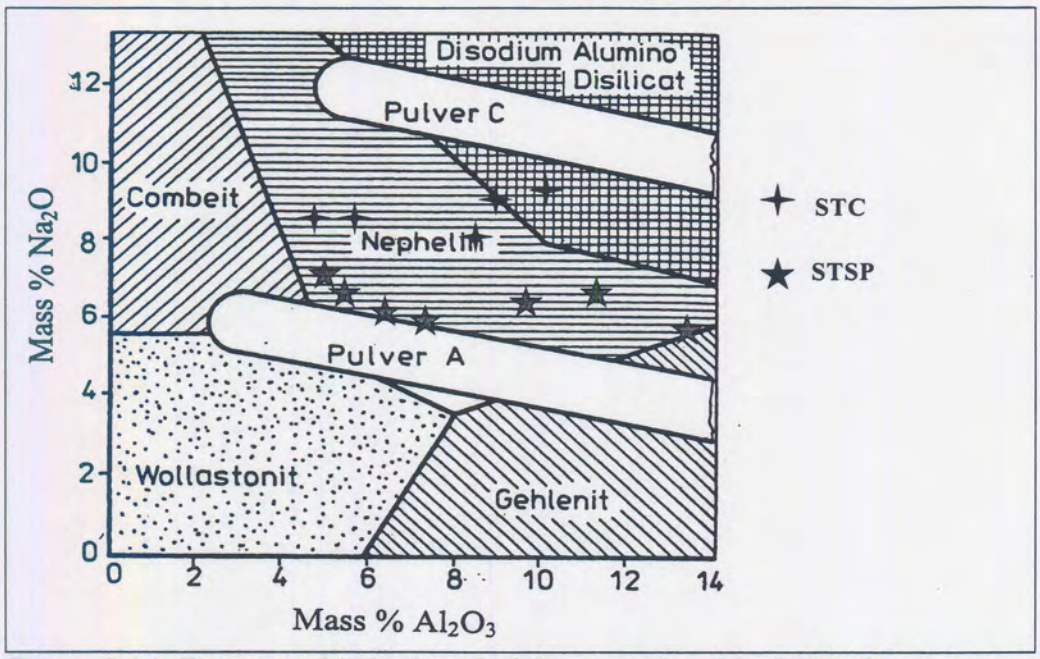

Figure 5.16: True mass % Na_2O and Al_2O_3 as analysed by EDX after viscosity measurements of both STSP and STC superimposed upon the stable mineral phase map measured by Hering et al [1992].

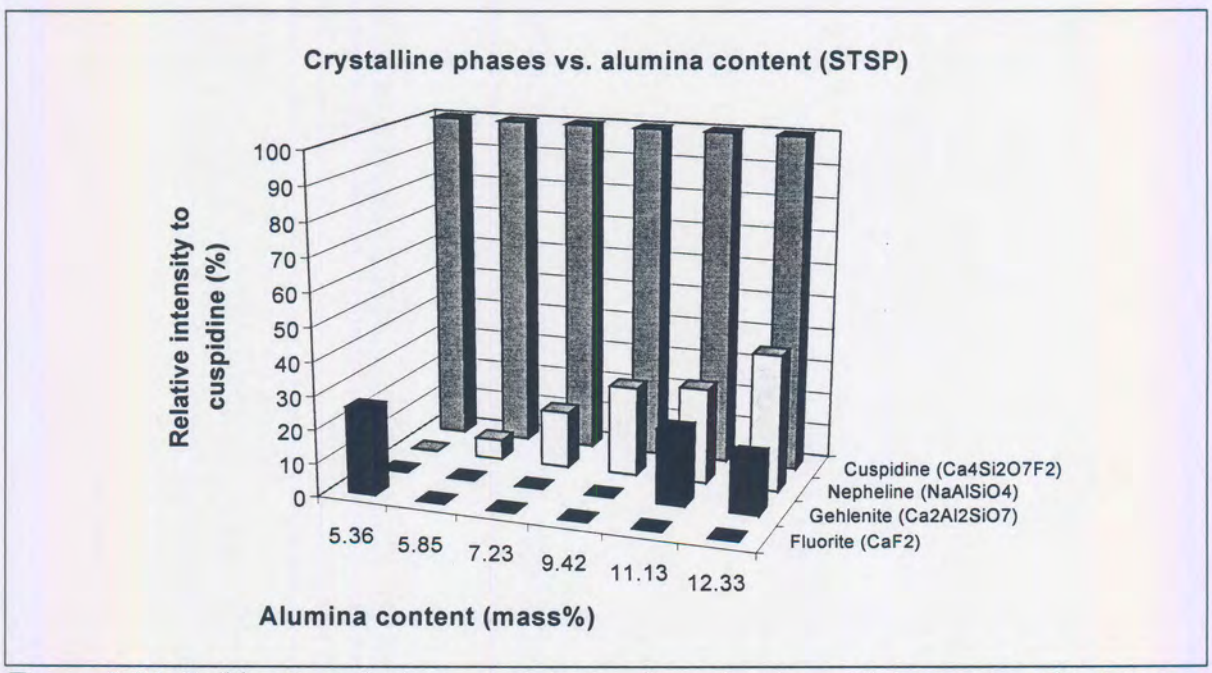

Figure 5.17: Stable mineral phase precipitating from the slag with increasing alumina content for powder STSP.

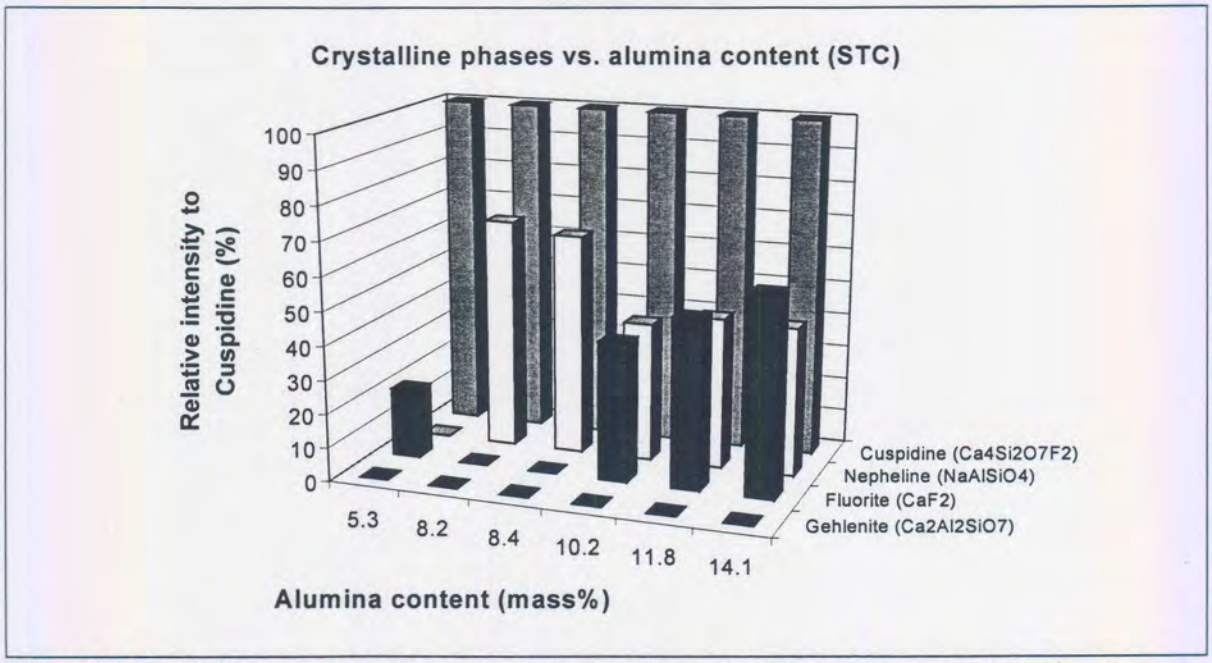

Figure 5.18: Stable mineral phase precipitating from the slag with increasing alumina content for powder STC.

5.3. Crystallisation of mould powders

Experimental work conducted brought this study right back to the fundamentals of the crystallisation process and provided valuable information as to why crystallisation is so hard to evaluate for the in-mould situation. The situation in the mould gap is of course a mixture of temperatures and times at these temperatures. There is no single and simple way to view crystallisation of mould powders in the mould, except if the whole thermal condition in the mould is known and full data is available for all possible time-temperature scenarios. The technique employed in this study is useful for the test of the influence of certain composition or thermal changes in the mould and may facilitate the design considerations of powders.

5.3.1. Difficulties and drawbacks of the hot thermocouple technique

Several areas were encountered that posed difficulties to interpreting the data obtained from usage of the thermocouple technique **(without concurrent microscope analyses)**. The current discussion will elaborate on these difficulties as background to the reason for the use of quench experiments.

The size of the sample used in each run differed to small extents, due to variability of applying the powder to the loop in the wire (as discussed in section 4.3.2). With small samples such as these, the amount of heat generated by crystallisation is extremely small and difficult to precisely interpret. A deviation from the set cooling curve may be small or indistinct enough so that discernment from electrical noise becomes ambiguous and irreproducible. The reason for the

small temperature arrests is the wide temperature range of crystallisation, as discussed below and shown in Figure 5.19.

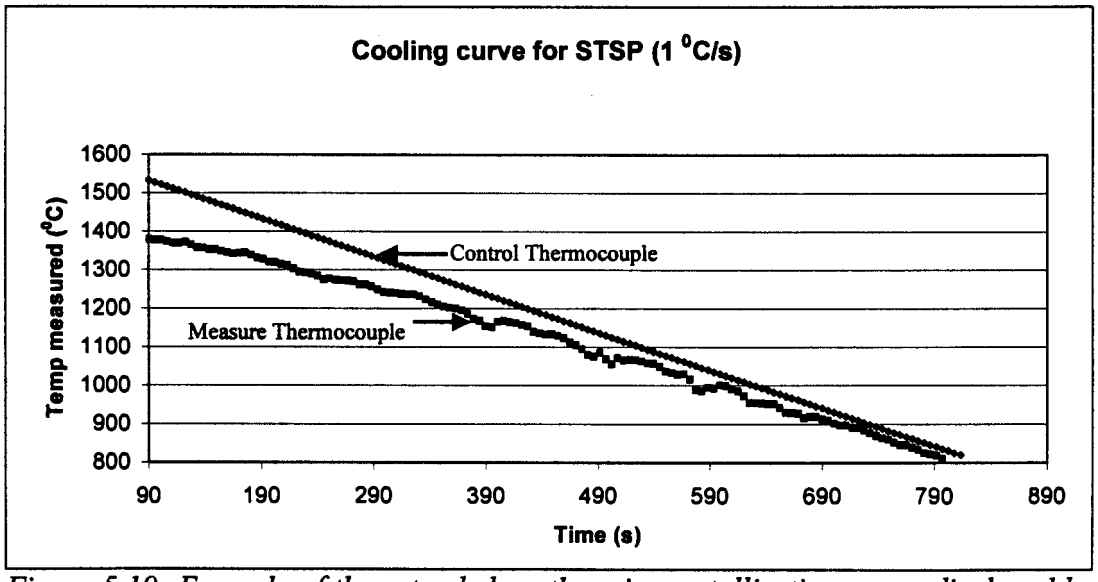

Figure 5.19: Example of the extended exothermic crystallisation range displayed by the cooling of the commercial casting powder at 2°C/s.

Imposed constant cooling of a sample that exhibits no phase transformation tendency will result in a linear cooling pattern. Any deviation from linearity is caused by endothermic or exothermic reactions. Figure 4.9 in chapter 4 shows an example of the single exothermic reaction of CaF_2. The deviation in the cooling curve of CaF_2 is clear due to the isothermal exothermic crystallisation reaction of CaF_2 at 1418°C (CaF_2 is a pure material with a congruent melting point). In real mould slag, crystallisation may occur over a wider range of temperature, making a deviation from the cooling curve indistinct. This was indeed found to be the case for real mould powders. The cooling curves on the temperature-time diagrams displayed some thermal activity that could be identified as an exothermic reaction, but with a number of small and indistinct peaks over a temperature range, even up to 200°C, as shown in Figure 5.19. Determining of a single temperature of crystallisation was by no means regarded as accurate or reproducible, for a deviation from the cooling curve was sometimes pronounced at a certain temperature for a fixed cooling rate, and on other occasions not. In a complex system like mould powders, it is necessary to incorporate the visual aspect of opaque crystal growth from the transparent liquid/glass to validate data.

Crystallisation in a mould powder occurs by the emergence and growth of crystals in the liquid pool. As the temperature of the sample is raised to above the melting point of the slag, the crystals that are present in the slag will dissolve into the liquid. If the time above the melting temperature is short enough, some crystals will still be present in the liquid and act as a heterogeneous site for new crystals to grow out of the liquid as the temperature is lowered. These heterogeneous sites require less initiation energy for a new crystal to form than does homogeneous nucleation in the liquid itself. On the other hand, if the cooling rate is low enough from very high temperature (1500°C), crystals will nucleate in the liquid and grow. The above-mentioned mechanism was observed in the collection of data. Both the peak temperature of the

sample and the length of time that the sample is maintained at that temperature will determine the mechanism of crystal formation in the liquid pool. In the case of complete melting of the sample and dissolution of all crystalline matter in the liquid at higher temperatures, new crystal nucleation was necessary for crystallisation. In the case of incomplete melting of the sample where there was still some undissolved crystalline matter present in the slag at lower temperatures and shorter times, crystallisation proceeded through growth of the existing crystals. In other words, it is possible to cool the sample as crystalline material at higher cooling rates from the lower temperatures where dissolution is incomplete, than would yield crystalline material from higher temperatures where crystals are completely dissolved. The above discussion predicts that the use of the same sample will yield different time, temperatures and fraction of crystallisation due to the elimination/addition or characteristic change of the nucleation sites in the sample.

Experiments done beforehand showed through EDX analyses that sodium and fluorine completely disappear from the powder when it is heated in the thermocouple loop. The powder often cooled as glass despite low cooling rates (as low as 1°C per second) due the lack of Na_2O and F in the matrix. Sodium Fluoride (together with potassium fluoride) has a high vapour pressure at high temperatures (as discussed in chapter 2, section 2.1.3). X-Ray Diffraction of the cooled sample after crystallisation revealed that the predominate crystalline phase, namely Cuspidine ($3CaO.2SiO_2.CaF_2$) that contains F, was absent as was a prominent phase like Nepheline ($Na_2O.Al_2O_3.2SiO_2$) that contains Na; and Gehlenite ($2CaO.Al_2O_3.SiO_2$) was the only phase present. In order to compensate for the lack of Na_2O, it was added along with Al_2O_3 to the powder as described in section 4.3.1.2, Chapter 4. Cuspidine is formed when the F content is typically between 4 and 10 mass percentage. Even though the Na_2O loss can be rectified through additions, the lack of fluoride remains a problem to be solved. The implication of the absence of the predominant crystal phase (Cuspidine) due to the absence of fluoride on the data obtained by the Hot Thermocouple Technique remains to be determined (in regard to the true crystallisation in the mould, where Fluorine is available).

5.3.2. Use of quench experiments

It is well known from classical nucleation theory that the onset of crystallisation in slag must be a function of the cooling rate, and that to determine the solidification behaviour of a liquid slag one must construct either isothermal time temperature transformation diagrams (TTT curves) or continuous cooling transformation diagrams (CCT curves). In addition, the growth rate, morphology and solidified fraction of the slag under varying cooling rates are important in the determination of the effect of crystallisation of the slag on heat transfer and rheology. The visual assessment of the crystallisation process at the high temperatures holds great promise in yielding understanding the temperature and time dependence of crystal formation and growth during cooling. Thermal data rather acts as an aid to visual observation to confirm the onset of crystallisation in the sample.

To compensate for the failure of the current technique to identify the temperature at which the slag crystallises, because of the temperature range of crystallisation, and the lack of high temperature microscopic video facilities, use was made of the conventional and established way of determining cooling diagrams together with time-temperature observations. The sample was

"quenched" by cutting the power supply to the platinum wire at different temperatures of the cooling cycle to construct a Continuous Cooling Transformation (CCT) diagram (keeping the initial cooling rate constant from a specified peak temperature). Cooling rates in excess of 300°C/s were achieved in the sample after the electric power was cut. The sample could then be visually studied at room temperature for the extent of crystallisation, if any.

It would also be possible (but was not performed) to construct TTT-diagrams in addition to the CCT diagrams mentioned above by heating the sample to 1500°C and keeping it there for 1 minute in order for the sample to achieve homogeneous composition and temperature and for all crystals to dissolve. After this the sample is "quenched" to the test temperature and kept there for a variable time. After each time the sample can be quenched and microscopically examined at room temperature for crystallisation. The test temperature will vary in order to obtain a classical TTT diagram

5.3.2.1. Results

Figure 5.20 shows crystals growing dentritically along the surface of a sample removed from the thermocouple wire, and is included to show the morphology of the crystalline material as seen under the optical stereo microscope (Figure 5.21 and 5.22).

TYPE JSM-5800 ACCV 10kV
WIDTH 132um MAG x1,000

Figure 5.20: Electron microscope picture showing crystals growing dendritically on the surface of the sample removed after a quench experiment – backscatter electrons was used to obtain the image.

To provide an example of the image obtained at room temperature under the stereo microscope for the determination of the extent of crystallisation, Figure 5.21 and 5.22 are included. The distinction between the vitreous and opaque parts in the photo provides the estimated percentage

crystallisation. Figure 5.21 shows crystals suspended in glass in the approximate ratio of 3 to 7. The crystals nucleating throughout the glass serve as an example of the nucleation and growth mechanism at work in the samples. The right part in this figure is more crystalline due to the slower cooling it was exposed to – which is a function of the geometry of the design of the thermocouple loop (see Figure 4.7 and 4.8, section 4.3.1.1). The design of the sample loop (measure thermocouple) was arranged such that the sample was exposed to a hotter side (right hand side of the measure thermocouple in Figure 4.7), adjacent to the control thermocouple, and a colder side (left hand side of the measure thermocouple in Figure 4.7). The colder side will cool faster due to the absence of heat input from the control thermocouple side, together with the cooling effect from the cooled side (in contact with water cooled clamp) of the thermocouple wire. The thermal inertia is small in this corner due to the small amount of molten slag in contact with this area. The faster cooling rate experienced in this top section in turn aids the super-cooling of glass. The consequence of this could be distinguished in some of the samples that were studied visually. The thermocouple is situated in the base of the loop (on the top right side of Figure 5.21) and the temperature measured strictly represents only the area adjacent to this contact point. The effect of this on the results could not be determined, but would be limited by the small size of the loop (less than 1mm in diameter). Figure 5.22 is a picture of a different sample that crystallised to a larger extent – 50 % crystalline material. It can be seen from this picture that the effect of non-uniform temperature distribution in the loop had less effect of the crystal distribution than Figure 5.21 (measure thermocouple situated at bottom of Figure 5.22).

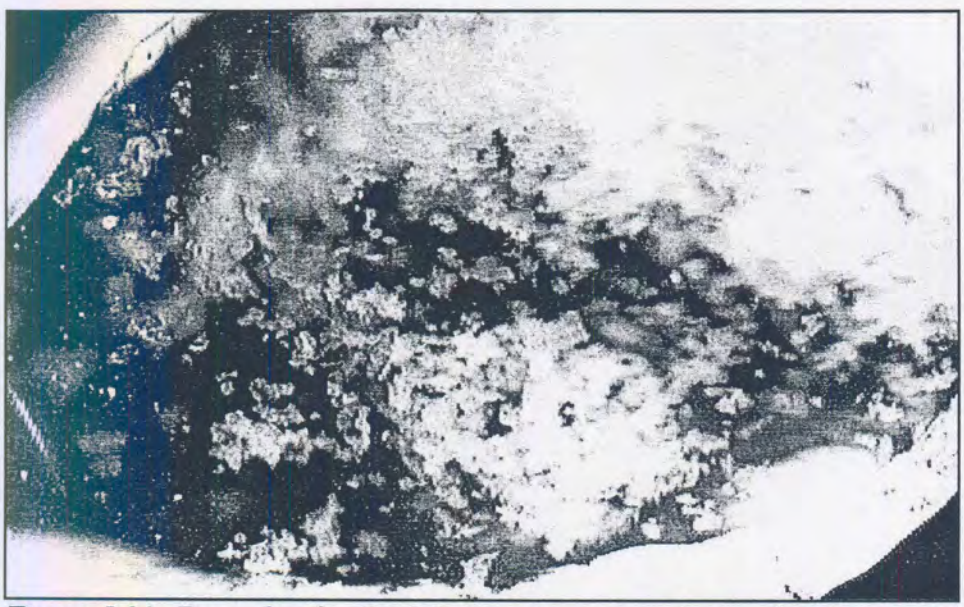

Figure 5.21: Example of optical stereo microscope picture showing crystals growing in the glass in the sample removed after a quench experiment (30% crystalline material, 70% glass).

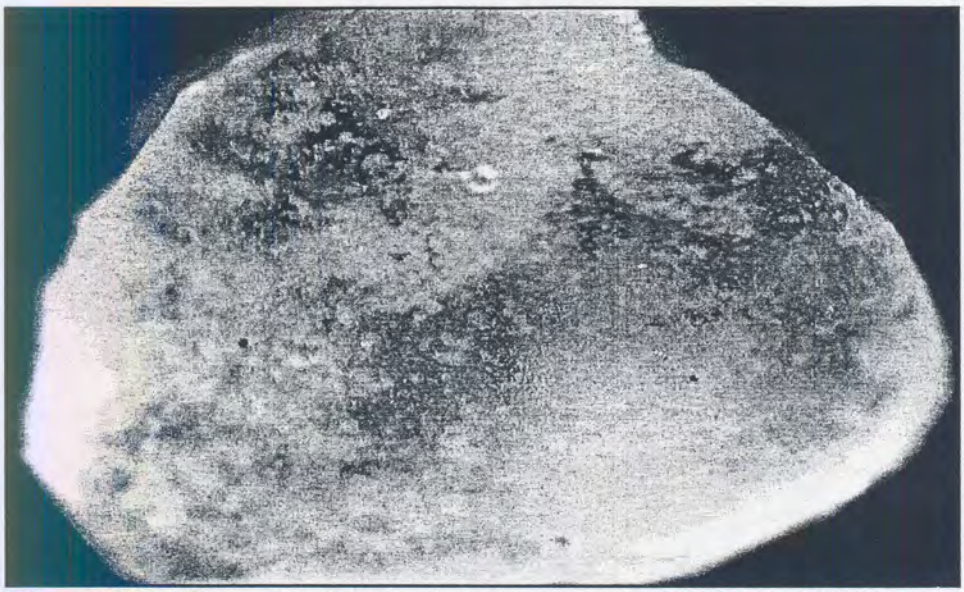

Figure 5.22: Example of optical stereo microscope picture showing around 50% crystal and 50% glass phase present in the sample removed after a quench experiment.

Before a detailed discussion of the influence of the heat cycle on crystallisation behaviour is presented, the influence of alumina on crystallisation will be discussed. Figure 5.23 shows how the crystallisation behaviour of the powder STSP changes as 5 and 10 percent alumina are added to the powder. Increasing alumina content decreases the percentage crystal present in the sample at the same quench temperature. This implies that the temperature at which crystals start precipitating in the sample is lowered as the alumina is increased. Let us consider the scenario in which powder STSP is enriched with respectively 5 and 10 mass percentage alumina during a sequence cast – considering the effect on both viscosity and crystallisation at the isothermal condition of 1300°C. According to Figure 5.6 the viscosity will rise from 2.5 Poise at 1300°C to 4 Poise when 5% alumina has been absorbed. 4 Poise viscosity of the slag moving next to the steel strand will not discernibly increase lubrication/friction (for a detailed discussion on lubrication/friction, refer to section 5.2.2). Slag feed at the meniscus area will remain sufficient with a viscosity of less than 2 Poise at 1550°C. Since STSP is a medium carbon steel grade powder, the crystallisation characteristic of the powder is especially important. In the 1300°C region of the mould, a powder that enriches with 5% alumina should consist of only 30% crystal, opposed to the 60% crystalline material of the original powder. The ability of the powder to restrict heat flux through the slag layer should significantly be influenced by 5% alumina increase, more significant than the viscosity increase the powder experiences. Since heat extraction is most critical in the high temperature area of the mould (1300°C and higher) to reduce cracking, the influence of alumina is considered to be significant to the process.

It must be emphasised that the percentage crystal that is depicted in Figure 5.23 results from a specific temperature cycle. The influence of changes in the temperature cycle will be discussed from Figure 5.24 to Figure 5.26. Every piece of slag in the mould area experiences a unique heat cycle and will crystallise accordingly. (Ho and Thomas [1992] estimated actual cooling rates between the steel shell and the mould of a continuous caster to range from less than 1°C per second to 20°C per second depending upon position in the mould. Furthermore, slag can move

down the mould length at the speed of the steel strand, or be almost stagnant in the partly solidified portion of the slag). At best this discussion does provide insight into the importance of considering the effect of alumina on the crystallisation behaviour of the powder, together with viscosity experiments.

Through following the trend of the viscosity rise in Figure 5.6, a viscosity increase (of the 10% added alumina sample) should be in the order of 2.5 Poise to 7 Poise. This influence is more substantial that the 5% and could restrict slag infiltration. For a 10% alumina increase, the percentage crystal present at 1300°C will decrease from 60% to approximately 15% (predominantly crystalline to almost pure glass phase). Clearly heat transfer in the mould is likely to be greatly increased and this may result in longitudinal cracking.

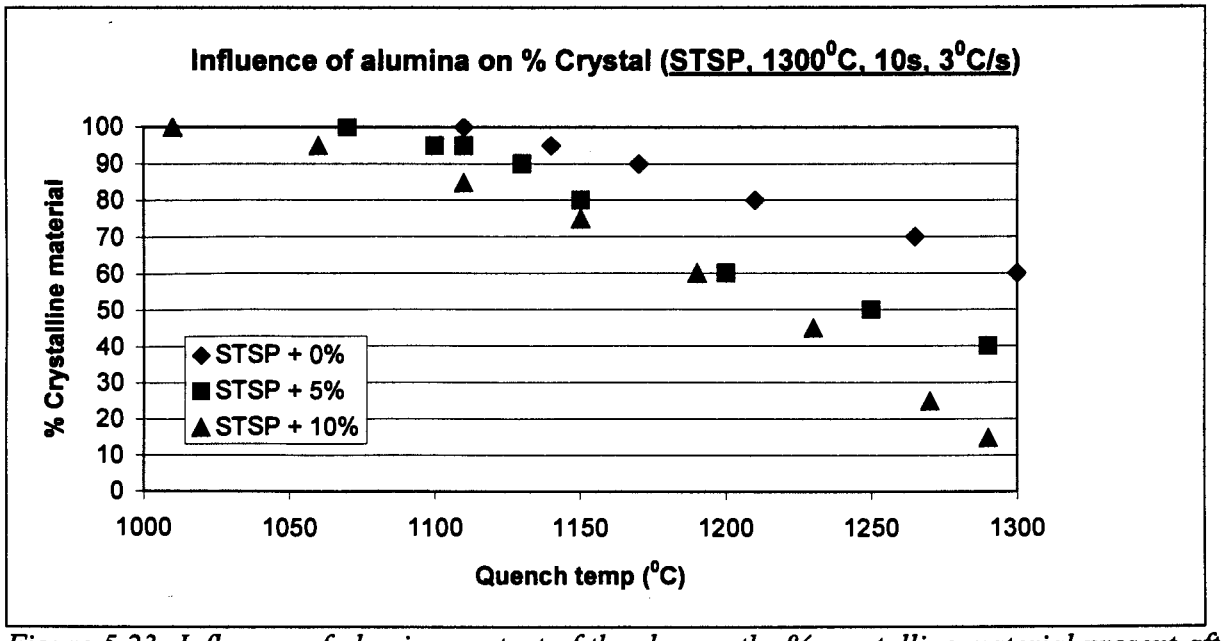

*Figure 5.23: Influence of alumina content of the slag on the % crystalline material present after interrupted crystallisation – Powder **STSP** + indicated alumina (Heat cycle: Held at 1300°C for 10s, cooled at 3°C/s and quenched from temperatures shown).*

We will now consider the strong effect of changes in the heat cycle on the crystal-forming ability of essentially the same sample. Figure 5.24 suggests how the peak temperature influences the residual crystals in the liquid before cooling progresses. The sample held at 1250°C for 10 seconds was still 85% crystalline. The amount increases and reaches 100% as the sample is allowed to cool to 1150°C at 3°C/s. When the sample was heated to 1400°C, **all crystalline material dissolves**. New crystal precipitation commenced only after the sample had cooled from 1400°C to around 1260°C at 3°C/s. The higher peak temperatures consistently yield less crystalline material at the same quench temperature and cooling rate.

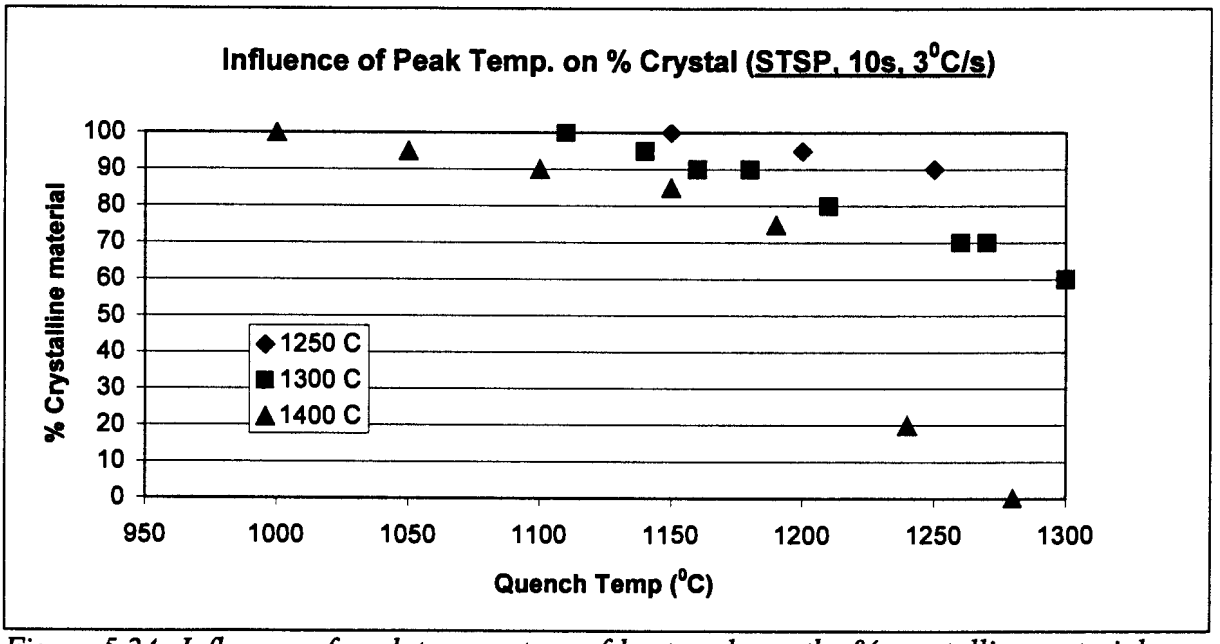

*Figure 5.24: Influence of peak temperature of heat cycle on the % crystalline material present after interrupted crystallisation - **STSP + 0% alumina** (Heat cycle: Held for 10s, cooled at 3°C/s and quenched from temperatures shown).*

From Figure 5.23 through 5.26 it can be seen that when the sample was quenched from 1300°C (after holding at 1300°C for 10s), it contained around 60% crystalline material. This value proved reproducible – as can be seen by the consistent values in Figure 5.23 through Figure 5.26, that were all obtained in separate experimental runs. Figure 5.25 suggests that crystalline material is somewhat less if the sample is kept for 30s relative to the 10s holding time. The explanation provided is continued dissolution of the crystals as the sample is kept at 1300°C for the longer period.

An interesting phenomenon is noted, as the holding time at the peak temperature is even longer. When the sample was controlled for 50s at 1300°C and then quenched at 1300°C, more crystalline material (70%) is reported. The value of 70% crystal remains constant when quench temperature is lowered – even up to 1200°C. No explanation can be offered for this documented behaviour. Reference is made to Figure 5.27 where the sample held for 50s of STSP+10% alumina exhibit the same behaviour.

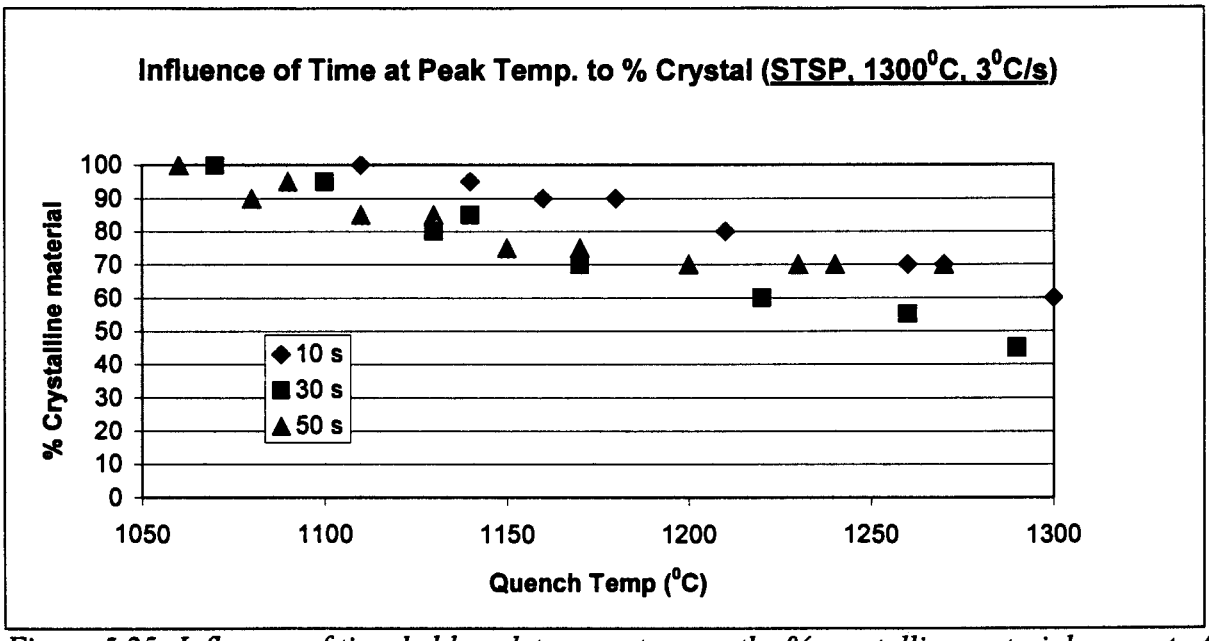

*Figure 5.25: Influence of time held peak temperature on the % crystalline material present after interrupted crystallisation - **STSP + 0% alumina** (Heat cycle: Held at 1300°C, cooled at 3°C/s and quenched from temperatures shown).*

Figure 5.26 at first glance serves to contradict the whole argument regarding the necessity of distinct well-documented cooling rates for crystallisation data, as discussed in the literature. Generally, cooling rate influences the undercooling (relative to equilibrium values) that a system will require for solidification to proceed. The lower cooling rates provide more time for crystal growth or nucleation than the higher cooling rates. In Figure 5.26, a marginal amount of increased crystal growth is reported at low quench temperatures (lower than 1200°C) for the lower cooling rates. Since the fraction of crystalline material is similar for the different cooling rates, it could be argued that the nucleation and growth rate of crystals remain constant and is not a strong function of the cooling rate. The only way to clarify the true reason for the documented behaviour will be to visually monitor crystal nucleation and growth as cooling proceeds by means of a hot stage microscope. (Since the number and morphology of the similar crystalline fractions in the samples may very well differ, the documented influence of cooling rate cannot be effectively evaluated without the aid of visual data).

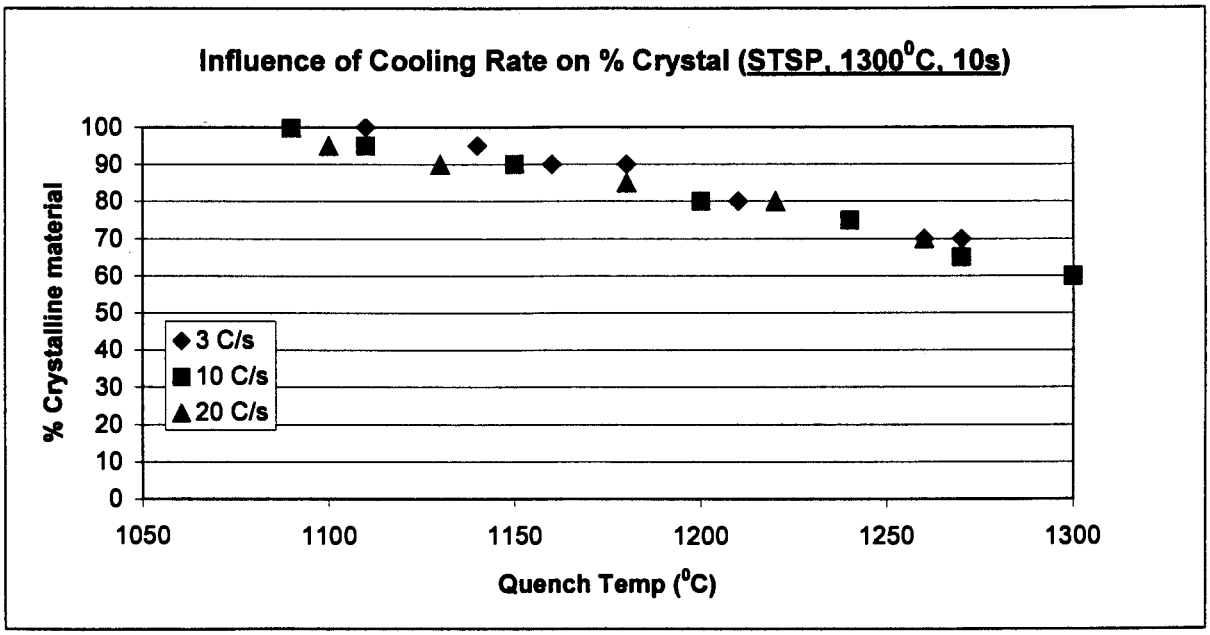

*Figure 5.26: Influence of cooling rate on the % crystalline material present after interrupted crystallisation - **STSP + 0%** alumina (Heat cycle: Held at 1300°C for 10s, cooled at different rates and quenched from temperatures shown).*

For interest's sake, similar data as Figure 5.25 and 5.26 have been included for the powder STSP with 10% alumina added. Figure 5.27 shows the influence of time at peak temperature and Figure 5.28 the influence of cooling rate on crystallisation of STSP + 10% alumina. The principles for the discussion of Figure 5.27 are the same as for Figure 5.25, and that of Figure 5.28 are the same as Figure 5.26. The percentage crystalline material is consistently less at the same quench temperature (for STSP + 10 % alumina) compared to the plain STSP powder.

From Figure 5.27 it can be seen that the sample held for 30s crystallises less than the sample held only for 10s. The reason is again the dissolution of some of the crystals still present. The sample held for 50s in this case display consistently more crystalline material than even the 10s sample.

In the case of STSP + 10% alumina, cooling rate appears to play even less of a role (Figure 5.28 compared to Figure 5.26).

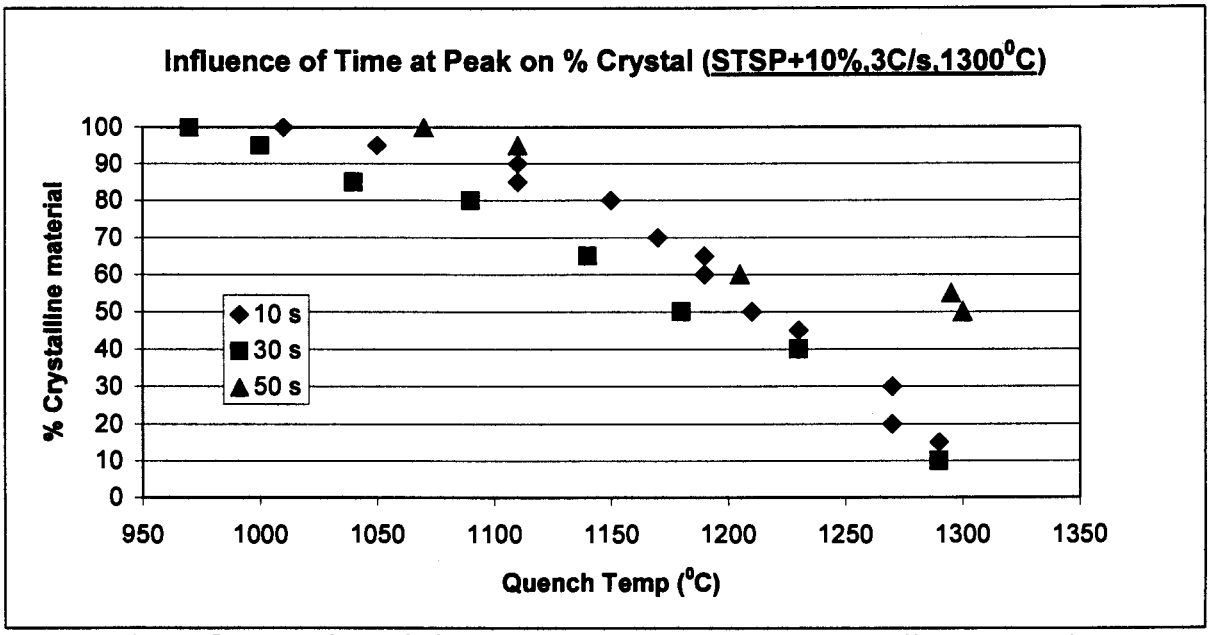

*Figure 5.27: Influence of time held peak temperature on the % crystalline material present after interrupted crystallisation - **STSP + 10%** alumina (Heat cycle: Held at 1300°C, cooled at 3°C/s and quenched from temperatures shown).*

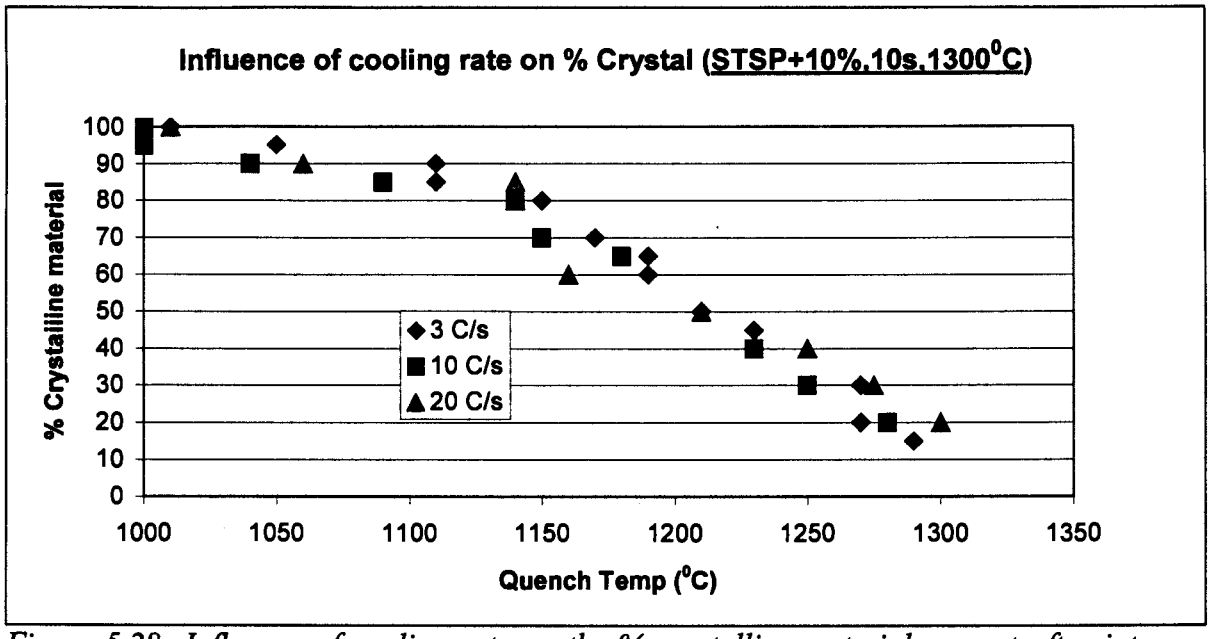

*Figure 5.28: Influence of cooling rate on the % crystalline material present after interrupted crystallisation for **STSP + 10%** alumina (Heat cycle: Held at 1300°C for 10s, cooled at different rates and quenched at temperatures shown).*

6. Conclusion

During the continuous casting of aluminium killed carbon steel, the molten casting powder on top of the liquid steel in the mould enriches in alumina to a steady-state value. With modern day clean steel practice between 2 and 4 mass % alumina are absorbed by the casting powder. The alumina content of the molten casting slag reaches the increased steady-state value within the first ladle of the sequence (the first 40 minutes of casting) and remains constant for the rest of the casting process.

As the alumina content of the slag increases, so the viscosity increases. The viscosity of the powder STC-89 (the low carbon powder used in this study and designed with low viscosity to reduce sticking in the mould) at 1300°C will be affected by a change in viscosity of about 0.3 Poise (raised from 2 Poise to 2.3 Poise) for a 4 mass % alumina increase. This constitutes a 15 % viscosity increase, and even less at higher temperatures. Neither infiltration into the mould-strand gap, nor liquid friction force (as a measure of lubrication), nor oscillation mark depth will be notably influenced by a 4 mass % alumina increase.

When problems occur in casting practice and alumina is not removed from the steel before casting, or re-oxidation takes place, the alumina increase of the casting slag may be pronounced. An alumina increase of 10% for powder STC-89 at 1300°C will cause a viscosity increase from 2 Poise to 5.7 Poise, a 185% increase, and poor feeding (especially at higher casting speeds) can be expected. At 1150°C (strand surface temperature at the bottom of the mould) the viscosity will have increased from 5.6 Poise to 22.7 Poise, a 305% viscosity increase. A partly crystalline mushy zone may be present in the slow moving viscous slag in this area. It is even possible that solid lubrication may be experienced at the bottom of the mould, depending on the heat cycle.

Models that predict viscosity vary in their predictive capability; their accuracy may vary from highly accurate to yielding a 10 Poise under-prediction. They are specifically sensitive to temperature and composition changes. Unfortunately, not one of the models used today for prediction of casting powder viscosity incorporates all the compositional elements found in casting powders. There is not a single model that always performs well, and the choice of a model should take account of the limitations of the model regarding the composition of the powder and the temperature (considering the possibility of partial crystallisation at different temperatures for different casting slags).

The crystallisation temperature of a casting slag is lowered as the alumina content increases and the stable mineral phases that precipitate change. Quench experiments used to determine the % crystalline material showed the sensitivity of crystallisation to the heat cycle that the sample had experienced. Heterogeneous nucleation sites (typically found in a mushy zone lower down the mould) promote crystallisation. Time at a temperature also has a strong effect (longer times increasing crystal growth). Cooling rate was found to have virtually no effect on the % crystalline material.

Casting powder STSP-232-BA (a medium carbon casting powder designed to crystallise in the mould area and reduce cracking) was used in quench experiments. A sample heated to 1300°C, held there for ten seconds and then quenched from 1300°C, should consist of only 30%

crystalline material if 5 mass % alumina is added to it, and only 10% crystalline material if 10 mass % alumina is added to it, opposed to 60% crystalline material of the original powder. Since heat extraction is most critical in the high temperature area of the mould (1300°C and higher) to reduce cracking, the influence of alumina is considered to be significant to the process – even more so than the viscosity influence.

The data from attempts to measure the crystallisation temperature of casting slag with DTA and Hot Thermocouple related techniques is difficult to interpret since the slag crystallises over a temperature range of up to 200°C. A further shortcoming to the use of the Hot Thermocouple Technique is the loss of fluorine from the sample, which excludes some of the stable mineral phases expected to crystallise.

7. References

Anzai E., Ando T., Shigezumi T., Ikeda M. & Nakano T., (July 1987), *Hydrodynamic Behavior of Molten Powder in Meniscus Zone of Continuous Casting Mold*, Nippon Steel Technology Report, no.34, 31-40.

Bommaraju R., (1991), *Optimum Selection and Application of Mold Fluxes for Carbon Steels*, 1991 Steelmaking Conference Proceedings, 131 - 146.

Branion R.V., (1987), *Mould Fluxes for Continuous Casting*, Mould Powders for Continuous Casting & Bottom Pour Teeming, Iron and Steel Society, 3-13.

Brimacombe J.K. & Samasekera I.V., (September 1979), *The Thermal Field in Continuous Casting Moulds*, Canadian Metallurgical Quarterly, Vol. 18, no. 3, 251 – 256.

Brookfield Engineering Laboratories, (July 1996), *More Solutions to Sticky Problems*, 13 – 16.

Carli R. & Ghilardi V., (June 1998), *Managing Technological Properties of Mold Fluxes,* Iron and Steelmaker, Vol. 25, no. 6, 43 – 46.

Diehl S., Moore J.A. & Phillips R.J., (April 1995), *Improved spherical granule mold flux*, 78th Steelmaking Conference, Nashville, Tennesee, U.S.A.

Feldbauer S., Jumbo I., Sharan A., Shimizu K., King W., Stepanek J., Harman J. & Cramb, A.W., (1995), *Physical Properties of Mold Slags that are Relevant to Clean Steel Manufacture*, 1995 Steelmaking Conference Proceedings.

Fonseca V.A., Afrange O.D.C., Lavinas A.O., Ramos A.A. & Valadares C.A.G., (1997), *Evaluation of Solidified Slag Films from Mould Powders Used in C.C, Taken From Shell/ Mold Interface*, Carboox.

Fox A. & Mills K. C., (June 1999), *Modelling the Viscosities of Slags in Steelmaking*, Results of global round robin compiled by NPL.

Hering L. & Fenzke H.W., (July 1992), *On-line Monitoring of Heat Flow Density in Slab Continuous Casting*, Stahl u. Eisen, Vol. 112, no.7, 61 - 65.

Hering L., Heller H.P. & Fenzke H.W., (August 1992), *Investigation of Flux Powder Selection in Slab Continuous Casting*, Stahl u. Eisen, Vol 112, no.8, 61 - 65.

Ho B. & Thomas, (1992), *Characterization of Interfacial Heat Transfer in the Continuous Slab Casting Process,* Masters Thesis, University of Illinois-Champagne.

Imai T., Kurose Y., Omiya S., Sorimachi K. & Suzuki K., (1986), *Influence of Gas on Lubrication of Mould Powder*, Transactions ISIJ, Vol. 26, 95.

Jablonka A., Harste K. & Schwerdtfeger K., (1991), *Thermodynamical Properties of Iron and Iron - Carbon Alloys: Density and Thermal Contraction*, Steel Research 62, no. 1, 28 – 33.

Jenkins M.S., (1995), *Characterisation and Modification of the Heat Transfer Performance of Mold Powders*, 1995 Steelmaking Conference Proceedings, 669 - 677.

Johnston W. & Brooks G., (1997), *Effect of Al2O3 and TiO2 Additions on the Lubrication Characteristics of Mould Fluxes*, Molten Slags, Fluxes and Salts ' 97 Conference, 845 - 850.

Kashiwaya Y., Cicutti C.E., Cramb A.W. & Ishi K., (1998a), *An Investigation of the Crystallisation of a Continuous Casting Mold Slag Using the Single Hot Thermocouple Technique*, ISIJ International, Vol. 38, no. 4, 357 – 365.

Kashiwaya Y., Cicutti C.E. Cramb A.W. & Ishi K., (1998b), *Development of Double and Single Hot Thermocouple Technique for In Situ Observation and Measurement of Mold Slag Crystallisation*, ISIJ International, Vol. 38, no. 4, 348 – 356.

Kawamoto M., Kanazawa T., Hiraki S. & Kumakura S., (1997), *Mold Flux for High Speed Continuous Casting*, Molten Slags, Fluxes and Salts '97 Conference, 777 - 780.

Kawamoto M., Nakajima K., Kanazawa T. & Nakai K., (1994), *Design Principles of Mould Powder for High Speed Continuous Casting,* ISIJ International, Vol. 34, no. 7, 593 – 598.

Kim J.W., Choi J., Kwon O.H., Lee I.R., Shin Y.K. & Park J.S., (1992), *Viscous Characteristics of Synthetic Mold Powder for High Speed Continuous Casting*, 4th International Conference on Molten Slags and Fluxes, 1992, Sendai, ISIJ, 468 - 473.

Kishi T., Tsuboi H., Takeuchi H., Nakano T., Yamamiya M. & Ando T., (July 1987), *Mold Powder Technology for Continuous Casting of Titanium-Stabilized Stainless Steel,* Nippon Steel Technical Report, no. 34, 11 – 20.

Koyama K., Nagano Y., Nagano K. & Nakano T., (July 1987), *Design for Chemical and Physical Properties of Continuous Casting Powders*, Nippon Steel Technical Report, no.34, 41 - 47.

Kyoden H., Diohara T. & Nomura O., (1987), *Development of Mould Powders for High Speed Continuous Casting of Steel*, Mould Powders for Continuous Casting and Bottom Pour Teeming, Iron and Steel Society, 45 – 51.

Mills K. C., (1991a), *The Performance of Casting Powders and Their Effect on Surface Quality*, 1991 Steelmaking Conference Proceedings, 121 – 129.

Mills K. C., (August 1991b), *Commission Report on Standard Reference Material (SRM) For High Temperature Viscosity Measurements*, NPL Report DMM(A) 30.

Mills K. C. & Machingawuta N., (August 1991), *SRM for High Temperature Viscosity Measurements: Results for Phase Two of Interlaboratory Comparison Program*, NPL Report DMM(A) 29.

Mills T.N. & Bhat B.N., (October 1973), *Development of Continuous Casting Mold Powders*, Iron and Steelmaker, Vol. 5, no. 10, 18 – 24.

Nakano T., Kishi T., Koyama K., Komai T. & Naitoh S., (1984), *Mould powder technology for continuous casting of aluminium-killed steels*, Transactions ISIJ, Vol. 24, 950 – 956.

Nakato H., Omiya S., Habu Y., Emi T., Hamagami K. & Koshikawa T., (March 1984), *Optimizing Mold Lubrication for High-Speed Continuous Casting of Slabs*, Journal of Metals, 44 - 49.

Neumann F., Neal J., Pedroza M.A., Castillejos E.A.H. & Acosta G., F.A., (1996), *Mold Fluxes in High Speed Thin Slab Casting*, 1996 Steelmaking Conference Proceedings, 249 - 257.

Ogibayashi S., Mukai T., Mimura Y., Nagano Y., Yamaguchi K., Takahashi T., Koyama K. & Nakano T., (July 1987), *Mold Powder Technology for Continuous Casting of Low-Carbon Aluminium-Killed Steel*, Nippon Steel Technical Report, no.34, 1 - 10.

Pinheiro C.A., Samarasekera I.V., & Brimacombe J.K., (February 1995), *Mould Flux for Continuous Casting of Steel*, Iron and Steelmaker, 37 – 39.

Riboud P.V. & Larrecq M., (1979), *Lubrication and Heat Transfer in a Continuous Casting Mold*, Steelmaking Proceedings 1979, Vol. 62, ISS-AIME, 54 - 62.

Riboud P.V., Olette M., Leclerc J. & Pollak W., (1983), *Continuous Casting Slags: Theoretical Analyses of Their Behaviour and Industrial Performance*, The Theory and Practise of Mold Fluxes Used in Continuous Casting, Iron and Steel Society, 13 – 19.

Sakai H., Kawashima T., Shiomi T., Watanabe K. & Iida T., (1997), *Crystallisation Behaviour of Molten Fluxes for High-Speed Continuous Casting of Middle Carbon Steel*, Molten Slags, Fluxes and Salts '97 Conference, 787 – 790.

Skoczylas G., (1996), *Recent Developments in High Viscosity Mold Powders for TiSULC Steel Grades*, 1996 Steelmaking Conference Proceedings, 269 – 275.

Susa M., Mills K.C., Richardson R., Taylor R. & Steward D., (1994), *Thermal Properties of Slag Films Taken From Continuous Casting Mould*, Ironmaking and Steelmaking, Vol. 21, no. 4, 279 – 286.

Turkdogan E. T., (1996), *Fundamentals of Steelmaking*, The Institute of Materials, 160.

Watanabe K., Suzuki M., Murakami K., Kondo H. & Shiomi T., (1996), *Development of Mould Powder for High Speed Casting of Middle Carbon Steel,* 1996 Steelmaking Conference Proceedings, 265 – 268.

Wolf M.M., (1987), *On the Interaction Between Mould Oscillation and Mould Lubrication,* Mould Powders for Continuous Casting and Bottom Pour Teeming , Iron and Steel Society, 33 – 44.

Yamauchi A., Sorimachi K. & Sakuraya T., (1992), *Heat Transfer Between Mold and Strand Through Mold Flux Film in Continuous Casting of Steel*, 4th International Conference on Molten Slags and Fluxes, 1992, Sendai, ISIJ, 415 -420.

Zaitsev A., Leites A., Litvina A. & Mogutnov B., (1994), *Investigation of the Mould Powder Volatiles During Continuous Casting*, Steel Research, Vol. 65, no. 9, 368 -374.

Zasowski P.J. & Sosinski D.J., (1990), *Control of Heat Removal in the Continuous Casting Mould*, 1990 Steelmaking Conference Proceedings, 253 - 259.